Interaction of curium with human serum albumin

Markus Keskitalo

Master's thesis

Department of Chemistry – Radiochemistry

University of Helsinki

September, 2018

HELSINGIN YLIOPISTO
HELSINGFORS UNIVERSITET
UNIVERSITY OF HELSINKI

MATEMAATTIS-LUONNONTIETEELLINEN TIEDEKUNTA
MATEMATISK-NATURVETENSKAPLIGA FAKULTETEN
FACULTY OF SCIENCE

Tiedekunta – Fakultet – Faculty	Koulutusohjelma – Utbildningsprogram – Degree programme
Faculty of Science	Department of chemistry - Radiochemistry

Tekijä – Författare – Author

Markus Keskitalo

Työn nimi – Arbetets titel – Title

Interaction of curium with human serum albumin

Työn laji – Arbetets art – Level	Aika – Datum – Month and year	Sivumäärä – Sidoantal – Number of pages
Master's thesis	10/2018	100

Tiivistelmä – Referat – Abstract

Actinides are heavy elements with no known physiological function in man, animals or plants. The actinides are radioactive without exception. In addition, the actinides exhibit metallotoxic properties. Due to these properties the actinides represent a health hazard to living organisms. This hazard can materialize should actinides be accidentally released into the environment. Decontamination regimes are used to treat humans contaminated with actinides. The knowledge of actinide bioinorganic chemistry inside the tissues and bodily fluids of humans is required for the development of internal decontamination therapies. Unfortunately, fairly little is known of the behaviour of actinides inside the human body at a molecular level.

Human serum albumin (HSA) is a blood plasma protein. With a concentration of circa 600 micromolar, it is the most ubiquitous of the blood-borne proteins. HSA has a multitude of physiological functions, one among them being the role of metal carrier. It is tempting to speculate that HSA might be an actor responsible for actinide distribution inside the human body.

In this study, the interaction between HSA and trivalent curium was investigated using time-resolved laser fluorescence spectroscopy (TRLFS) in a bid to obtain information useful in decontamination therapy development. TRLFS is a highly sensitive technique that allows the determination of speciation data even at trace level concentrations. Cm(III) has excellent optical properties, making it amenable for study using TRLFS and a convenient representative of trivalent actinides in general. In addition to Cm(III) the trivalent actinide analogue Eu(III), which is also a good fluorescent probe, was also utilized. Nuclear magnetic resonance (NMR) spectroscopy was used in an experiment aimed at resolving the site of interaction.

The experiments revealed the existence of a CmHSA complex. It was discovered that 90 % of available Cm(III) was in the CmHSA complex at physiological pH and temperature (7,4 and 310 K, respectively). A pH 8,0 conditional stability constant log K of 6,8 $\pm$ 0,5 and a Cm(III):HSA reaction stoichiometry of 1:1 were determined for the complex. In addition, the thermodynamic parameters ΔH and ΔS were determined. The number of non-water ligands in the first coordination sphere of Cm(III) was determined to be five or six. Furthermore, a combined TRLFS and NMR approach revealed the HSA binding locus of Cm(III) and Eu(III). Based on the results, a model could be presented, in which trivalent actinides bind HSA at the amino-terminus of the protein and that the site shares at least some of its ligands with the canonical Cu(II) binding site of HSA.

Avainsanat – Nyckelord – Keywords

human serum albumin, curium, time-resolved laser fluorescence spectroscopy

Säilytyspaikka – Förvaringställe – Where deposited

E-thesis

Muita tietoja – Övriga uppgifter – Additional information

Contents

1. Introduction 1

1.1. Chemical properties of actinides 2

1.1.1. Differences between actinides and lanthanides 4

1.1.2. Oxidation states 5

1.2. Spectroscopic properties of actinides 6

1.2.1. Spin-orbit coupling 6

1.2.2. Term symbols 7

1.2.3. Relative energies of terms and levels 8

1.2.4. jj-coupling and intermediate coupling 8

1.3. Curium 9

1.3.1. Oxidation states of curium 9

1.3.2. Electronic structure and properties of curium 11

1.3.3. Cm(III) spectroscopy 12

1.3.4. Spectroscopic properties of the trivalent actinide analogue Eu(III) 17

1.3.5. The Cm(III) aquo ion 20

1.3.6. Aqueous chemistry of curium 21

1.3.7. Curium in the geosphere 28

1.3.8. Curium in man 32

1.4. Human serum albumin 37

1.4.1. The structure of human serum albumin 37

1.4.2. Fatty acid binding properties of HSA 38

1.4.3. Drug binding properties of HSA 40

1.4.4. Metal ion binding properties of HSA 40

2. Experimental 47

2.1. Aims of the study 47

2.2. Materials and methods 48

2.2.1. Purification of HSA 48

2.2.2. Sample preparation 49

2.2.3. Time-resolved laser fluorescence spectroscopy 50

2.2.4. Nuclear magnetic resonance 52

2.2.5. pH measurement 54

2.3. Results and discussion 55

2.3.1. Interaction between Cm(III) and HSA at room temperature 55

2.3.2. Interaction between Cm(III) and HSA at physiological temperature 58

2.3.3. Kinetics of the CmHSA complex 59

2.3.4. The fluorescence lifetime of CmHSA 61
2.3.5. Stoichiometry and the conditional stability constant of CmHSA 63
2.3.6. Thermodynamics of Cm-HSA interaction 66
2.3.7. Displacement of Cm(III) from HSA by divalent metals 69
2.3.8. Interaction of Eu(III) with HSA 72
2.3.9. Eu(III) induced transitions in the proton NMR spectrum of HSA 75
2.3.10. The nature of the CmHSA complex 77
2.4. Summary and outlook 78
3. References 81

Abbreviations and symbols

An	Actinide
DAHK	L-Aspartyl-L-alanyl-L-histidyl-L-lysine
DTHK	L-Aspartyl-L-threonyl-L-histidyl-L-lysine
DTPA	Diethylenetriaminepentaacetic acid
EDTA	Ethylenediaminetetraacetic acid
FA	Fulvic acid
HA	Humic acid
HSA	Human serum albumin
ICCD	Intensified charged-couple device
Ln	Lanthanide
MBS	Multi-metal binding site
MWCO	Molecular weight cut-off
NMR	Nuclear magnetic resonance
NTA	Nitrilotriacetic acid
NTS	N-terminal site
PDB	Protein data bank
RT	Room temperature
TF	Transferrin
TFR	Transferrin receptor
TMS	Tetramethylsilane
TRIS	Tris(hydroxymethyl)aminomethane
TRLFS	Time-resolved laser fluorescence spectroscopy
WATERGATE	Water suppression by gradient tailored excitation
YAG	Yttrium aluminum garnet

1. Introduction

Actinides are a series of elements stretching from thorium (Z = 90) to lawrencium (Z = 103). Actinium (Z = 89) is also often included in the series. The pseudoelement symbol An is often used when referring to actinides. The characteristic property of an actinide is the filling of the seven 5f orbitals. In this regard the actinides are similar to another series of f-block elements, the lanthanides. The chemistry of actinides, however, is much more complex than that of lanthanides. Furthermore, actinides are radioactive without exception. (Choppin *et al.* 2013; Lehto & Hou 2010)

The actinides present in the environment can be categorized as either anthropogenic or natural. Anthropogenic actinides are artificial actinide nuclides created by man. Natural actinides belong to one of three natural radioactive decay chains. These decay chains originate from two isotopes of uranium (^{235}U and ^{238}U) or a single isotope of thorium (^{232}Th) and terminate in stable isotopes of lead. The chain-initiating actinides possess half-lives comparable to or even in excess of the age of the earth, and have been present since earth's formation. Such radionuclides are called primordial radionuclides. (Choppin *et al.* 2013; Eisenbud & Gesell 1997; Lehto & Hou 2010)

Since the discovery of nuclear fission by Hahn, Strassman, and Meitner mankind has harnessed the power of the nucleus for both power generation and destruction. Both of these activities have resulted in the release of anthropogenic and natural actinides into the environment (Eikenberg *et al.* 2004). The major and most relevant source of environmental actinides from 1945 to 1980 was the atmospheric test detonations of nuclear weapons (Beck & Bennett 2002; UNSCEAR 2000). Since the cessation of atmospheric nuclear weapon tests in 1980 actinides have been released in nuclear power plant accidents at Chernobyl and Fukushima (Högberg 2013; Steinhauser *et al.* 2014; UNSCEAR 2008; Zheng *et al.* 2012). Other notable releases of actinides have occurred at plutonium production, nuclear fuel reprocessing, and waste storage facilities (Garland & Wakeford 2007; Hunt & Smith 1999; Jones 2008; Nikipelov *et al.* 1989), during atmospheric burn-up of nuclear power generators carried on satellites (Krey 1967; Krey *et al.* 1979; USDOE 1978), and in incidents

involving bomber aircraft armed with nuclear weapons (García-Olivares & Iranzo 1997; Ikäheimonen *et al.* 2002; Montero & Sánchez 2001; USAF 1970).

Actinides are of special health interest due to the significant amounts handled in both power generation and the nuclear weapons industry, as well as their presence in global fallout and use in munitions (Choppin *et al.* 2013). Actinides are inherently harmful due to their metallotoxic and radioactive nature and no element of the actinide series is known to have an essential biochemical function in man, animals or plants. The very long-lived natural isotopes of thorium and uranium present both a chemical and radiological hazard, whereas the toxicity of the other actinides that possess shorter half-lives is dominated by the radiotoxicity component. (Karpas 2015; Nesmerak 2013) Indeed, the majority of long-term radiotoxicity of spent nuclear fuel originates from plutonium and minor actinides, which has implications regarding the long-term storage of spent nuclear fuel (Stacey 2007). To further highlight the health-threatening potential of actinides, the majority of the common radionuclides belonging to the very high radiotoxicity group are actinides (Piciu 2012). The investigation of actinide uptake and tissue retention in biological systems has been a major focus of actinide biology research as both subjects have implications for the protection of workers and the public (Durbin 2006).

1.1. Chemical properties of actinides

The electronic structure of actinides is based on the radon electron core in addition to which the 7s, 6d, and 5f orbitals are filled to varying degrees depending on the actinide and its oxidation state (Cotton 2006). Actinide cations are hard Lewis acids as defined by Pearson (Pearson 1963; Wiberg *et al.* 2001). Actinides form a multitude of complexes with halides, carbonates, chalcogens, and other ligands. Many oxides of actinides are known, often multiple per actinide. (Cotton 2006) Actinides tend to undergo hydrolysis, the intensity of which is dependent on the chemical form of the actinide (Lehto & Hou 2010). The coordination chemistry of actinides is rich and a coordination number higher than 6 is the norm for actinide coordination complexes. The organometallic chemistry of actinides is in like manner abundant. (Cotton 2006) Furthermore, some actinide complexes are catalysts in homogenous catalysis (Karmel *et al.* 2015).

In many respects, the chemistry of actinides bears a resemblance to lanthanide chemistry. As with lanthanides, the dominant oxidation state from americium to lawrencium at the end of the series is +III (Cotton 2006). Thermodynamic properties and trends are relatively similar between analogous actinides and lanthanides and the hydration properties are likewise similar between the two series (D'Angelo *et al.* 2013; David 1986). Electronegativities of actinides and lanthanides are comparable and distinct from other groups of elements (Pauling 1988). In addition, a trend resembling the lanthanide contraction phenomenon is observed in the actinide series: the ionic radii of actinide ions of the same oxidation state decrease with increasing atomic number (Lehto & Hou 2010). Ionic radii of actinides and lanthanides of the same oxidation state and coordination number are shown in Figure 1.1.

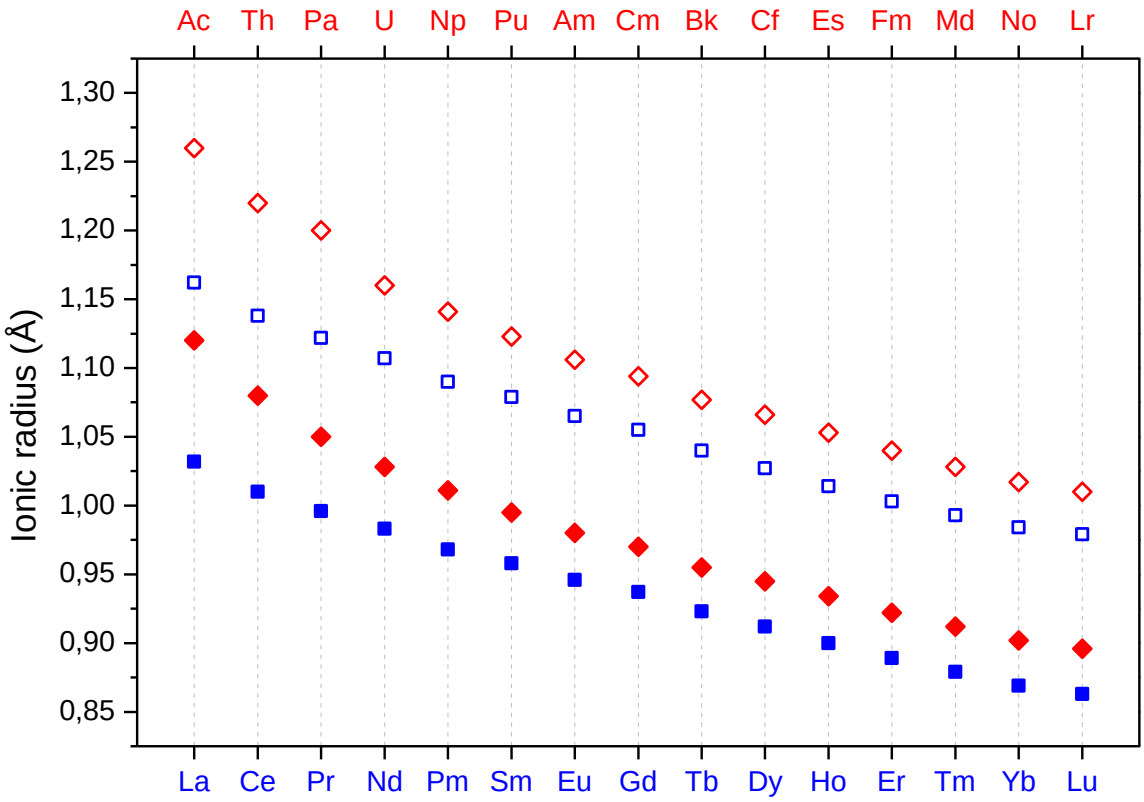

Figure 1.1. Ionic radii of actinides (red diamonds) and lanthanides (blue squares). Radii shown are for +III oxidation state ions in coordination number of either 6 (filled symbols) or 8 (empty symbols). Values are from David (1986).

1.1.1. Differences between actinides and lanthanides

Although similarities exist between the actinides and lanthanides, differences between the two series are known to exist as well. The differences stem from relativistic effects that have appreciably more impact on actinides than lanthanides. Unlike lighter elements, the velocity of electrons of heavy elements starts to approach the speed of light to a significant extent. This in turn increases the mass of the electrons in a phenomenon known as relativistic mass increase. (Kaltsoyannis & Scott 1999) Relativistic effects cause the s shells to contract. Contraction of a lesser magnitude is seen with p shells. The contraction of s and p shells shields the d and f shells from the nuclear charge, hence these shells tend to expand and destabilize. As actinides are the heavier of the two sets of elements, they experience stronger relativistic effects and the 5f orbitals of actinides are relatively larger than the 4f orbitals of lanthanides. This leads to weaker nuclear binding of actinide 5f electrons and increased chemical activity. (Cotton 2006) However, as the atomic number and nuclear charge increase across the actinide series, the 5f orbitals begin to contract and retreat into the radon electron core. As a results of this, the behavior of late actinides is more lanthanide-like than the early actinides' (Orchard 2003).

The consequences of stronger relativistic effects are multifold. A bigger range of oxidation states is available to the actinides, especially the early actinides. The ground-state electron configurations between actinides and lanthanides differ early in the series. As the actinide 5f orbitals are relatively higher in energy than the lanthanide 4f orbitals, they start to fill later in the series: the electronic structure of thorium is $[Rn]6d^27s^2$ instead of $[Rn]5f^16d^17s^2$, as could be expected from the electronic structure of the analogous lanthanide, cerium. In addition, the energy difference between the outermost d and f orbitals is smaller in actinides, and early actinides up to neptunium all have at least one d electron in their ground-state electron configurations. Compared to lanthanides, actinides form covalent bonds more readily, especially in the case of ions such as AnO_2^+ and AnO_2^{2+}. (Cotton 2006) The crystal structures of metallic early actinides are unlike the lanthanides' and appear more like that of the 3d transition metals (Edelstein *et al.* 2011). Crystal field effects are stronger for the early actinides than for their corresponding lanthanides (Orchard 2003). Relative to lanthanides, actinides show an increase in spin-orbit coupling (Kaltsoyannis & Scott 1999).

1.1.2. Oxidation states

The 5f electrons of actinides are shielded by the outer 6d and 7s orbitals in a fashion similar to the 4f electrons of lanthanides. The radial distribution of the 5f electrons in early actinides is such that the shielding of 5f electrons is smaller in magnitude than the shielding of 4f electrons (Edelstein 1995). This leads to 5f, 6d, and 7s electrons of early actinides being near-degenerate, thus making the 5f electrons available to participate in chemical bonding. (Lehto & Hou 2010) As a result, a wider range of available oxidation states is observed for the early actinides relative to lanthanides or late actinides. The behavior of early actinides resembles that of transition metals in that the highest available oxidation state is dictated by the number of electrons that can be taken out from the outermost orbitals. Later in the series, when the near-degeneracy of 5f, 6d, and 7s orbitals is abrogated, the +III state is established as the most common oxidation state. (Cotton 2006) The oxidation states of actinides are listed in Table 1.1.

Table 1.1. The oxidation states of actinides. A filled circle indicates that the oxidation state is common and an empty circle indicates that the oxidation state is known. Data are from Cotton (2006), MacDonald *et al*. (2013), Windorff *et al*. (2017), and Dutkiewicz *et al*. (2017).

	+II	+III	+IV	+V	+VI	+VII
Ac		●				
Th		○	●			
Pa		○	○	●		
U	○	○	●	○	●	
Np	○	○	○	●	○	○
Pu	○	○	●	○	○	○
Am	○	●	○	○	○	
Cm		●	○	○		
Bk		●	○			
Cf	○	●	○			
Es	○	●				
Fm	○	●				
Md	○	●				
No	●	○				
Lr		●				

Actinides in oxidation states +V and +VI do not appear as free cations but as so-called actinyl ions, AnO_2^+ and AnO_2^{2+}, respectively. Under acidic conditions, some unstable oxidation states of actinides may undergo disproportionation, in which the unstable species are transformed into other species. Plutonium is an especially interesting example of the disproportionation phenomenon, as even the most stable oxidation state of +IV disproportionates into +III and, possibly via a transient +V intermediate, +VI states. (Lehto & Hou 2010)

1.2. Spectroscopic properties of actinides

1.2.1. Spin-orbit coupling

An electron has an inherent spin angular momentum, characterized by the spin quantum number *s*, of ½. Should the azimuthal quantum number *l* be non-zero, the electron also possesses an orbital angular momentum. Both phenomena generate magnetic momenta and the interaction of these momenta is referred to as spin-orbit coupling. The summation of the spin and orbital momenta vectors gives the total angular momentum quantum number, *j*. (Atkins & De Paula 2010)

In a system with multiple electrons residing outside the closed shells, the coupling of all the spin and orbital angular momenta has to be considered. This is facilitated by the Russell-Saunders coupling scheme, also known as LS-coupling (Haigh 1995), in which vector sums of orbital and spin angular momenta of electrons are formed separately to yield *L* and *S*, respectively. Russell-Saunders coupling is based on the assumption of weak spin-orbit coupling relative to Coulomb interactions. (Atkins & De Paula 2010) The Russell-Saunders scheme is commonly used for lanthanides (de Bettencourt-Dias 2014). The Clebsch-Gordan series gives the permitted values of *L* and *S* (Atkins & De Paula 2010).

For a two electron system with azimuthal quantum numbers l_1 and l_2 and spin quantum numbers s_1 and s_2, possible values of L and S are

$$L = l_1 + l_2, l_1 + l_2 - 1, \dots, |l_1 - l_2| \quad (1)$$

$$S = s_1 + s_2, s_1 + s_2 - 1, \dots, |s_1 - s_2| \quad (2)$$

Subsequent coupling of L and S gives the total angular momentum J, with allowed values again given by the Clebsch-Gordan series (Engel & Reid 2014).

$$J = L + S, L + S - 1, \dots, |L - S| \quad (3)$$

Whereas the quantum number j conveys the information concerning the orientation of spin and orbital angular momenta relative to one another for a single electron, the quantum number J conveys the same information for multiple electrons (Atkins & De Paula 2010).

1.2.2. Term symbols

The L, S, and J values of different configurations are given by term symbols. Term symbols take the form of ${}^{2S+1}L_J$. The multiplicity of a term is represented by a number, the result of $2S+1$. Pairing up all the electrons abolishes net spin and means that $S = 0$. This leads to $2S+1$ equaling 1 and so a singlet term. Similarly, a single, unpaired electron with $S = s = ½$ leads to a doublet term as in this case $2S + 1 = 2$. Furthermore, two unpaired electrons leads to a triplet state as $S = 1$ and $2S + 1 = 3$, and so on. (Atkins & De Paula 2014)

The total orbital angular momentum L is represented by a capital letter, as listed in Table 1.2. S and L define the term of a configuration. Spin-orbit coupling splits terms into levels, which are represented by the possible values of J. (Engel & Reid 2014) The splitting of terms into levels gives rise to the fine structure in a spectrum (Atkins & De Paula 2010). In a term symbol, the numerical values of J given by (3) are used denote the different levels of a term.

Table 1.2. The letters used to denote *L* in term symbols. After F the letters are assigned in alphabetical order. Note that the letter J is not used. (Weller *et al.* 2014)

Value of *L*	0	1	2	3	4	5	6	7	…
Letter	S	P	D	F	G	H	I	K	…

1.2.3. Relative energies of terms and levels

A set of three empirical rules govern the relative energies of different terms and levels of a configuration. Referred to as Hund's rules after their discoverer, Friedrich Hund, the rules facilitate the prediction of the term that is lowest in energy and the level of lowest energy within a term. (Engel & Reid 2014)

Rules one and two deal with the relative energies of terms, whereas rule three concerns the relative energies of levels. Rule one states that the term with the highest spin multiplicity is the lowest in energy. Rule two sets forth that if multiple terms share the same spin multiplicity value, then the term that is lowest in energy is the one with the highest orbital angular momentum. And finally, rule three states that if a partially filled subshell is precisely or more than half full, the level that has the lowest energy is the one with the highest value of *J*. Conversely, if the subshell is less than half full then the level of lowest energy is the one with the lowest *J* value. (Engel & Reid 2014)

1.2.4. jj-coupling and intermediate coupling

The strength of spin-orbit coupling is dictated by the nuclear charge and therefore spin-orbit interaction is stronger in heavier atoms. For this reason the Russell-Saunders coupling scheme fails when the *Z* of an atom is large. (Atkins & De Paula 2010)

A better scheme for heavy atoms with strong spin-orbit couplings, like actinides, is jj-coupling, in which the spin and orbital momenta are coupled separately for each individual electron in partially filled subshells to yield an electron-specific total angular momentum *j*. The electron specific total angular momenta are then coupled, which gives the resultant grand total angular momentum *J*. (Haigh 1995)

No atom displays pure Russell-Saunders or jj-coupling. Rather, all atoms adhere to both schemes to varying degrees: light atoms more to Russell-Saunders coupling, heavy atoms more to jj-coupling. Although jj-coupling is the more fitting scheme for heavy atoms, different energies of heavy atoms can still be labeled using term symbols compliant with the Russell-Saunders coupling scheme, as a correspondence exists between the two schemes. (Atkins & De Paula 2010) However, the best scheme to represent the 5f states is the intermediate coupling scheme that accounts for both the electrostatic and spin-orbit interactions (Moore & van der Laan 2009). In intermediate coupling, the eigenstates are derived from linear combinations of different Russell-Saunders terms that possess the same total angular momentum *J* (Dodson & Zia 2012).

1.3. Curium

Curium, the 96th element of the periodic table, is named in honor of Marie and Pierre Curie. As curium does not occur in nature, all terrestrial curium is anthropogenic. The first isotope of curium to be produced was ^{242}Cm in 1944 by Seaborg, James, and Ghiorso by way of bombarding ^{239}Pu with helium ions (He^{2+}) in a cyclotron. (Lumetta *et al.* 2011) Another route to ^{242}Cm discovered early was successive neutron captures by plutonium followed by β^--decay to first produce an intermediate americium nuclide ^{241}Am, which upon neutron capture and subsequent β^--decay transmutes to ^{242}Cm (Choppin *et al.* 2013).

Curium is the heaviest element that is available in gram amounts. Isotopes ^{242}Cm, ^{244}Cm, and ^{248}Cm are available in quantities that allow a more thorough chemical investigation. However, the rarity of ^{248}Cm and high specific radioactivities of ^{242}Cm and ^{244}Cm place constraints on the characterization of curium chemistry. In all, 14 isotopes of curium are known, with their mass numbers ranging from 238 to 251. (Lumetta *et al.* 2011) The nuclear properties of curium isotopes are listed in Table 1.3.

1.3.1. Oxidation states of curium

In contrast to earlier actinides, the +III oxidation state of curium is very stable and resistant to oxidation and reduction. The stability is postulated to arise from a half-filled 5f orbital

($5f^7$), a relatively stable electron configuration. Due to its stability, the chemical behavior of Cm(III) resembles that of lanthanides. (Lumetta *et al.* 2011)

Table 1.3. The known isotopes of curium and their associated half-lives and decay modes with intensities. ε = electron capture, SF = spontaneous fission. Data are from Audi *et al.* (2017).

Mass number	Half-life	Decay modes and intensities (%)
238	2,2 h	ε = ?; α = 3,84; SF = 0,048
239	2,5 h	$\beta^+ \approx 100$; $\alpha = 6{,}2 \times 10^{-3}$
240	27 d	α ≈ 100; ε < 0,5
241	32,8 d	ε = 99; α = 1
242	162,8 d	α = 100
243	29,1 a	α ≈ 100; ε = 0,29
244	18,1 a	α = 100
245	8,25 ka	α = 100
246	4,706 ka	α ≈ 100; SF = 0,02615
247	15,6 Ma	α = 100
248	348 ka	α = 91,61; SF = 8,39
249	64,15 min	$\beta^- = 100$
250	about 8,3 ka	SF ≈ 74; α ≈ 18; $\beta^- \approx 8$
251	16,8 min	$\beta^- = 100$

Oxidation states other than +III do exist, however. Oxidation of Cm(III) to Cm(IV) requires very strong oxidizing agents and only two compounds of curium in the tetravalent state are known (Lumetta *et al.* 2011). Curium dioxide, CmO_2, can be produced via air ignition of some Cm(III) species (Asprey *et al.* 1955). The synthesis of curium tetrafluoride, CmF_4, involves fluorination of curium trifluoride with fluorine gas (Asprey *et al.* 1957). Aqueous CmF_4 requires the inclusion of 15 M CsF and is not stable due to radiolytic reduction of Cm(IV) to Cm(III) (Keenan 1961). Transient Cm(IV) and Cm(II) states have been detected by subjecting Cm(III) to pulse radiolysis in aqueous perchlorate media (Sullivan *et al.* 1976).

No isolated Cm(II) compounds are known (Lumetta *et al.* 2011) and data for curium oxidation states greater than +IV are sparse (Lehto & Hou 2010).

1.3.2. Electronic structure and properties of curium

Curium has the ground electron configuration of $[Rn]5f^7 6d^1 7s^2$ and upon ionization to Cm(III) it sheds the s and d electrons to attain a half-filled f shell configuration $[Rn]5f^7$. Curium's ground and trivalent cation electron configurations are identical with its lanthanide analogue, gadolinium ($[Xe]4f^7 5d^1 6s^2$ for Gd(0), $[Xe]4f^7$ for Gd(III)), except that the outermost shell numbers are one smaller in Gd. (Cotton 2006)

Hund's rules state that the term with the highest spin multiplicity is the ground term (Engel & Reid 2014). For Cm(III), and for Gd(III), the highest multiplicity is attained when all seven of the f electrons are unpaired. As every suborbital of the f orbital is now filled with a single, unpaired electron, there is no effective orbital angular momentum and so the ground term is expected to be $^8S_{7/2}$. However, the strong spin-orbit coupling in Cm(III) mixes other J = 7/2 states into the ground state. While the ground term of Gd(III) is about 97 % of $^8S_{7/2}$ parentage, the larger spin-orbit coupling in Cm(III) mixes excited states into the ground manifold and splits the ground term. (Edelstein *et al.* 2006) This results in the ground term $^8S'_{7/2}$ having about 78 % $^8S_{7/2}$ parentage with other states, mostly $^6P_{7/2}$ at 19 %, mixed in (Lindqvist-Reis *et al.* 2006).

As the maximum multiplicity ground state is relatively stable, the energy required to excite one of the equivalent, unpaired f electrons to the next highest multiplet is relatively high. Therefore, in both Cm(III) and Gd(III), a large energy gap is formed between the ground octet state and excited sextet states as the result of electrostatic interactions between the equivalent electrons of the half-filled f shell. In free Gd(III) ion with a spatially more compact 4f shell, the gap is over 30 000 cm^{-1}. However, in free Cm(III) ion the greater extent of the 5f shell reduces the intensity of electron-electron interactions, resulting in a smaller gap of about 16 800 cm^{-1}. (Edelstein *et al.* 2006) In trivalent aquo ions the gap is 32 200 cm^{-1} for Gd (Carnall *et al.* 1968a) and 17 095 cm^{-1} for Cm (Carnall & Rajnak 1975). Another reason for the smaller transition energy between the ground and first excited multiplets in Cm(III) is the greater spin-orbit coupling in Cm (Edelstein *et al.* 2006). The free-ion energy

levels of Gd^{3+}(aq) and Cm^{3+}(aq) are presented in Figure 1.2. Conveniently, the first excited multiplet of Cm(III) resides in the visible region and the large energy difference across the gap gives rise to strong fluorescence (Edelstein *et al.* 2006).

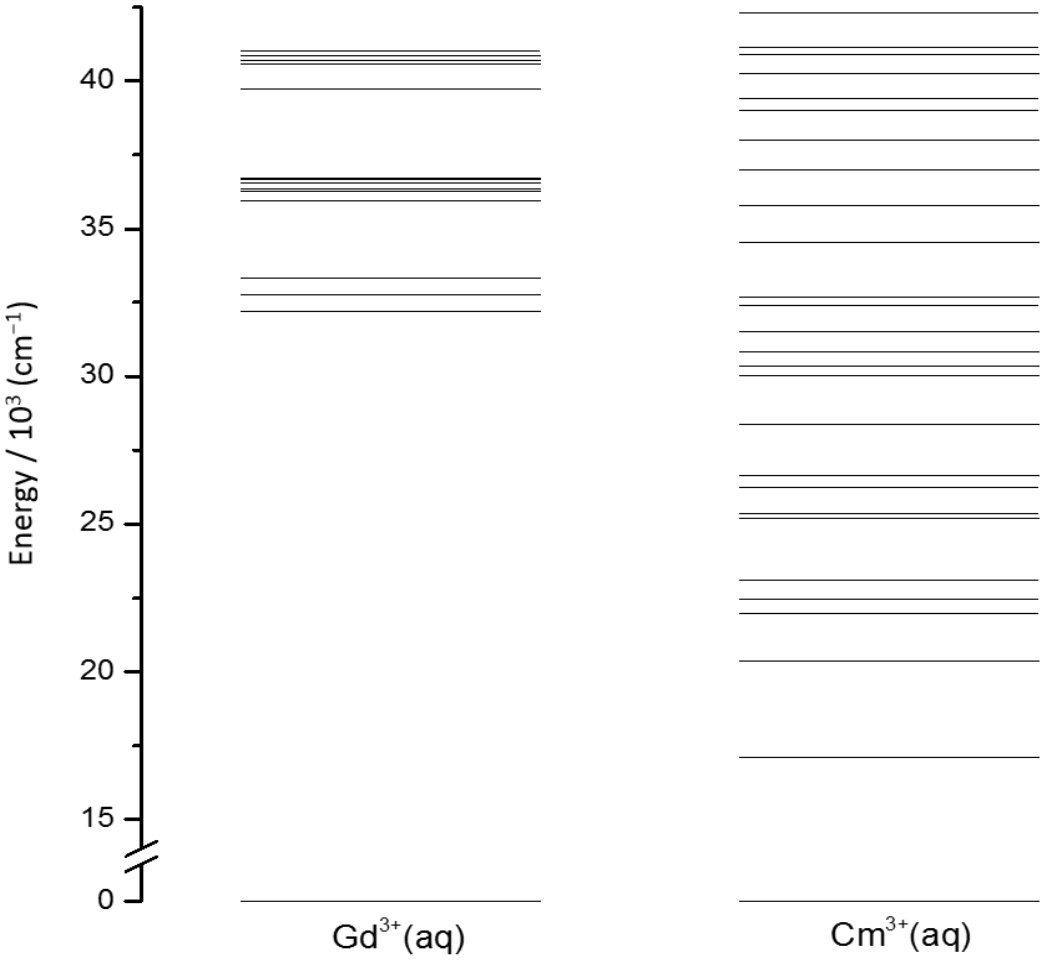

Figure 1.2. Experimental free-ion energy levels of the Gd(III) and Cm(III) aquo ions up to 42 500 cm^{-1}. Values for Gd^{3+}(aq) and Cm^{3+}(aq) are from Carnall *et al*. (1968a) and Carnall & Rajnak (1975), respectively.

1.3.3. Cm(III) spectroscopy

As curium is often present or available only in trace amounts, very high sensitivity is required from the methods applied in its study. Many commonly used spectroscopic techniques, such as conventional optical spectroscopy, fail to fulfill the sensitivity requirement. (Edelstein *et al.* 2006) The application of laser-based methods to observe 5f-

transitions in actinides was suggested by Beitz and Hessler in 1980 and time-resolved laser fluorescence spectroscopy (TRLFS), in particular, was found to be a suitable technique for the study of Cm(III), with an estimated limit of detection in the sub-nanomolar range (Beitz & Hessler 1980). Experimental TRLFS detection limits of $1{,}8 \times 10^{-11}$ (Beitz *et al.* 1988) and 3×10^{-11} (Kim *et al.* 1991) molar Cm(III) have since been reported. In addition, TRLFS is very capable of discrimination between chemical species (Nouhi *et al.* 2018).

The absorption spectrum of the Cm(III) aquo ion is dominated by three intense f-f transitions from the $^{8}S'_{7/2}$ ground state Z to three separate excited states. These three absorption lines were originally identified as the F, G, and H bands. (Carnall & Rajnak 1975) Excitation of Cm(III) to any of these states is followed by nonradiative decay to a $^{6}D'_{7/2}$ state, the A band. The nonradiative decay path is thought to involve predominantly electronic-to-vibrational energy transfer from the Cm^{3+} to the surrounding water molecules (Beitz 1991). A radiative decay from the excited A state to the ground state Z results in an emission at 593,9 nm (Figure 1.3). No emissions from the higher excited states are observed. (Beitz & Hessler 1980) The fluorescence process is summarized in Figure 1.4.

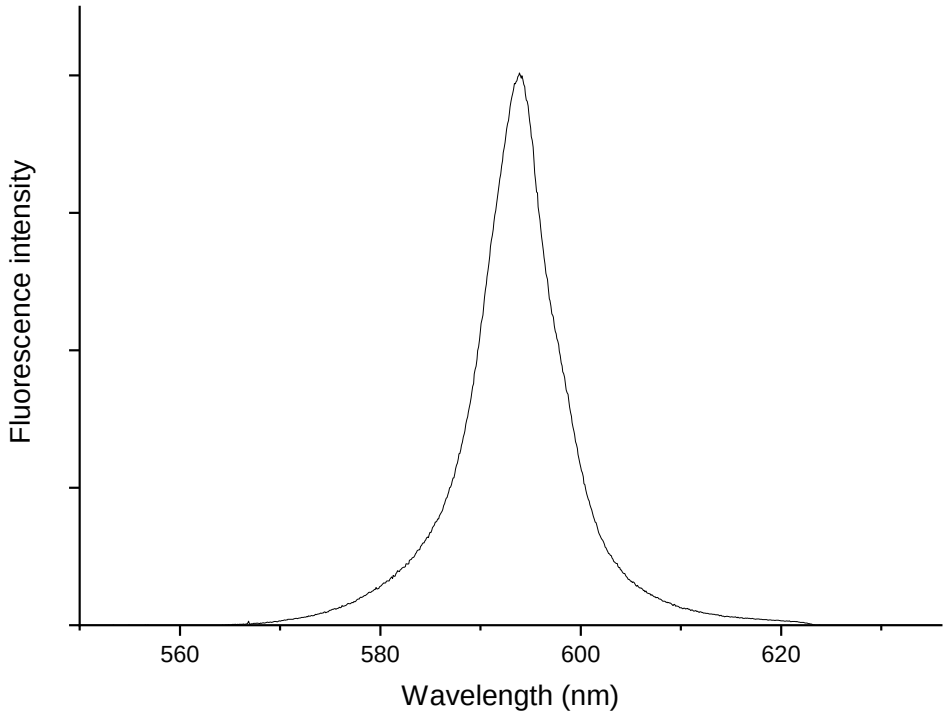

Figure 1.3. The $^{6}D'_{7/2} \rightarrow {}^{8}S'_{7/2}$ emission band of the Cm(III) aquo ion.

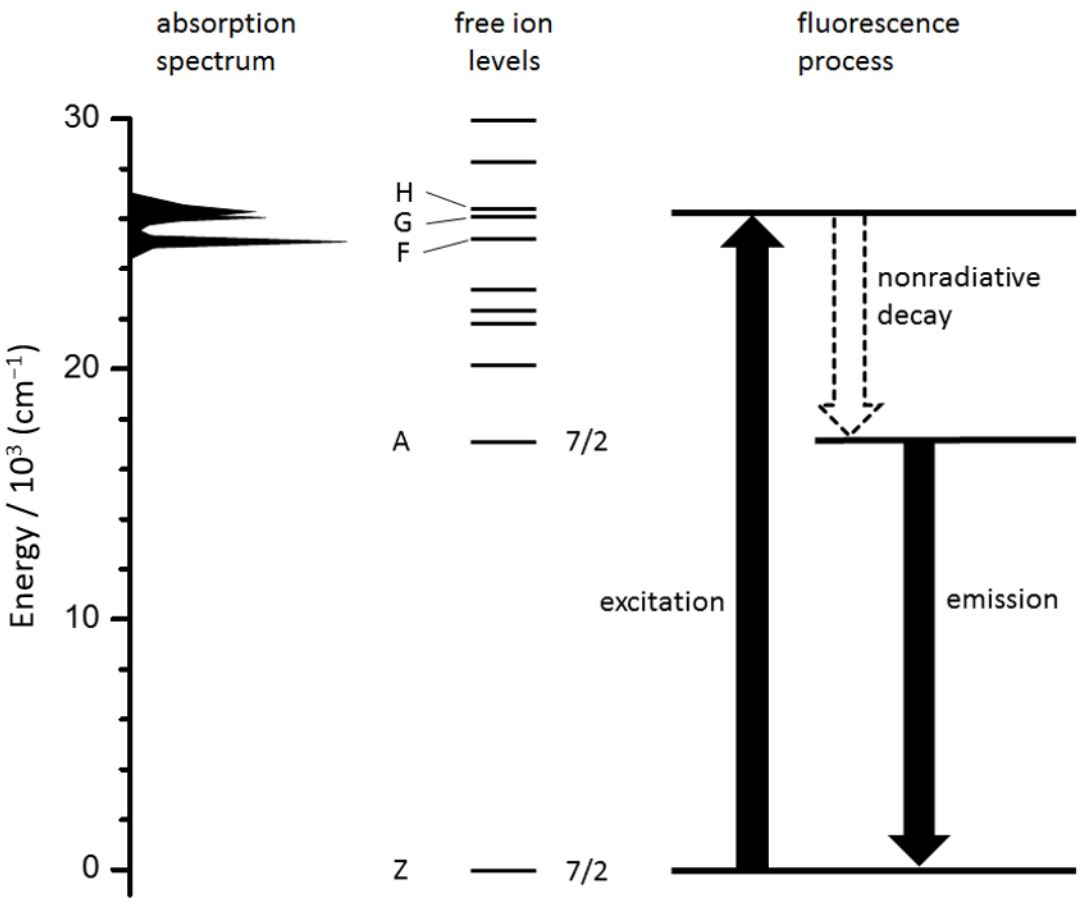

Figure 1.4. Overview of the fluorescence process in Cm^{3+}(aq). The dominant absorption lines arising from the F, G, and H states are shown on the left. Their relation to the emissive excited state A and the ground state Z is shown in the center. The *J* values of A and Z states are shown to the right of their respective free ion level bars. The overall fluorescence process is shown on the right. Excitation of the system is followed by a nonradiative decay process that takes the system down to the emissive excited A state. The remainder of the absorbed energy is then lost through emission of electromagnetic radiation, following which the system is again at ground state. In TRLFS, the energy required for excitation is supplied by a pump laser. Figure adapted and modified from Beitz (1991) and Kim *et al*. (1991).

The radiative decay rate constant of the Cm(III) aquo ion has been directly measured and the radiative lifetime of 65 µs has been shown to be temperature and isotope effect independent (Tian *et al.* 2011; Wimmer, Klenze *et al.* 1992). Using D_2O as the solvent instead of H_2O results in the removal of OH oscillators from the first coordination shell of Cm^{3+} and extends the fluorescence lifetime to 1270 µs (Kimura & Choppin 1994). The fluorescence quantum yield of Cm(III) in H_2O was first estimated to be 0,03, with later measurements suggesting that the quantum yield is temperature-dependent and has a

value ranging from 0,0323 to 0,0289 at temperatures 10 and 85 °C, respectively (Beitz & Hessler 1980; Tian *et al.* 2011). Some processes may alter the fluorescence intensity of Cm(III). Reduction in intensity may occur through transfer of energy to low-lying levels of other ions or ligands. On the other hand, energy transfer from an excited ligand to Cm(III) may give rise to sensitized and markedly more intense fluorescence. (Edelstein *et al.* 2006)

A crystal field splits both the $^{8}S'_{7/2}$ ground state and the $^{6}D'_{7/2}$ excited state of the Cm(III) aquo ion into four crystal field levels. An emission spectrum is expected to red-shift should the strength of the crystal field increase. (Lindqvist-Reis *et al.* 2006) Whereas the ground state splitting of the Cm(III) aquo ion is thought to be negligibly small (Carnall & Rajnak 1975), the excited state is split by several hundred cm^{-1}. The crystal field splitting is dependent on the strength of the crystal field in a manner where a strong field strength results in large splitting. This behavior is showcased in Figure 1.5. The quantity N'_v, derived from the scalar crystal field strength parameter N_v, is used for comparison of crystal field magnitudes and is a good indicator of splitting magnitude. At room temperature, the lowest crystal field level of the excited multiplet is the most populated and transitions from this level are the most prominent in an emission spectrum. Transitions from the higher crystal field levels that are populated to a lesser extent result in an asymmetrical broadening of the emission spectrum by unresolved hot bands. (Edelstein *et al.* 2006)

The inner-sphere coordination environment has a profound impact on metal ion fluorescence, and changes in the coordination environment can lead to changes in spectral shape, decay lifetimes and fluorescence intensity. The differentiation between chemical species using TRLFS is based on monitoring and recording these alterations. (Collins *et al.* 2011) The emission spectra of organic or inorganic complexes of Cm(III) are red-shifted relative to the aquo ion in an aqueous environment (Edelstein *et al.* 2006). The spectroscopic characteristics of some Cm(III) species are listed in Table 1.4. Whereas the changes in excitation and emission spectra are probably of prime importance and interest, measurement and analysis of the lifetime of fluorescence arising from Cm(III) yields some useful information as well.

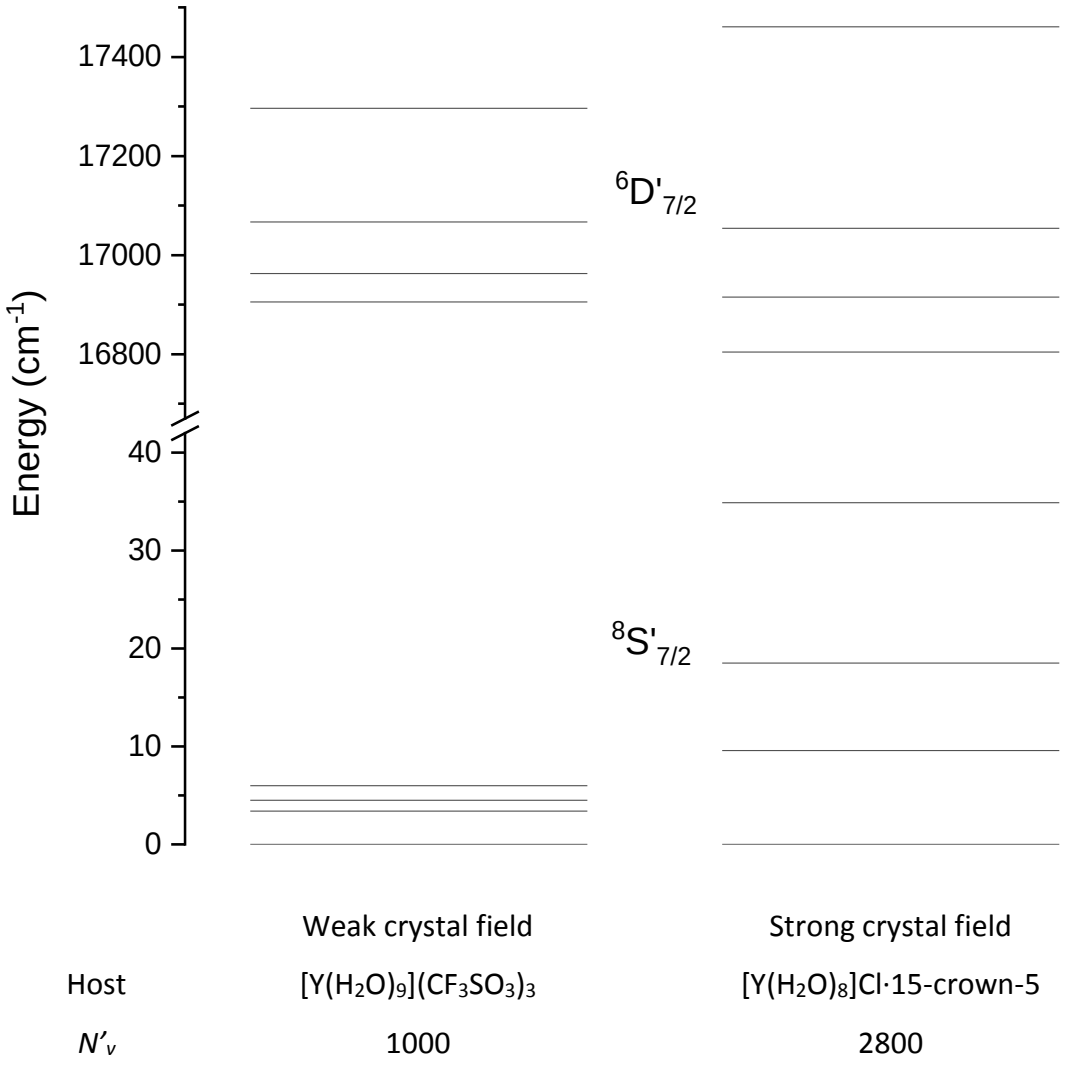

Figure 1.5. Splitting of the ground state $^{8}S'_{7/2}$ and the excited state $^{6}D'_{7/2}$ into crystal field levels in, relatively, weak and strong crystal fields. Data for $[Y(H_2O)_9](CF_3SO_3)_3$ is from Lindqvist-Reis *et al*. (2009) and data for $[Y(H_2O)_8]Cl$·15-crown-5 is from Lindqvist-Reis *et al*. (2006).

The number of water molecules in the first coordination shell can be estimated using the empirical Kimura equation

$$n_{H_2O} = 0{,}65 \times k_{obs}[\mathrm{Cm(III)}] - 0.88 \qquad (4)$$

where k_{obs}[Cm(III)] is the decay constant, equal to the reciprocal of the observed fluorescence lifetime (in ms).

Table 1.4. Spectroscopic characteristics of selected aqueous Cm(III) species. Data are from Wimmer *et al*. (1992).

Species	Excitation wavelengths (nm)			Emission wavelength (nm)	Fluorescence lifetime (µs)
Cm^{3+}	375,4	381,3	396,5	593,8	65
$CmOH^{2+}$	376,0	381,6	397,5	598,8	72
$Cm(OH)_2^{+}$	377,4	384,2	399,2	603,5	80
$CmCO_3^{+}$	376,5	382,5	397,5	598,0	85
$Cm(CO_3)_2^{-}$	377,5	384,5	398,9	605,9	105
$Cm(CO_3)_3^{3-}$	377,5	384,1	399,9	607,6	215

The inherent uncertainty of hydration numbers calculated using (4) is ±0,5 water molecules. (Kimura & Choppin 1994) Decay lifetimes can be useful in qualitative analysis if the spectra of the different species overlap. The fluorescence lifetimes of Cm(III) species are usually in the microsecond range (Kimura *et al.* 1996). Thus, a time-gate can be used to separate the fluorescence signals originating from Cm(III) and most organic compounds, as the fluorescence lifetimes of the latter tend to be shorter. (Collins *et al.* 2011) TRLFS permits the determination of thermodynamic data, as the fluorescence quantification and speciation information provided by TRLFS can be used to calculate thermodynamic parameters (Edelstein *et al.* 2006). The spectroscopic properties of selected aqueous Cm(III) species are listed in Table 1.4.

1.3.4. Spectroscopic properties of the trivalent actinide analogue Eu(III)

Europium (Eu) is an element belonging to the lanthanide series. With a ground electron configuration of $[Xe]4f^7 6s^2$, it is the lanthanide congener of americium. While +III is the only relevant oxidation state for most lanthanides, europium is stable also at oxidation state +II, as the loss of two electrons results in a half-filled 4f shell. Perhaps unsurprisingly then, the +II oxidation state of europium is the most stable of the series. At oxidation states +II and +III, the electronic configuration of Eu is $[Xe]4f^7$ and $[Xe]4f^6$, respectively. (Cotton 2006) It is the most reactive element of the lanthanide series (Moreno 2011). The behavior of

trivalent lanthanides mirrors that of trivalent actinides, and Eu(III) in particular is commonly used as a trivalent actinide analogue (Lehto & Hou 2010).

Hund's rules dictate that the ground term level of Eu(III) is $^7F_0$. However, unlike in Cm(III), where the ^8S ground term is split only to a relatively minor degree, the ^7F ground term of Eu(III) is extensively split into *J* states. The split $^7F_{0–6}$ states in free ion Eu(III) are calculated to be separated by energies from a few hundred to up to about thousand cm^{-1}. (Binnemans 2015) Splitting of similar magnitudes has been observed in Eu^{3+}(aq) (Carnall *et al.* 1968b).

The luminescence spectrum of Eu(III) is significantly more complex than that of Cm(III) due to the splitting of the ground term. For spectroscopic purposes Eu(III) is often excited to the $^5L_6$ level, the most intense absorption transition of Eu(III) in the UV-Vis region. Subsequently, some of the excitation energy is lost through non-radiative mechanisms and Eu(III) adopts the $^5D_0$ level, which is non-degenerate. From here, most or all of the remaining excitation energy is lost in a radiative emission to the different ground term levels, giving rise to multiple possible transitions of different energies. Transitions from ^5D term levels other than $^5D_0$ term are possible, but uncommon. (Binnemans 2015) The general features of $^5D_0 \rightarrow {}^7F_J$ transitions are summarized in Table 1.5. The fluorescence process scheme for Eu^{3+}(aq) is presented in Figure 1.6.

Table 1.5. Summary of the $^5D_0 \rightarrow {}^7F_J$ emissive transitions of Eu(III). Data are from Binnemans (2015). vw = very weak, w = weak, m = medium, s = strong, vs = very strong.

Transition	Wavelength range (nm)	Relative intensity
$^5D_0 \rightarrow {}^7F_0$	570-585	vw to s
$^5D_0 \rightarrow {}^7F_1$	585-600	s
$^5D_0 \rightarrow {}^7F_2$	610-630	s to vs
$^5D_0 \rightarrow {}^7F_3$	640-660	vw to w
$^5D_0 \rightarrow {}^7F_4$	680-710	m to s
$^5D_0 \rightarrow {}^7F_5$	740-770	vw
$^5D_0 \rightarrow {}^7F_6$	810-840	vw to m

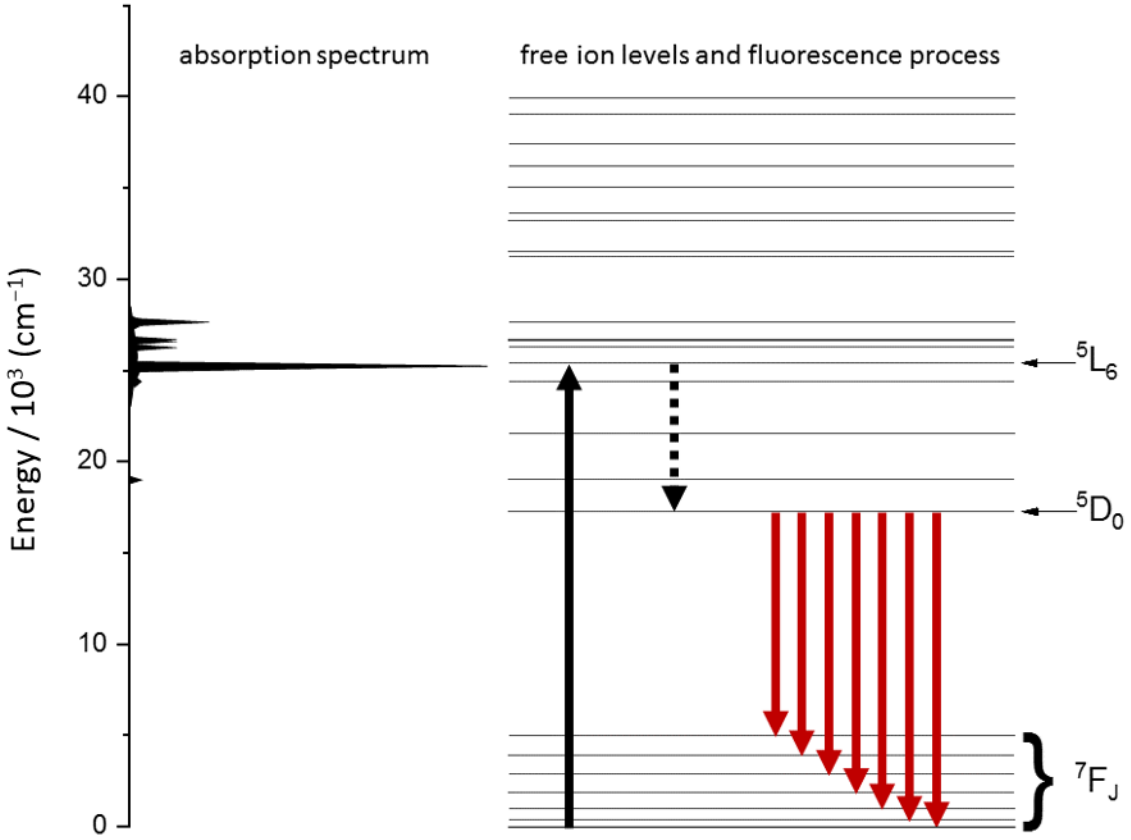

Figure 1.6. The absorption bands, energy levels and fluorescence process of Eu^{3+}(aq). Approximate, relative absorption bands up to 30 000 cm^{-1} are shown on the left whereas the free ion levels up to 40 000 cm^{-1} are shown on the right. The $^5L_6 \leftarrow {}^7F_0$ excitation is shown as a solid, black arrow, the $^5L_6 \rightarrow {}^5D_0$ non-radiative relaxation as a dotted arrow, and the $^5D_0 \rightarrow {}^7F_J$ emissive transitions as red arrows. Data are from (Carnall *et al.* 1968b).

Eu(III) is a convenient spectroscopic probe due to the high luminescence intensity of its compounds facilitated by the large $^5D_0 \rightarrow {}^7F_J$ energy gap. The crystal field may split the energy levels by a couple hundred cm^{-1} or less and the spacing of the ^7F_J levels guarantees that in the vast majority of cases there is no overlap of crystal field levels of different $^5D_0 \rightarrow {}^7F_J$ emission bands. In addition, only a small number of crystal field levels are possible for the important $^5D_0 \rightarrow {}^7F_{0-2}$ transitions. The crystal field levels are of use in assessing the point group symmetry of Eu(III), as in principle it is possible to establish the point group from the number of observed crystal field components of a transition, though a small crystal field splitting and overlap of peaks often make it difficult. (Binnemans 2015)

Of the transitions listed in Table 1.5, $^5D_0 \rightarrow {}^7F_1$ and $^5D_0 \rightarrow {}^7F_2$ are particularly interesting. The strong $^5D_0 \rightarrow {}^7F_1$ transition is largely independent of the environment and the integral of the transition intensity may be used to normalize Eu(III) spectra. (Binnemans 2015) The $^5D_0 \rightarrow {}^7F_2$ transition, on the other hand, is hypersensitive and thus very attuned to the microenvironment of the fluorescing Eu(III) ion. This feature is of use in Eu(III) speciation, as the intensity of the transition increases upon complexation. (Plancque *et al.* 2003) The $^5D_0 \rightarrow {}^7F_2$ transition intensity is dependent on ligand polarizability in a fashion where the intensity is very strong in the presence of highly polarizable ligands, and *vice versa*. In addition, the $^5D_0 \rightarrow {}^7F_2$ transition intensity may be utilized as a measure of Eu(III) site asymmetry, as the intensity of the transition in a centrosymmetric environment is usually weak (Binnemans 2015). The lifetime of Eu(III) fluorescence is sensitive to the immediate environment akin to Cm(III) and the determination of the number of first hydration shell water molecules can be estimated with the empirical equation

$$n_{H_2O} = 1{,}07 \times k_{obs}[\mathrm{Eu(III)}] - 0.62 \qquad (5)$$

where k_{obs}[Eu(III)] is the fluorescence decay constant, the reciprocal of the fluorescence lifetime (in ms), and the inherent uncertainty of the equation is ±0,5 water molecules (Kimura & Choppin 1994).

1.3.5. The Cm(III) aquo ion

The hydration number of trivalent actinide aquo ions is predicted to be either eight or nine with a gradual transition from nine to eight taking place from Cm to Es (David & Vokhmin 2003). Therefore, a hydration number of nine or eight is expected for Cm^{3+}(aq). Quantum chemical studies and molecular dynamics simulations have indicated that the first hydration shell of Cm^{3+}(aq) consists of nine water molecules with an additional 21 water molecules in the second hydration shell (Yang & Bursten 2006). Single-crystal x-ray diffraction investigation of a curium triflate salt suggested a structure in which nine water molecules in a tricapped trigonal-prismatic geometry are in coordination with a central Cm^{3+} ion (Lindqvist-Reis *et al.* 2007). Nonahydration of Cm^{3+}(aq) in solution has also been suggested by extended X-ray absorption fine structure (EXAFS) and high energy X-ray

scattering (HEXS) experiments. The prismatic waters are thought to reside closer to the central Cm^{3+} ion than the capping water molecules. (Skanthakumar *et al.* 2007) In like manner, luminescence studies have indicated a hydration number of nine (Kimura & Choppin 1994; Kimura *et al.* 1996). The Cm(III) aquo ion has been suggested to exist as an equilibrium species. At room temperature most of the Cm(III) is nonahydrated and a smaller fraction is present as the octahydrated species. Raising the temperature shifts the equilibrium towards the octahydrated species. (Lindqvist-Reis *et al.* 2005) A schematic representation of nonahydrated Cm^{3+}(aq) is shown in Figure 1.7. In contrast to curium, the aquo ion of the analogous lanthanide, gadolinium, is octahydrated as the transition from nona- to octahydration comes earlier in the lanthanide series (Rizkalla & Choppin 1991; Steele & Wertz 1976).

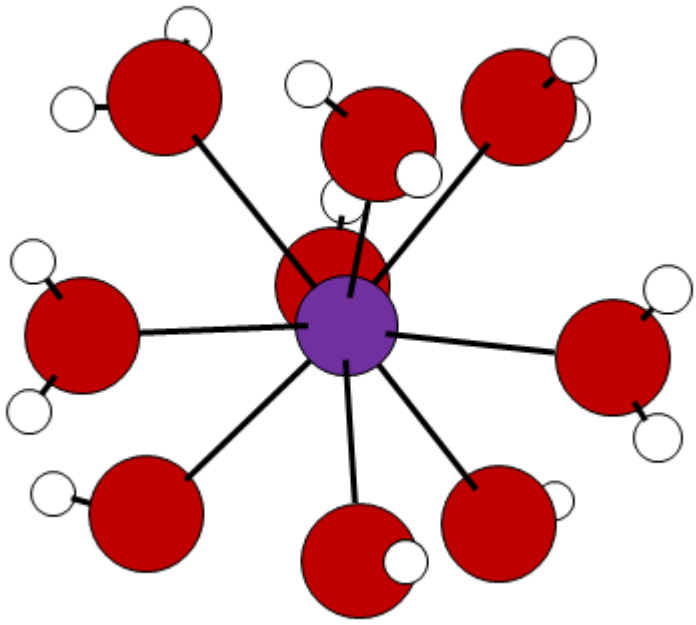

Figure 1.7. A schematic representation of the nonahydrated Cm^{3+}(aq) ion. Curium is shown in purple, oxygen in red and hydrogen in white. Adapted and modified from Skanthakumar *et al.* (2007)

1.3.6. Aqueous chemistry of curium

As oxidation states other than +III are highly unstable, nearly all curium chemistry in solution involves Cm(III). Curium chemistry in solvents other than water is not very well

characterized, except for chemistry with environmental implications or relevant to chemical separations. The reactions and behavior of Cm(III) in aqueous solutions are similar to those of other trivalent actinides. Especially the higher fluorides, iodates, phosphates, hydroxides, and oxalates of Cm(III) are sparingly soluble in water, whereas the iodides, chlorides, sulfates, nitrates and perchlorates are water-soluble. As a hard metal ion, curium forms complexes far more readily with non-polarizable donors like fluoride and oxygen than with polarizable donors such as sulfur and chloride. (Lumetta *et al.* 2011) Reported stability constants of selected aqueous complexes of Cm(III) are given in Table 1.6 at the end of this chapter.

Complexation with inorganic ligands

As a trivalent actinide ion, the formation of relatively strong hydrolysis complexes of Cm(III) is expected (Altmaier *et al.* 2013). Indeed, Cm(III) readily undergoes hydrolysis reactions under aqueous conditions (Mohapatra & Khopkar 1989). Both the monohydroxo $Cm(OH)^{2+}$ and the dihydroxo $Cm(OH)_2^{+}$ hydrolysis species have been characterized in solution. The formation of the monohydroxo species reportedly starts at around pH 6 and reaches its maximum relative concentration at about pH 8. The dihydroxo species is first observed when the pH is raised above 7. From about pH 8 upwards, the only relevant species are the two hydrolysis species, and from about pH 10 upwards, only the dihydroxo species is present in the solution. (Wimmer, Klenze *et al.* 1992) The distribution of Cm^{3+}(aq), $Cm(OH)^{2+}$, and $Cm(OH)_2^{+}$ as a function of pH is shown in Figure 1.8. Increasing concentrations of sodium chloride in aqueous solution shift the pH at which the hydrolysis reactions initiate to lower pH values, and thus promote hydrolysis (Fanghänel *et al.* 1994). The trihydroxo species $Cm(OH)_3$ is a quantitative precipitant and the characterization of the hydrolysis species in solution is, in general, marred by solubility issues (Penneman & Keenan 1960; Wimmer, Klenze *et al.* 1992). High concentrations of $CaCl_2$ are, however, able to bring hydrolysis species up to the hexahydroxo $Cm(OH)_6^{3-}$ into solution, possibly through the formation of ternary Ca-Cm(III)-OH complexes, under basic conditions (Rabung *et al.* 2009).

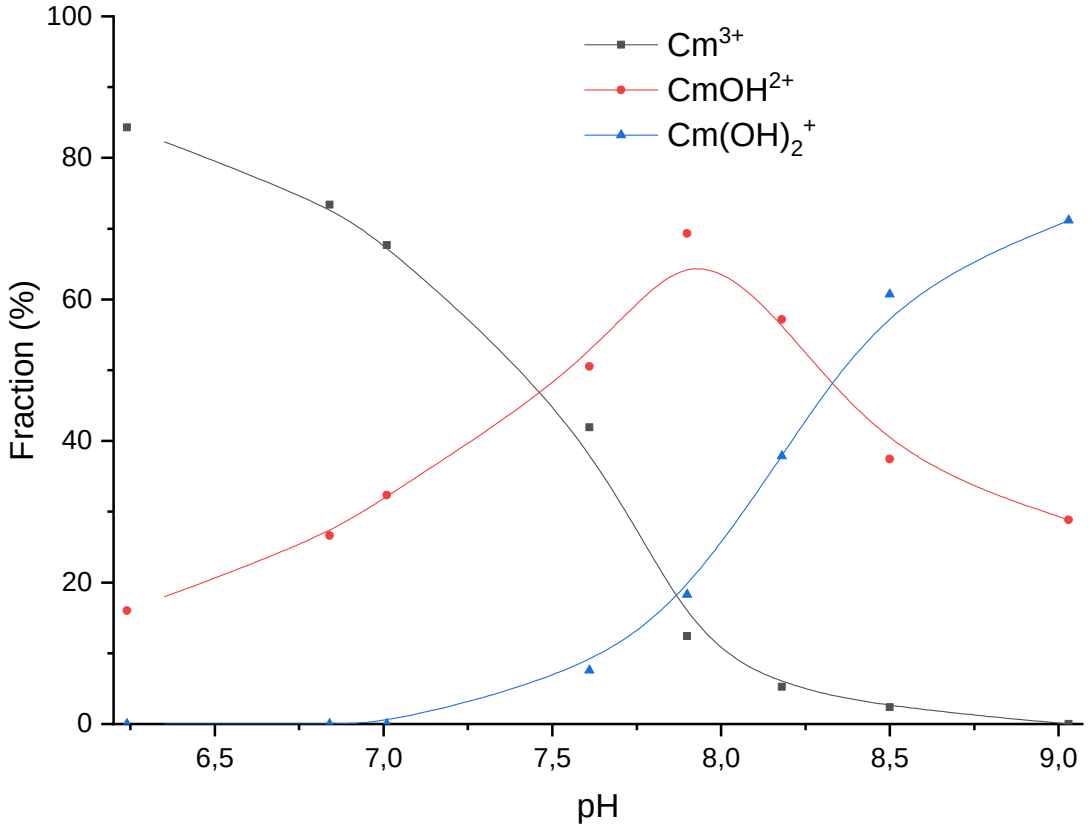

Figure 1.8. The distribution of Cm^{3+}(aq), $Cm(OH)^{2+}$, and $Cm(OH)_2^+$ as a function of pH. The lines drawn are approximations and are not the result of curve fitting. Data are from Wimmer *et al.* (1992).

As the carbonate anion is classified as a hard base and ligand (House 2013), strong complexation with curium can be expected. A curium bicarbonate complex and curium carbonate species up to the tetracarbonate $Cm(CO_3)_4^{5-}$ have been characterized (Vercouter *et al.* 2005; Wimmer, Kim *et al.* 1992). The formation of mixed hydroxo carbonates has been suggested for americium, but no evidence of mixed hydroxo carbonates of curium exists despite the relatively similar formation constants of the curium monohydroxo and monocarbonate species. (Fanghänel *et al.* 1998) It is postulated that Cm(III) might, under certain conditions, form a $Cm_2(CO_3)_3$ precipitate with carbonate, a reaction observed with Am(III) (Meinrath & Kim 1991).

Cm(III) forms relatively strong complexes with fluoride, a hard base (Aziz & Lyle 1969). As with the study of hydrolysis products of Cm(III), the study of higher fluoride complexes in

solution is made difficult by precipitation of curium as CmF_3(s), and so only CmF^{2+} has been properly characterized in aqueous solvent. The magnitude of the curium-fluoride complexation constant is dependent on the ionic strength of the solvent. (Aas *et al.* 1999) Relative to fluoride, chloride forms noticeably weaker inner sphere complexes with Cm(III). The formation of $CmCl^{2+}$ and $CmCl_2^{+}$ species has been established experimentally (Khopkar & Mathur 1980). Elevated $CaCl_2$ concentrations appear to promote the formation of the chlorido complexes. (Fanghänel *et al.* 1995) However, the formation of curium chlorido complexes becomes relevant only at high chloride concentrations due to the weakness of the chloride ion ligand (Könnecke *et al.* 1997). In addition, the formation of inner sphere chlorido complexes is suggested by a gradual drop in the hydration number when Cm(III) is in HCl solutions of above 5 molar, as the lost coordinating water molecules are suspected to be replaced by chloride ions (Kimura *et al.* 1998). Curium nitrate complexes have been characterized in nitric acid and ammonium nitrate media (Khopkar & Mathur 1980). In HNO_3 solutions the hydration number decreases as in HCl solutions, but the hydration number starts to drop immediately with the addition of HNO_3, suggesting the formation of curium nitrato complexes. Aqueous complexes between curium and sulfate are known (de Carvalho & Choppin 1967; Khopkar & Mathur 1980). Sulfato complexes of curium have been characterized up to the trisulfato complex $Cm(SO_4)_3^{3-}$ (Skerencak *et al.* 2013). However, the trisulfato complex is stable only at very high concentrations of sulfate and no evidence of the tetrasulfato species has been found. (McDowell & Coleman 1972; Paviet *et al.* 1996) The phosphate complexes $CmH_2PO_4^{2+}$ and $CmHPO_4^{+}$ are formed under acidic conditions. In addition, Cm-phosphate colloids are generated in conjunction with the formation of $CmHPO_4^{+}$. (Moll *et al.* 2011) The thiocyanate complexes $CmSCN^{2+}$ and $Cm(SCN)_2^{+}$ have been reported (Khopkar & Mathur 1974).

Complexation with organic ligands

Complexation reactions between Cm(III) and different organic ligands are of interest due to their presence in high level radioactive waste (HLW) solutions (Campbell *et al.* 1994; Toste *et al.* 1995; Toste 2001). In addition, low molecular weight organic ligands are present in geological formations that have been put forward as potential host rocks for radioactive waste disposal (Courdouan *et al.* 2007a; Courdouan *et al.* 2007b). Small organic molecules containing carboxylic acid groups act as hard ligands and should eagerly form complexes

with Cm(III). Indeed, multiple complexes of Cm(III) and carboxylic acid ligands have been characterized, such as acetate (Fröhlich *et al.* 2014; Grenthe 1963), oxalate (Thakur *et al.* 2006), and citrate (Mathur *et al.* 2007). In the case of citric acid, the alcohol group may deprotonate and partake in complexation. (Heller *et al.* 2012) Humic and fulvic acids (HA and FA, respectively), both of which are important environmental organic ligands, form complexes with Cm(III) (Buckau *et al.* 1992; Czerwinski *et al.* 1996; Kim *et al.* 1991; Moulin Valérie *et al.* 1992). These two acids and other ligands that are paramount to the behavior of curium in the environment will be discussed in more detail in the following chapter.

Water-soluble as well as water-insoluble heterocyclic N-donor ligands have been investigated with regard to their potential application in Ln/An partitioning, where they prefer complexation with actinides over lanthanides (Panak & Geist 2013). It is thought that the interactions between these ligands and 5f orbitals of actinides are more covalent in nature than the interactions with the 4f orbitals of lanthanides, and that this might account for the An selectivity of these ligands. (Hudson *et al.* 2013) Complexation of curium with hydrophilic 2,6-bis(1,2,3-triazin-3-yl)-pyridine (BTP) derivative N-donor partitioning ligands has been reported (Ruff *et al.* 2012; Trumm *et al.* 2016).

The chemistry of Cm(III) with chelating agents such as ethylenediaminetetraacetatic acid (EDTA) is of interest due to their potential and actual use in nuclear decontamination operations (Flora & Pachauri 2010; Means & Alexander 1981; Spoor 1977). The Cm(III)-EDTA system in particular has been investigated in detail and EDTA is known to form strong complexes with curium (Thakur, Conca *et al.* 2009). Based on the structures of analogous Ln-EDTA complexes, the hexadentate EDTA can be expected to chelate Cm(III) with four carboxylates and two nitrogens (Sakagami *et al.* 1999). In a binary complex, the remaining coordination sites of Cm(III) are occupied by water, resulting in a total coordination number of nine (Mathur *et al.* 2006). Chelation by EDTA appears to protect Cm(III) from hydrolysis, as hydrolysis reactions of Cm(III) in the $Cm(EDTA)^-$ complex initiate at elevated pH values relative to Cm^{3+}(aq) (Griffiths *et al.* 2013; Thakur, Conca *et al.* 2009). A similar phenomenon has been observed for iron and its EDTA complex (Milić *et al.* 1989). Multiple ternary complexes of Cm(III), EDTA, and an additional ligand have been characterized. The studied additional ligands include carbonate and many small, organic ligands known to co-exist

with EDTA and Cm(III) in nuclear waste and other solutions (Griffiths *et al.* 2013; Mathur *et al.* 2007; Thakur, Pathak *et al.* 2009; Thakur *et al.* 2006). As a testament to the Cm(III) complexation potential of EDTA, it appears to outcompete another ubiquitous chelator, nitrilotriacetatic acid (NTA), for Cm(III) binding. In a ternary complex the usually tetradentate NTA is left to bind Cm in a tridentate manner while EDTA binding to Cm is unaffected. Some of the other chelators studied with regard to Cm(III) complexation are diaminocyclohexanetetraacetatic acid (CDTA), propanoldiaminetetraacetatic acid (PDTA), (Thakur, Conca *et al.* 2009), and diethylenetriaminepentaacetatic acid (DTPA). DTPA is an especially interesting chelator as it has also been proposed as a potential decontamination therapy agent and is thought to be critical in the separation of trivalent actinides and lanthanides in the Trivalent Actinide Lanthanide Separation with Phosphorus-reagent Extraction from Aqueous Komplexes (TALSPEAK) process (Gray *et al.* 1995; Spoor 1977). (Tian *et al.* 2015)

Table 1.6. Stability constants of selected complexes formed between Cm(III) and small molecules. TRLFS = Time-resolved laser fluorescence spectroscopy, RT = Room Temperature.

Ligand	Stability constant(s) (log_{10} scale)		Conditions	Reference
OH^-	β_{11}	6,44	TRLFS, I = 0	Fanghänel *et al*. (1994)
	β_{12}	12,30		
OH^-	β_{11}	6,67	TRLFS, I = 0,1 M, T = 25 °C	Wimmer, Klenze *et al.* (1992)
	β_{12}	12,06		
CO_3^{2-}	β_{11}	7,11	TRLFS, I = 0, T = 25 °C	Fanghänel *et al*. (1999)
	β_{12}	13,00		
	β_{13}	15,20		
	β_{14}	13,00		
CO_3^{2-}	β_{11}	6,65	TRLFS, I = 0,1 M	Wimmer *et al*. (1992)
HCO_3^-	β_{11}	1,9	TRLFS, I = 1 m	Fanghänel *et al*. (1999)
F^-	β_{11}	3,16	TRLFS, I = 0	Aas *et al*. (1999)

Table 1.6. (continued)

Ligand	Stability constant(s) (log_{10} scale)		Conditions	Reference
F^-	β_{11}	3,34	Extraction, pH 3,6, *I* = 0,50	Aziz & Lyle (1969)
	β_{12}	6,18		
	β_{13}	9,08		
Cl^-	β_{11}	0,20	Extraction, *I* = 1,0	Khopkar & Mathur (1980)
	β_{12}	−0,05		
Cl^-	β_{11}	−1,70	TRLFS, *I* = 6,8 m, *T* = 25 °C	Fanghänel *et al*. (1995)
	β_{12}	−3,15		
Cl^-	β_{11}	0,23	TRLFS, *I* = 0, *T* = 25 °C	Könnecke *et al.* (1997)
	β_{12}	−0,70		
NO_3^-	β_{11}	0,3	Extraction, *I* = 1, *T* = 30 °C	Khopkar & Mathur (1980)
	β_{12}	0,1		
SO_4^{2-}	β_{11}	0,93	TRLFS, *I* = 3 m	Paviet *et al*. (1996)
	β_{12}	0,61		
SO_4^{2-}	β_{11}	1,3	Extraction, pH = 3,0, *I* = 2,0, *T* = 25 °C	de Carvalho & Choppin (1967)
	β_{12}	1,9		
SCN^-	β_{11}	0,18	Extraction, *I* = 1 M, *T* = 30 °C	Khopkar & Mathur (1974)
	β_{12}	0,61		
EDTA	β_{11}	17,86	Extraction, *I* = 0,1 M, *T* = 25 °C	Thakur *et al*. (2009)
EDTA	β_{11}	16,06	Extraction, *I* = 6,60 m, *T* = 25 °C	Cernochova *et al*. (2009)
NTA	β_{11}	10,82	Extraction, *I* = 6,60 m, *T* = 25 °C	Mathur *et al*. (2006)
DTPA	β_{11}	21,67	Fluorometry, *I* = 1,0 M, *T* = 25 °C	Tian *et al*. (2015)
Citrate	β_{11}	5,90	Extraction, *I* = 6,60 m, *T* = 25 °C	Mathur *et al*. (2007)
	β_{12}	10,30		

Table 1.6. (continued)

Ligand	Stability constant(s) (log_{10} scale)		Conditions	Reference
Citrate	β_{11}	9,3	TRLFS, I = 0, T = RT	Heller *et al*. (2012)
	β_{12}	13,2		
Oxalate	β_{11}	5,34	Extraction, I = 6,60 m, T = 25 °C	Thakur *et al*. (2006)
	β_{12}	8,61		
Humate	β_{11}	6,52	TRLFS, I = 0	Czerwinski *et al*. (1996)
Humate	β_{11}	6,22	TRLFS, I = 0,1 M	Wimmer *et al.* (1992)
Fulvate	β_{11}	5,90	TRLFS, I = 0,1 M	Buckau *et al*. (1992)

1.3.7. Curium in the geosphere

Most of the curium encountered in nature today has been generated by atmospheric detonations of nuclear weapons. In addition, spatially confined contaminations have occurred as the result of accidental or intentional discharges. The highest concentrations of environmental curium are found near discharge sites. Sources of discharge include nuclear fuel reprocessing plants, waste disposal sites and nuclear power plants. The Chernobyl incident for one is known to have contaminated hundreds of square kilometers with radionuclides, including curium. (Atwood 2010) Hundreds of kilograms of curium have been produced in nuclear reactors to date and the global inventory of curium is expected to increase hand-in-hand with the growth of the nuclear power industry (Runde & Neu 2006).

The behavior of actinides in the environment is extremely complex and multifaceted, with many different mechanisms and both physical and chemical phenomena at play. To add to the complexity, every environment is unique. Environmental parameters affecting actinide behavior include, but are not limited to, redox potential, rock and mineral composition, soil composition, the presence and flow of water, organic and inorganic ligands, and temperature. (Runde 2000) Furthermore, depending on the environmental variables, it is possible for a specific ligand to form actinide complexes of different types or phases

(Atwood 2010). Some environmental phenomena affecting actinide behavior in the environment are shown in Figure 1.9. For curium the scheme is somewhat less complex than for the earlier actinides, as curium is stable only as Cm(III) and so redox reactions are not pertinent.

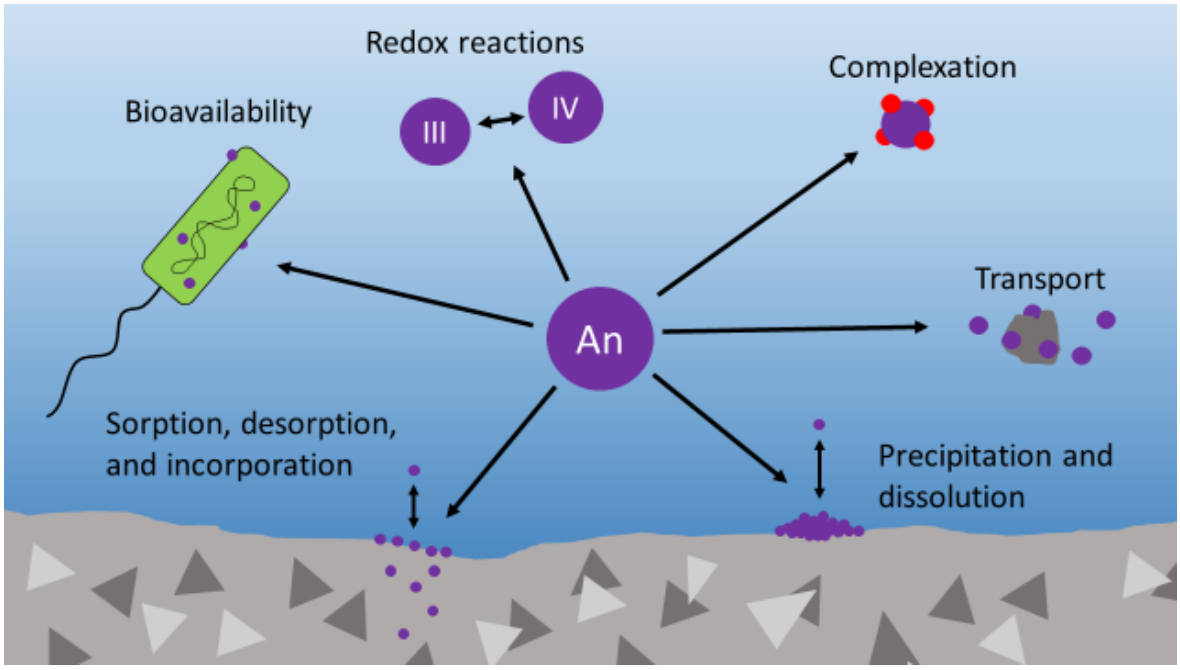

Figure 1.9. Some chemical and physical phenomena affecting the behavior of actinides in the environment. Oxidation state is one of the determinants of environmental behavior of actinides and redox reactions may take place depending on the local redox potential, resulting in behavioral changes. Complexation with organic or inorganic ligands can inhibit surface reactions with rocks and minerals and thus keep the actinide in solution. Migration through the solution phase can be facilitated by sorption onto colloids and solution species of an actinide may precipitate and form solid compounds. Sorption onto minerals, rocks and particulates is particularly important at low actinide concentrations and incorporation into the aforementioned materials may take place through diffusion or coprecipitation. Actinides can sorb onto or be taken in by microbes, both of which may affect the mobility of an actinide. Actinides taken in by a microbe may subsequently undergo redox reactions catalyzed by the cellular machinery. (Runde 2000)

As a hard Lewis acid, curium strongly adsorbs onto mineral and rock surfaces. Iron(oxy)hydroxides, clay minerals, carbonate minerals, phosphates, and oxides are thought to be the rocks and minerals chiefly responsible for curium retention. (Atwood 2010) In addition to surface adsorption, curium is known to incorporate into the bulk crystal

structure of minerals (Cavellec *et al.* 1998; Stumpf *et al.* 2006; Stumpf & Fanghänel 2002). Interactions between Cm(III) and clay minerals (Huittinen *et al.* 2010; Schnurr *et al.* 2015), silica (Chung *et al.* 1998), aluminum hydroxides and oxides (Huittinen *et al.* 2009; Stumpf *et al.* 2001; Thomas *et al.* 2009), feldspar (Silvia *et al.* 2009), phosphate minerals (Cavellec *et al.* 1998), and calcite (Stumpf *et al.* 2006; Stumpf & Fanghänel 2002), among other substances, have been confirmed in direct experiments.

Experimental solubilities of curium in natural ground waters are in the nano to picomolar range, depending on the composition of the ground water (Bruno *et al.* 1997). Unsurprisingly then, the concentration of aqueous curium in natural aquifers is usually low (Atwood 2010). In the absence of other ligands the behavior of trivalent actinides, including curium, in aqueous environments is mostly governed by hydroxide and carbonate ions, the most relevant environmental ligands (Runde 2000). The speciation of curium in natural ground waters has been probed by direct experiments, where curium has been added to ground water samples. In a study where ground waters from Gorleben, Germany were used, the speciation of curium is dominated by carbonate and humic acid species with a small fraction of free aquo ion present. In water samples with high organic content, only the CmHA species could be seen. No hydrolysis species were observed under any of the tested conditions. (Wimmer, Kim *et al.* 1992) Another study in which ground water samples from the same area were used suggested that ternary complexes of carbonate or hydroxide, humic acid, and curium are formed, specifically in the form of monohydroxo or monocarbonato humate complexes. Between the carbonate and the hydroxide ions, the former appears to form the more stable ternary complexes, and so the speciation is dominated by $Cm(CO_3)HA$. (Panak *et al.* 1996) A comparative study found no major differences in curium complexation between humic acids derived from dissimilar sources (Shin *et al.* 1995). Therefore, it is reasonable to assume that the results discussed above may apply in ground waters other than those used in the experiments. The transport of curium in aqueous solutions is thought to be facilitated in part by adsorption onto colloids or other mobile bodies (Atwood 2010). Another factor capable of affecting the mobility and solid-water distribution of curium in natural aquifers is the adsorption of humic and fulvic acids onto minerals, which creates scaffolds for the formation of ternary curium-HA/FA-mineral complexes (Takahashi *et al.* 2002; Wang *et al.* 2009).

Microbial activity may influence the behavior of actinides directly and/or indirectly. Direct mechanisms include uptake and enzymatic reduction or oxidation by microbes, or sorption onto microbial cell surface layers. Indirect mechanisms involve microbial secretion of acids, strongly complexing ligands, and reactive intermediate compounds that go on to oxidize or reduce actinides. (Bruynesteyn 1989; Francis 1998; Francis *et al.* 1998; J. R. Lloyd *et al.* 2002) Sorption of Cm(III) onto cellular surfaces of microbes and algae have been reported. In one study, curium was found to associate with the cell envelope of a gram-negative, sulfate-reducing bacterium, *Desulfovibrio äspöensis* strain DSM 10631^{T}, in a pH-dependent manner. However, no uptake of curium by the cells was observed. (Moll *et al.* 2004) Curium was found to sorb onto the alga *Chlorella vulgaris* and the interaction site was inferred to reside within the cellulose layer of the algal cell wall (Ozaki *et al.* 2003). In another study the interaction of curium with different archae, algae and both gram-positive and gram-negative bacteria under acidic conditions was investigated. Curium sorbs onto every tested organism with no evidence of cellular uptake. Sorption was again determined to be pH-dependent, with pH affecting both the distribution coefficient and the kinetics of sorption. Curiously, desorption of curium from some algae and archae was observed over time. These incidents were attributed to the production of exudates that contained high affinity ligands by the organisms. (Takuo *et al.* 2009) Indeed, compounds secreted by microbes have been found to complex curium in direct experiments in which pyoverdin and hydroxamate class bacterial siderophores were seen to form highly stable complexes with curium (Moll, Glorius *et al.* 2008; Moll, Johnsson *et al.* 2008).

Most environmental curium resides in soils and sediments (Atwood 2010). Migration of surface-deposited curium through soil layers is thought to be slow, as indicated by soil core sample analyses of curium fallout from Chernobyl (Mboulou *et al.* 1998). One possible route for curium to enter humans is through digestion of contaminated vegetation. Therefore, any information on curium uptake by agricultural crops and other plants is of interest. In most cases, the uptake of transuranium elements by the roots of plants is thought to be low, and lower plants are expected to accumulate significantly more radionuclides than higher plants (Ben-Bolie *et al.* 2014). An early study compared the uptake of Np, Pu, Am, and Cm by weeds, cereals, and legumes in a setting that simulated a natural environment. The concentration ratios, the quotient of radionuclide concentration

in the plant divided by radionuclide concentration in soil, were estimated to be 0,4 for Np, 0,002 for Am and Cm, and 0,0001 for Pu. Interestingly, radionuclide concentrations in seeds and peas were significantly lower than in other parts of the plant. (Schreckhise & Cline 1980)

1.3.8. Curium in man

The protection of workers handling radioactive material is naturally of paramount importance, and the establishment of maximum allowed intake limits for every individual radionuclide is the basis of biological actinide research (Stone 1951). To this end, the *in vivo* behavior of many different radionuclides has been studied in multiple model organisms for different timescales. The effect of intake route has likewise been studied. For radiation protection purposes the data on biokinetics and toxicology are particularly interesting and important. (Durbin 2006)

For obvious reasons the behavior of curium in the human body has not been a subject of systematic study. Instead, the *in vivo* distribution and retention of trivalent curium has been studied in rodents, canines, and primates. In a study in which rats were exposed to Cm(III), most of the curium that was injected was seen to rapidly migrate to the liver and skeleton (Table 1.7). The liver fraction, however, decreased over time. At the end of the 256 day observation period, while about three quarters of the administered curium had been excreted by the animal, the vast majority of the curium retained in the tissues was in the bone fraction. Interestingly, no uptake of curium introduced via a stomach tube was observed, suggesting that curium is not taken up by the gastrointestinal tract (Scott *et al.* 1949) In a canine study, the liver and the skeleton were again seen to be the primary targets of intravenously administered curium (Table 1.8). Interestingly, the retention of curium by the liver was seen to be much greater in the dogs compared to the rats, while the rate of excretion was slower. (R. D. Lloyd *et al.* 1974) In another canine study in which curium was administered via inhalation the curium was seen to migrate from the lungs to the skeleton and the liver in a matter of days, and these fractions then remained constant for the full 256 day duration of the study. (McClellan *et al.* 1972)

Table 1.7. Recovery- and absorption-corrected distribution of intramuscularly delivered curium in rodents at 1, 4, 16, 64, and 256 days post-injection. Values represent the average of measurements from three rats. Calculated from values presented in Scott *et al*. (1949).

		Days post-injection				
		1	4	16	64	256
% of injected dose retained in tissues	Liver	59,6	40,2	20,9	2,8	1,1
	Bone	25,1	29,4	29,7	27,2	21,9
	Skin	1,9	1,4	1,1	0,4	0,1
	Muscle	2,2	1,3	1,9	1,2	0,5
	Other	6,6	7,7	3,2	1,4	0,8
	Total	95,4	80,0	56,8	33,0	24,4
% of injected dose excreted	Urine	1,7	1,3	5,9	1,7	6,0
	Feces	2,9	18,7	37,3	65,3	69,6
	Total	4,6	20,0	43,2	67,0	75,6

Table 1.8. Distribution of intravenously delivered curium in canines at 6, 13, and 20 days post-injection. Each time point represents a single dog. Calculated from values presented in Lloyd *et al*. (1974).

		Days post-injection		
		6	13	20
% of injected dose retained in tissues	Liver	39,4	34,5	34,4
	Skeleton	36,5	44,7	42,7
	Pelt	2,1	2,2	1,5
	Muscle	2,3	2,4	1,8
	Other	9,0	6,7	6,6
	Total	89,3	90,5	87,0
% of injected dose excreted	Urine	8,6	6,6	11,0
	Feces	2,1	2,9	2,0
	Total	10,7	9,5	13,0

A study in which primates were injected with curium supports the canine and rodent study results in that the liver and the skeleton are the primary tissues of curium deposition in mammals. The elimination of curium from the primate skeleton was seen to be slow, with a half-life of several years, while the half-life of curium in the liver was on the order of 40 days. In addition, rapid clearance of injected curium from the blood fraction was reported. (Lo Sasso *et al.* 1981) This is in good agreement with the curium plasma clearance rate reported for rats (Turner & Taylor 1968).

While *in vivo* curium distribution data from humans may be lacking, the interaction of curium with many isolated components of the human and other mammalian bodies as well as with the constituents of different body fluids has been studied. Among small biomolecules, the nucleotide adenosine triphosphate (ATP) and amino acids threonine and phoshothreonine have been shown to complex curium (Moll *et al.* 2005; Moll & Bernhard 2007). In natural urine samples, curium is found to complex with citrate present in urine if the pH is slightly acidic. In near-neutral pH urine, however, another ternary complex of yet unknown composition is thought to be present. (Heller *et al.* 2011) A ternary complex between curium, carbonate, and phosphate dominate the speciation of curium in saliva. The excess negative charge of the complex is thought to be balanced out by calcium. A significant portion of curium not accounted for by the aforementioned ternary complex in saliva is bound to the digestive enzyme α-amylase (Amy). (Barkleit *et al.* 2017) The interaction between curium and α-amylase in the absence of other interfering ligands has been reported and it is suggested that Cm(III) interacts with Amy at the carboxyl groups of glutamate and aspartate residues. It has been proposed that two complexes are formed with Cm(III):α-amylase stoichiometries 1:1 and 1:3. (Barkleit *et al.* 2016)

Blood, an extracellular fluid, consists of cells and the aqueous liquid in which the cells are suspended. The liquid component is commonly referred to as plasma. (Reddi 2014) Blood serum, on the other hand, is blood plasma with fibrinogen and other clotting-related factors removed (Harris & Winter 2012). The main components of blood plasma are presented in Table 1.9. As in any near-neutral aqueous medium containing organic and inorganic ligands, the behavior of curium in blood is expected to be a balancing act between hydrolysis and complexation. The vast majority of curium in blood is thought to be

associated with the plasma and not the cellular components of blood. (Taylor 1998) Citrate, present in plasma at 135 µM concentration (Mycielska *et al.* 2009), is thought to be the only plasma ligand capable of outcompeting hydrolysis in the case of curium (Durbin 2006).

Table 1.9. The mean, normal plasma concentrations of main blood plasma constituents. Values are from Reddi (2014).

Constituent	Normal plasma concentration (mM)
Na^+	142
K^+	4
Ca^{2+}	2,5
Cl^-	104
HCO_3^-	25
HPO_4^{2-} and $H_2PO_4^-$	1,3
Organic acids	5,5
Proteins	0,9

In addition to the relatively small organic and inorganic molecules, proteins are available in plasma for curium complexation. Indeed, experiments with rats have indicated that the majority of intravenous curium is protein-bound and that the uptake of intravenous curium by plasma proteins is rapid. Globulins, a protein fraction accounting for about 42 % of the total plasma protein mass (Domino *et al.* 1975), appear to be the favored protein complexation partners of curium in plasma. (Turner & Taylor 1968)

Of the globulins, serum transferrin (TF) is of particular interest with regard to curium and actinide complexation in general. Transferrin is a 79,6 kDa (Sun *et al.* 1999), 679 residue glycoprotein that structurally consists of two lobes linked together by a short peptide (Wally *et al.* 2006). The structure of human serum transferrin is depicted in Figure 1.10.

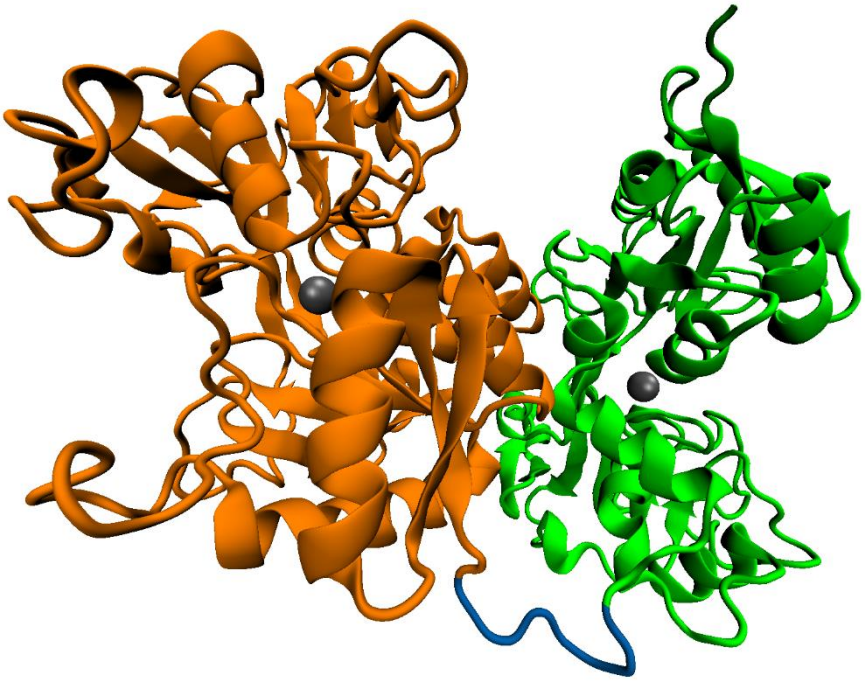

Figure 1.10. The structure of human transferrin. The N-terminal lobe is shown in green, the linker peptide in blue, and the C-terminal lobe in orange. Two Fe(III) ions are resolved in the structure and are shown here as grey spheres, one in each lobe. Rendered from Protein Data Bank (PDB) ID 3QYT.

The physiological function of TF is the facilitation of iron transport, which it accomplishes by binding a single Fe(III) ion at each of the two lobes. The iron ions are then internalized into cells through a transferrin receptor (TFR) mediated mechanism. (Sun *et al.* 1999) As transferrin is capable of internalizing trivalent iron from the blood stream into cells, it is relevant to question whether TF might play a part in internalization of Cm(III) as well. What is known is that curium appears to interact with TF. Direct laser spectroscopic experiments show Cm(III) interacting with both the full-length TF and a recombinant construct comprised of only the N-terminal lobe of TF. Binding is thought to take place at the Fe(III) binding sites of both lobes and at a yet unspecified, additional binding site. (Bauer *et al.* 2014; Bauer *et al.* 2015) *In vitro* interaction between curium-loaded TF and TFR has been reported (Sturzbecher-Hoehne *et al.* 2013), but results showing cellular uptake of curium through the TF-TFR mechanism are yet to be published.

1.4. Human serum albumin

Human serum albumin (HSA) is a monomeric protein of 585 amino acids with a molecular mass of about 66,5 kDa found mainly in blood plasma. HSA is expressed in the liver and from there it is introduced into the blood stream. It leaves the intravascular space by either passing through the walls of fenestrated or sinusoidal capillaries or via a receptor-mediated mechanism. Numerous putative albumin receptors have been identified (Merlot *et al.* 2014). With a plasma concentration level of circa 600 µM, it is the most ubiquitous plasma protein. It is of vital importance in maintaining the colloid osmotic pressure of plasma and the central contributor to the vascular Gibbs-Donnan effect. (Kragh-Hansen 2016) It can carry an astonishing number of different exogenous and endogenous ligands and act as a depot for ligand molecules. It is known to affect the pharmacokinetics and pharmacodynamics of drugs. (Mauro *et al.* 2008; Yamasaki *et al.* 2013) The ligand binding scheme of HSA is very complex and is modulated by pH and allosterically by fatty acids and drug molecules (Birkett *et al.* 1977; Gabriella *et al.* 2007; Solomon *et al.* 1968; Wilting *et al.* 1980a; Wilting *et al.* 1980b). Due to its many titratable acidic and basic amino acid residues it is very soluble in aqueous media and may act as a buffering agent in blood (Kragh-Hansen 2016). In addition, HSA is known to possess catalytic and antioxidant properties (Anraku *et al.* 2013; Kragh-Hansen 2013; Marjolaine *et al.* 2008). Furthermore, HSA is a highly useful disease biomarker (Fanali, di Masi *et al.* 2012).

1.4.1. The structure of human serum albumin

Structurally, HSA is comprised of three homologous domains (I-III) that form a heart-shaped assembly (Figure 1.11). Each of the three domains is further comprised of two helical subdomains (A and B) that share common structural motifs and are connected by a random coil. (He & Carter 1992; Mauro *et al.* 2008; Sugio *et al.* 1999) HSA is about 67 % α-helical and contains no β-sheets (Kragh-Hansen 2016). The three dimensional conformation is held together by a total of 17 disulfide bridges (Markus & Karush 1957). In fact, HSA has but a single free sulfhydryl group located at position Cys37 (Sugio *et al.* 1999). A lone tryptophan residue is located at position 214 (Dugaiczyk *et al.* 1982). The structural conformation of HSA undergoes transitions with changing pH. At pH values under 2,7, an extended (E) conformation is adopted. From pH 2,7 up to 4,3, a fast-migrating (F) form is the dominant conformation. A neutral (N) conformation is assumed at pH range 4,3 to 8,0.

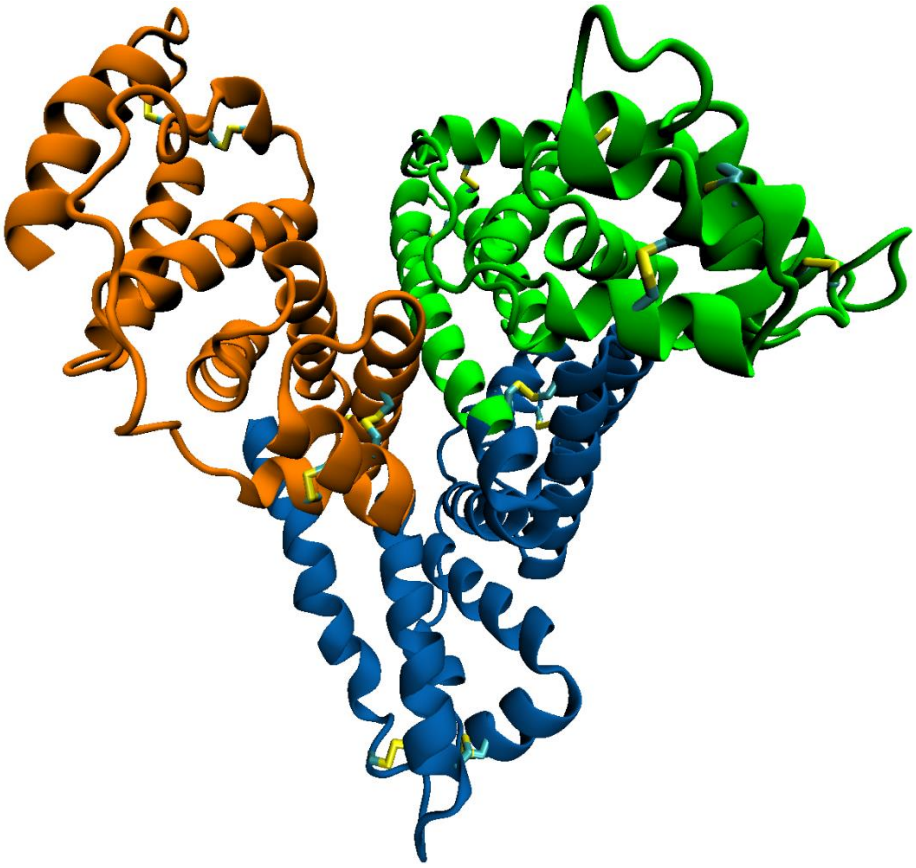

Figure 1.11. The structure of human serum albumin. Domains I, II and III are shown in green, blue and orange, respectively. Cysteine residue sidechains are drawn as stick models in which carbon atoms are shown in cyan and sulfur atoms in yellow. Rendered from PDB ID 1AO6.

And finally, above pH 8,0, HSA adopts a basic (B) conformation. (Fanali, di Masi *et al.* 2012) The N-B transition is thought to arise from the changes in protonation states of histidine residues (Bos *et al.* 1989). The overall structure of HSA in neutral and basic conformations is nevertheless similar (Handing *et al.* 2016).

1.4.2. Fatty acid binding properties of HSA

HSA is known to possess the binding capacity for up to seven long-chain fatty acid molecules at locations shown in Figure 1.12 (Mauro *et al.* 2008). One of the sites resides in sub-domain IB, one in a cleft between IA and IIA, two in IIIA, and one in IIIB (Curry *et al.* 1998). A sixth site is located at the interface between sub-domains IIA and IIB, and the seventh binding site is located in subdomain IIA, homologous to but smaller than the one found in IIIA. Most of the sites have a basic amino acid residue in place to interact with the carboxylate group of the fatty acid. All of the seven sites are known to bind, at minimum,

saturated fatty acids ranging in length from C10:0 to C18:0. Some sites are capable of accommodating multiple medium chain length (C10:0) fatty acids. In addition, two medium-chain binding sites are located at the crevice between domains II and III. Binding of fatty acids brings about a change in the overall conformation of HSA, with domains I and III deviating significantly from their relative positions in defatted HSA (Bhattacharya *et al.* 2000) The chain length of a fatty acid affects its HSA binding properties: longer chain fatty acids seem to have higher affinity towards HSA, possibly explained by the importance of hydrophobic effects in HSA-fatty acid interactions (Kragh-Hansen *et al.* 2006). The interactions between fatty acids and HSA are important and of interest, as they are known to modulate, among other things, the metal (Lu *et al.* 2012; Stewart *et al.* 2003), drug (Petitpas *et al.* 2001; Sudlow *et al.* 1976; Yamasaki *et al.* 2017), and heme binding properties of HSA (Fanali *et al.* 2005).

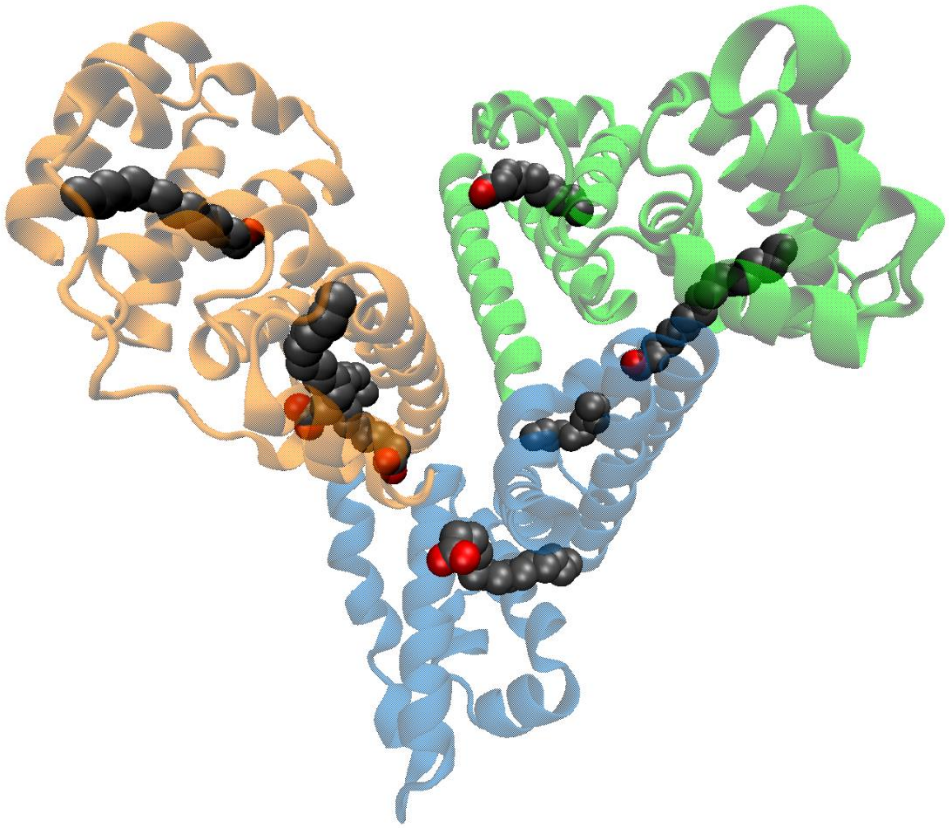

Figure 1.12. The structure of HSA with seven palmitate molecules (C16:0) bound at the seven principal long-to-medium length fatty acid binding sites. Color scheme for HSA is the same as in Figure 1.11. The structure of HSA is shown as a transparent model for clarity. Palmitates are shown as space-filling models in which dark grey spheres represent carbons and red represent oxygen. Rendered from PDB ID 1E7H.

1.4.3. Drug binding properties of HSA

Although other drug binding sites exist on HSA, two are of major importance: the so-called Sites I and II (Sudlow *et al.* 1975). Indeed, some of the other, minor sites may act as secondary binding sites for drug molecules that preferably bind at the two major sites. Structurally, the sites are preformed hydrophobic cavities with specific areas densely packed with polar residues (Ghuman *et al.* 2005). Site I resides in subdomain IIA, whereas Site II can be found in subdomain IIIA (He & Carter 1992; Mauro *et al.* 2008). Site I is composed of multiple subsites, each capable of binding their own, unique ligands with high affinity (Yamasaki *et al.* 1996). Warfarin, phenylbutazone, and iodipamide are examples of Site I binding drugs (Yamasaki *et al.* 1996). Site II shares some structural similarities with Site I, but is smaller, with only a single sub-compartment. In addition, whereas site I has two areas of polar residues, site II appears to have only one. (Ghuman *et al.* 2005) Examples of Site II binding drugs include benzodiazepines and ibuprofen (Maruyama *et al.* 1985; Sudlow *et al.* 1976).

1.4.4. Metal ion binding properties of HSA

Most mammalian albumins have four principal metal binding sites and HSA is no exception in this regard. The sites are structurally distinct and have unique metal ion specificity profiles. The four metal binding sites are the N-Terminal Site (NTS), the cysteine residue at position 34, the Multi-Metal Binding Site (MBS), and the so-called Site B. (Bal *et al.* 2013)

The N-Terminal Site

The N-Terminal Site is the primary binding site for Cu(II) and Ni(II) on HSA and is an Amino-Terminal Copper and Nickel (ATCUN) binding motif (Fanali, di Masi *et al.* 2012; Harford & Sarkar 1997; Laussac & Sarker 1984). The site is not resolved in crystal structures of intact HSA and is thought to be unstructured in nature (Handing *et al.* 2016; He & Carter 1992). This has led to a situation where much of the work on the geometry and conformation of the site is based on model peptide and HSA fragment studies (Bal *et al.* 2013). Both Cu(II) and Ni(II) form square-planar complexes with the first three N-terminal residues of HSA: Aspartic acid, alanine and histidine. Structural studies on mimetic peptides complexed with Cu(II) indicate the presence of an apically coordinated water molecule (Christelle *et al.* 2011). Co(II) is known to bind at the same site, although in a distorted octahedral geometry

(Mothes & Faller 2007). Co(II), however, also binds at two additional sites in HSA and of the three sites, NTS has the lowest affinity towards Co(II) (Sokołowska *et al.* 2009). The site also binds V(IV)O (Correia *et al.* 2012). Specifically, the chemical entities involved in the complexation are the N-terminal primary amine Nα of Asp1, the deprotonated peptide bond Nα amides of Ala2 and His3, and the Nπ of His3 sidechain imidazole (Sadler *et al.* 1994) Axial coordination of metal centers complexed at NTS by the carboxyl group located in the sidechain of Asp1 has been suggested by some (Laussac & Sarker 1984), but disputed by others (Valko *et al.* 1999). Both Cu(II) and Ni(II), however, bind to an NTS mimetic peptide of sequence Gly-Gly-His (Zhang *et al.* 2000), indicating that the Asp1 sidechain is not essential for binding. An imidazole sidechain at position 3 is thought to be paramount for specific binding of Cu(II) and Ni(II) (Ramasubbu *et al.* 2005). This argument is backed by reports that both dog (DSA) and chicken serum albumins (CSA) that lack a histidine at position 3 are incapable of specific Cu(II) or Ni(II) binding at the NTS (Appleton & Sarkar 1971; Dixon & Sarkar 1974; Predki *et al.* 1992). Others, however, have claimed that DSA, in which His3 is substituted with tyrosine, is capable of specific Cu(II) high affinity binding at the N-terminus, and that the chelating role of the His3 imidazole group may be overtaken by non-nitrogenous residues from the main body of the protein (Masuoka & Saltman 1994; Valko *et al.* 1999). The indirect, structural involvement of the lysine residue at position 4 in the complex formation has been postulated (Sadler *et al.* 1994), though it is doubtful to be essential, as tripeptides lacking a Lys4 are capable of binding Co(II), Ni(II), and Cu(II) (Bar-Or *et al.* 2001; Valko *et al.* 1999). A schematic structure of the HSA NTS is shown in Figure 1.13 and selected metal-specific binding constants for the NTS under physiological-like conditions are listed in Table 1.10.

Cys34

The only free-thiol cysteine residue in HSA is found at position 34. The residue is located in a turn between two helices and is partially inaccessible to solvent (He & Carter 1992). The reactivity of Cys34 is controlled by spatially nearby amino acids and structural features of HSA. The pK_a of the thiol is suggested to be around 8 (Bonanata *et al.* 2017; Ottavia *et al.* 2011; Stewart *et al.* 2005). About one fourth of serum albumin in healthy male adults is modified at Cys34, likely conjugated to other thiols like cysteine and glutathione or oxidized to higher sulfur oxidation products (Hayashi *et al.* 2000), and do not, therefore, contain a

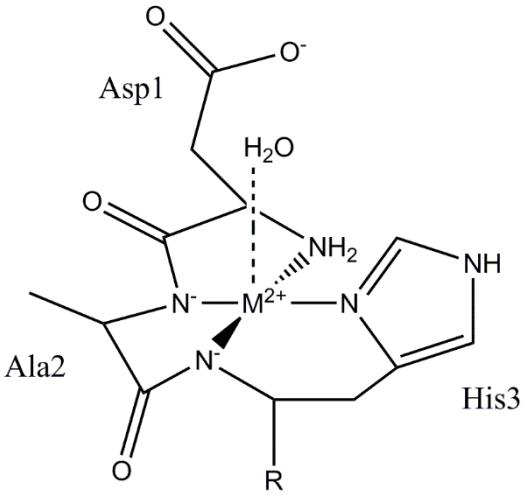

Figure 1.13. A schematic representation of the HSA NTS in complex with a divalent metal cation. The first three amino acids of HSA are shown.

Table 1.10. Reported metal binding constants for NTS under physiological-like conditions.

Metal	log *K*	Reference
Cu(II)	12	Rózga *et al*. (2007)
Ni(II)	6,8	Sokołowska *et al*. (2002)
Co(II)	3,6	Sokołowska *et al*. (2009)
V(IV)O	9,1	Correia *et al*. (2012)

free thiol (Masaru *et al.* 1985). Other Cys34 modifications include, for example, S-nitrosylation (Stamler *et al.* 1992). The residue is thought to be the primary binding site of some Au(I) complexes and possibly a secondary binding site for Pt(II) from the platinum-based drug, cisplatin (Ivanov *et al.* 1998; Shaw 1989). The binding of Ag(I) has been postulated based on the presence of vibration bands corresponding to Ag-S bond formation in Raman spectroscopy (Shen *et al.* 2003). Given the high reactivity of mercury towards biological thiols (Vallee & Ulmer 1972), it is perhaps not surprising that Cys34 has been put forward as the primary binding site of Hg(II) on HSA (Li *et al.* 2007).

The Multi-metal Binding Site

The MBS is the main binding site for Zn(II) residing between domains I and II. The structure of the MBS with a bound zinc ion is shown in Figure 1.14. Divalent zinc is bound to the site in a tetrahedral fashion. The primary complexing ligands at the site are the sidechains of His67, His247, Asp249, and a solvent water molecule. In addition, Asn99 sidechain amide involvement in Zn(II) complexation was previously suggested (Stewart *et al.* 2003), but crystal structure analysis of the ZnHSA complex appears to rule out direct involvement of the residue. (Handing *et al.* 2016) The complexing water molecule is thought to be replaceable by a chloride ion at sufficiently high chloride concentrations (Stewart *et al.* 2003) The site was originally identified in ^{113}Cd NMR studies and referred to as Site A (Sadler & Viles 1996). It was discovered that Cd(II) shares the binding site with Zn(II), as zinc appears to displace cadmium from the site (Stewart *et al.* 2003). Besides Zn(II) and Cd(II), the site has been reported to bind Cu(II), Ni(II), Mn(II), and V(IV)O (Bal *et al.* 1998; Correia *et al.* 2012; Fanali, Cao *et al.* 2012). Of the three Co(II) binding sites on HSA, the MBS has

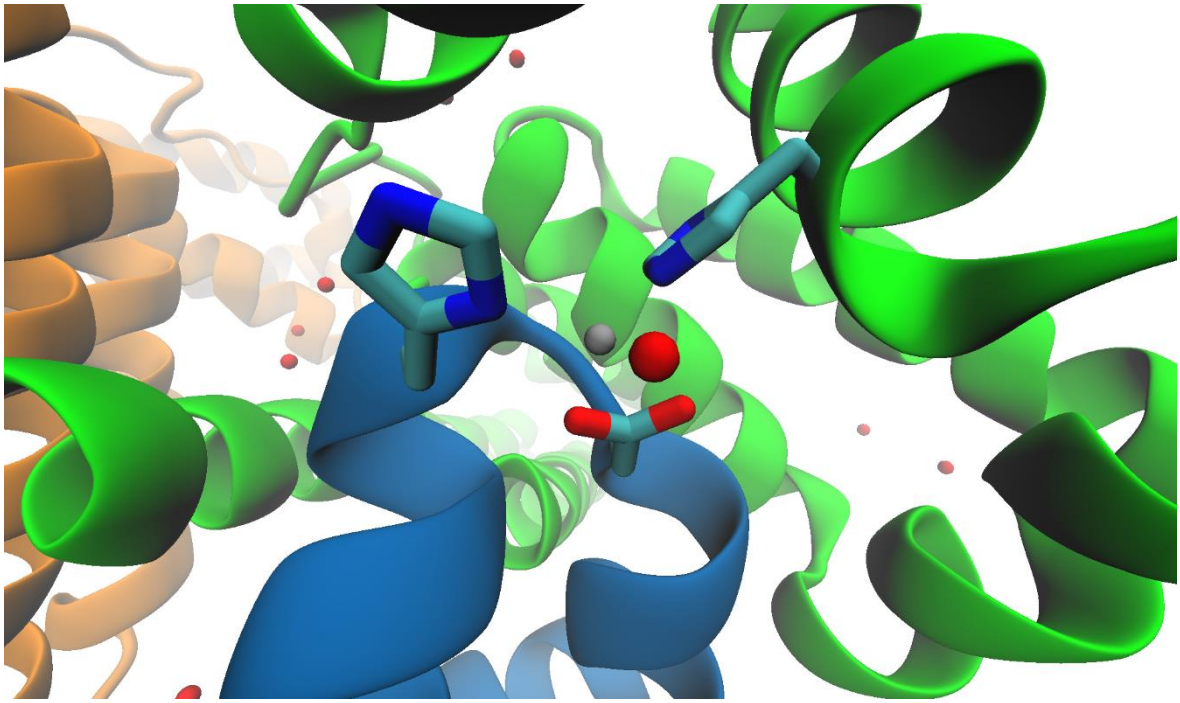

Figure 1.14. The structure of the Multi-metal Binding Site. Color scheme for HSA is the same as in Figure 1.11. The sidechains of His67, His247 and Asp249 are drawn as stick models in which carbon is cyan, nitrogen is blue, and oxygen is red. The tetragonally coordinated Zn^{2+} ion and the oxygen atoms of resolved water molecules are drawn as gray and red space-filling spheres, respectively. Rendered from PDB ID 5IJF.

the second highest affinity towards the metal (Sokołowska *et al.* 2009). Metal binding at the MBS appears to be allosterically modulated by fatty acids, as the complexation behavior of both Zn(II) and Cd(II) has been shown to be affected by the presence of fatty acids (Kassaar *et al.* 2015; Sadler & Viles 1996). Selected metal-specific binding constants for the MBS under physiological-like conditions are listed in Table 1.11.

Table 1.11. Reported metal binding constants for MBS under physiological-like conditions. Cu(II) log *K* is for a ternary complex with buffer components.

Metal	log *K*	Reference
Cu(II)	8,0	Sokołowska *et al*. (2010)
Ni(II)	4,9	Sokołowska *et al*. (2002)
Co(II)	4,0	Sokołowska *et al*. (2009)
Zn(II)	7,0	Giroux & Henkin (1972)

Site B

Akin to the MBS, site B was first identified in ^{113}Cd NMR experiments as another HSA site capable of binding Cd(II). While the location of site B on HSA and the exact nature of the complexing ligands are unclear, based on the chemical shifts it has been postulated that the site is rich in oxygen-containing ligands, likely Asp and Glu residues, and that it contains most a single nitrogenous ligand. (Sadler & Viles 1996) Site B is purportedly the highest affinity binding site of Co(II) in HSA with a log *K* of 5,0 at 298 K (Sokołowska *et al.* 2009).

Binding of actinides by HSA

Interactions between HSA and multiple different actinides and lanthanides have been reported and some of the available binding constants are summarized in Table 1.12. Binding of U(VI) by HSA has been described in many published articles (Ali *et al.* 2016; Michon *et al.* 2010; Montavon *et al.* 2009), though the site or sites of interaction are unknown. NTS may serve as a U(VI) interaction site, as an NTS mimetic DAHK peptide, representing the first four amino acid residues of HSA, forms ternary complexes with uranyl and carbonate (Huang *et al.* 2005). However, the HSA analogue bovine serum albumin

(BSA), with an N-terminal sequence of DTHK, appears to not bind U(VI) at the NTS. Instead, U(VI) seems to bind BSA at two non-equivalent binding sites and is displaced by Zn(II) and Ni(II) ions. (Duff & Kumar 2006) Contrary to the two reported binding sites on BSA, the reported stoichiometries for U(VI)-HSA interaction range from 1:1 to 5:1 (Ali *et al.* 2016; Michon *et al.* 2010).

Table 1.12. Reported An-HSA and Ln-HSA binding constants.

Metal	log *K*	Method	Conditions	Reference
U(VI)	4,3	Fluorescence quenching	*T* = 298 K, pH 7,4	Ali *et al*. (2016)
U(VI)	K_1 6,1 K_2 4,8	Fluorescence quenching	*T* = 295 K, pH 7,4	Michon *et al*. (2010)
U(VI)	10,8	Competition titration	*I* = 0, *T* = 296 K, pH 7,4	Montavon *et al*. (2009)
Th(IV)	4,1	Fluorescence quenching	*T* = 298 K, pH 7,4	Ali *et al*. (2016)
Eu(III)	6,4	Equilibrium dialysis	*I* = 0,15, *T* = 310 K, pH 7,4	Schomäcker *et al*. (1988)

Quantitative binding information for An-HSA interactions other than U(VI)-HSA is sparse. Among tetravalent actinides, both plutonium and thorium reportedly bind to HSA. In serum, despite the noticeably higher concentration, HSA is outcompeted by transferrin for Pu(IV) binding, and studies with isolated proteins suggest only very limited Pu(IV) association with HSA (Chipperfield & Taylor 1968; Stover *et al.* 1968), suggesting that the binding affinity is low. The interaction between Th(IV) and HSA appears to result in a drastic alteration of HSA secondary structure when Th(IV) is present in excess of HSA. Th(IV) seems to have affinity towards the less structured regions of HSA, as the number of Th(IV) in interaction with HSA increases in tandem with increasing Th(IV) concentration and thus increasing degree of structural change. (Ali *et al.* 2016) Of the trivalent actinides, association of Am(III) with HSA has been suggested based on the overlapping elution

profiles of Am(III) and HSA after human serum spiked with Am(III) was subjected to gel filtration (Boocock & Popplewell 1966). Binding of the trivalent actinide analog Eu(III) by HSA has been reported and characterized (Schomäcker *et al.* 1988).

2. Experimental

2.1. Aims of the study

Actinides are known to be hazardous to human health due to their metallotoxic and radioactive nature (Nesmerak 2013). Internal decontamination by actinides may occur should an unprotected person inhale, ingest, or be wounded by radioactive material. Wounds, cuts, and burns can allow actinides to bypass the epithelial barrier and enter the circulatory system. (Kumar *et al*. 2010) Most blood-borne actinides are transported in the plasma fraction of blood (Taylor 1998). The high concentration of human serum albumin (HSA) in blood plasma makes it tempting to speculate that it might act as a complexation partner for actinides in blood. In spite of this potential, the interaction of HSA with trivalent actinides has so far been studied only superficially at a qualitative level.

Internal decontamination therapies aim to both reduce the absorption of radionuclides and to enhance their elimination via excretion mechanisms. The distribution of a radionuclide in the body is dependent on the physical and chemical properties of the radionuclide, and these properties therefore dictate the type of decontamination therapy to be used. For actinides, the chelating agent diethylenetriaminepentaacetatic acid (DTPA) is used to enhance the rate of excretion. (Domínguez-Gadea & Cerezo 2011)

The aim of the present study was to identify and characterize the interaction between human serum albumin and trivalent curium in an effort to produce results that are relevant to the development of internal radionuclide decontamination therapies. Cm(III) was selected to represent the trivalent actinides due to its excellent optical properties (Edelstein *et al.* 2006). Time-resolved laser fluorescence spectroscopy (TRLFS) was primarily used to study the Cm-HSA system. TRLFS is a very sensitive spectroscopic method that allows both the investigation of Cm(III) fluorescence at trace level concentrations and the acquisition of speciation information (Beitz 1991; Collins *et al.* 2011). To address the premise of the study, determination of the speciation behavior of Cm(III) in the presence of HSA at room and physiological temperature was deemed paramount. Other parameters of interest were determined to be the stability constant of the complex and the kinetics and thermodynamics of the complexation reaction. The fluorescence lifetime of Cm(III) can

also reveal interesting information regarding the chemical environment of the ion and was therefore investigated. In addition, efforts were made to identify the Cm-HSA interaction locus using both TRLFS and nuclear magnetic resonance (NMR) techniques. As Cm(III) is not a feasible option for NMR studies where high metal concentrations are required, the trivalent actinide analogue Eu(III) was used instead. The complexation of Eu(III) in the Eu-HSA system was also determined using TRLFS.

2.2. Materials and methods

Unless stated otherwise, all chemicals were purchased from Merck or Sigma-Aldrich and used as received. The solutions used were prepared with ultrapure water as the solvent (Millipore, 18,2 MΩ cm). All data analysis was performed using the OriginPro software suite.

2.2.1. Purification of HSA

All protein that was used in experiments was subjected to a gel filtration prior to use. The gel filtration was performed using a glass column packed with Sephadex G-25 column material (GE Healthcare). TRIS buffer (10 mM TRIS, 150 mM NaCl) was used to equilibrate the column and the protein was dissolved in it before introduction into the column. Elution fractions containing the protein were identified by running TLC. The plates were dipped in a $KMnO_4$ solution and protein-containing fractions identified from the yellowish spots seen at the site of sample application. The fractions were pooled and concentrated using an Amicon Centrifugal Filter Unit (30 kDa MWCO). The concentrated protein was then clarified by 15 minute centrifugation at maximum rpm in a benchtop centrifuge. The protein concentration was determined by measuring absorbance at 280 nm using an extinction coefficient of 38 553 M^{-1} cm^{-1} for HSA (Gill & von Hippel 1989; Schönenberger 1955).

For metal competition measurements, the interfering TRIS buffer was removed from the HSA stock solution with three cycles of buffer exchange against 150 mM NaCl solution utilizing the same centrifugal filter units that were used in sample concentration. The concentration of the protein sample was re-established after the buffer exchange.

2.2.2. Sample preparation

The Cm(III) stock solution used was $3{,}33 \times 10^{-6}$ M in $HClO_4$ and of isotopic composition 89,7 % ^{248}Cm, 9,4 % ^{246}Cm, and ≤ 1 % ^{243}Cm, ^{244}Cm, ^{245}Cm, and ^{247}Cm. The Eu(III) stock used was $1{,}065 \times 10^{-3}$ M in 0,01 M $HClO_4$. All TRLFS samples were prepared in a sealable 1 cm path length quartz cuvette. All measurements were performed at room temperature (296 K) unless stated otherwise. HCl or NaOH solutions of 1, 0,1, or 0,01 M concentration were used for pH adjustment.

Curium-containing samples that were used in pH titrations, kinetic studies, and determination of thermodynamic parameters were prepared by mixing together curium stock solution, purified HSA and TRIS buffer in a quartz cuvette to yield a 1 ml total volume with 1×10^{-7} M (30 µl) Cm and 5×10^{-6} M HSA. Sample pH was then adjusted to the required pH. For pH titrations two samples were prepared, both initially adjusted to pH 7,4. One was then made more acidic in a stepwise fashion while the other was made more basic to cover a pH range of 3,5 – 11,5. Samples used in the fluorescence lifetime measurements were prepared similarly, except that HSA concentrations of either 5×10^{-6} M or 1×10^{-5} M were used.

For titration of Cm(III) with HSA a 1 ml sample of Cm(III) stock solution and TRIS buffer with a final Cm(III) concentration of 1×10^{-7} M was used. Solution pH was then adjusted to 8,0 and HSA stock solution added in a stepwise fashion until a final concentration of $7{,}08 \times 10^{-6}$ M was reached. The pH was monitored after every HSA addition step and adjusted to 8,0 if it was found to deviate from it.

The metals used in competition assays (Zn, Cd, and Cu) were purchased as dichlorides and solubilized in 150 mM NaCl solution. A sample containing 5×10^{-6} M HSA and 1×10^{-7} M Cm(III) was then prepared and pH adjusted to 8,5. Metal solutions were then added in a stepwise fashion. pH was monitored and re-adjusted if necessary after every titration step.

For pH titrations with Eu(III) and HSA, final concentrations of $1{,}0 \times 10^{-5}$ M Eu(III) and $1{,}8 \times 10^{-5}$ M HSA in TRIS buffer were used. Two initial samples of 1 ml total volume and pH 7,4 were prepared, one to cover the acidic and the other to cover the basic pH conditions in

the pH range 3,5 – 11,5. For HSA titration of Eu(III), a sample with an initial total volume of 500 µl and a Eu(III) concentration of 5×10^{-6} M in TRIS buffer at pH 8,0 was used. HSA stock solution was then added in a stepwise fashion until a concentration of $2{,}7 \times 10^{-4}$ M was reached.

For NMR Eu-HSA studies a sample with a total volume of 600 µl containing 1 mM HSA and 10 % D_2O with TRIS buffer as the main solvent was prepared. The sample pH was adjusted to 8,0 (not corrected for D_2O). After measurement of the HSA spectrum, 1 molar equivalent (1 mM) of Eu(III) from the stock solution was added and the pH re-adjusted to 8,0. After the 1:1 HSA:Eu spectrum was acquired, a second molar equivalent of Eu(III) was added, the pH re-adjusted to 8,0 and the 1:2 HSA:Eu spectrum measured.

2.2.3. Time-resolved laser fluorescence spectroscopy

A laser, an acronym standing for light amplification by stimulated emission of radiation, is an apparatus in which radiation of a certain frequency is used to stimulate an excited state to emit a photon of corresponding energy. Lasers can produce high power, monochromatic, coherent, pulsed, and collimated light beams. (Atkins & De Paula 2010)

Positive-feedback is a quintessential feature of a laser: the more photons of the appropriate frequency are present, the more photons of same frequency can be stimulated to be emitted. A metastable excited state is required for a laser to function. The metastable state must have a lifetime long enough to allow for the stimulation of photon emission. In addition, the metastable state must be more populated than the ground state if there is to be net emission of radiation. As the opposite is true at thermal equilibrium, a population inversion, after which the metastable excited state is more populated than the ground state, needs to be achieved. This is achieved using flash of light of high intensity, so-called pumping. Commonly, the lasing medium is excited to an intermediate state, which then decays to the metastable state in a non-radiative fashion. The metastable state then decays to the ground state in the stimulated emission. A laser operating under such principles is called a three-level laser. If the excited metastable state decays in the stimulated emission to an excited state of lower energy, which then subsequently non-radiatively decays to ground, the laser is then called a four-level laser. (Atkins & De Paula 2010)

A common type of laser is the neodymium laser. In a Nd-YAG laser, low concentrations of Nd^{3+} ions are deposited in yttrium aluminum garnet (YAG, $Y_3Al_5O_{12}$). Nd-YAG lasers are four-level lasers. The most common emission band of Nd-YAG lasers is at 1064 nm, but light with a wavelength that is a quotient of 1064 nm, such as 532 and 355 nm, can be produced with high-order harmonic generation (Lewenstein *et al.* 1994). The transitions involved in the operation of a Nd-YAG laser are presented in Figure 2.1. (Atkins & De Paula 2010)

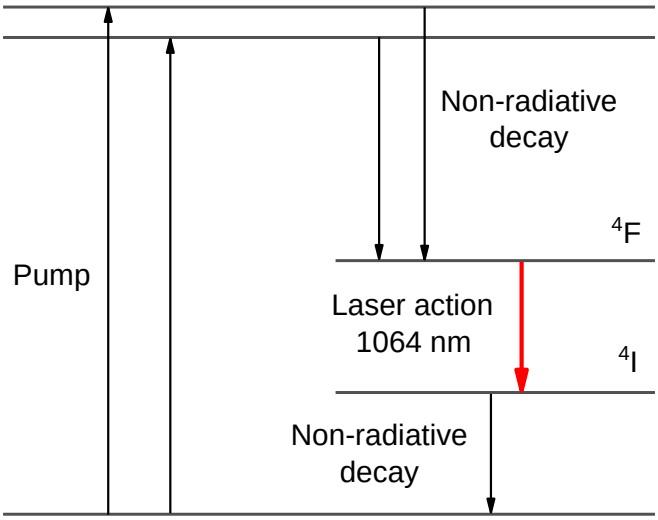

Figure 2.1. The transitions involved in the operation of a Nd-YAG laser. The levels are those of Nd^{3+}. Data are from Atkins & De Paula (2010).

One application of lasers is in the spectroscopic technique time-resolved laser fluorescence spectroscopy. In TRLFS, a laser is used to excite target molecules, atoms or ions. The fluorescent light emitted by the excited entities is then collected. As the intensity of fluorescence is dependent on the intensity of the excitation source, the fluorescence intensity produced by TRLFS is greater than the fluorescence intensities obtained using more conventional fluorescence spectroscopic methods. This in turn leads to increased sensitivity of TRLFS compared to conventional techniques. (Chatwal & Anand 2008). Observing the fluorescence emitted by the sample as a function of time allows for the determination of fluorescence lifetimes. In addition, interfering fluorescence from sources other than the chemical entity under study may be filtered out (Collins *et al.* 2011).

A TRLFS instrument typically consists of a laser system, a spectrograph, and a detector. The types of lasers used include Nd-YAG, nitrogen gas, Ti-sapphire, and excimer lasers. In tunable laser systems the laser is used to pump an optical parametric oscillator or a dye (Hänsch 1972). The emitted fluorescence is measured using a spectrograph, which may have multiple different gratings, and an intensified charged-couple device (ICCD). The time delay between the laser pulse and the ICCD operation is provided by an optical delay circuit or a delay generator. (Collins *et al*. 2011)

For TRLFS investigations in this study, a Nd-YAG (Continuum Surelite Laser) pumped dye laser system (NARROWscan D-R Dye Laser) with a 10 Hz repetition rate was used. Excitation of Cm(III) was achieved using a wavelength of 396,6 nm. The sample was inserted into a cuvette holder that permitted the adjustment of sample temperature. Fluorescence signal was collected at a 90° angle relative to the excitation light beam. A spectrograph (Shamrock 303i) was used for spectral decomposition using a grating of 1199 lines per millimeter. Ultimately the spectra were recorded using an ICCD camera (iStar Gen III, ANDOR) that was fitted with an integrated delay controller. A 1 µs delay time window was used to filter out short-lived fluorescence stemming from organic compounds.

Cm-HSA pH titration spectra series were collected at 296 and 310 K. The spectra that were measured in order to determine the thermodynamic parameters of the Cm-HSA interaction were collected in the temperature range 283 – 308 K using 2,5 K steps.

For the measurement of fluorescence lifetimes, a series of spectra were collected in which the measurement start delay window was cumulatively increased by either 15 or 20 µs after the measurement of every individual spectrum. A total of 50 spectra were collected per experiment.

2.2.4. Nuclear magnetic resonance

Nuclear magnetic resonance (NMR) spectroscopy is a technique that is used to investigate the properties of molecules that contain magnetic nuclei. This is achieved by exposing a molecule to a strong external magnetic field and observing the frequencies at which the nuclear spins come into resonance with an electromagnetic field. The Larmor frequency is

the rate of precession of a magnetic moment, such as the spin angular momentum of a nucleus, about an external magnetic field. For a spin-½ nucleus, the resonance condition states that for a resonance to occur, the frequency of an electromagnetic field must match the Larmor frequency. At the magnetic fields commonly applied in NMR, the Larmor frequencies of nuclei reside in the radiofrequency part of the electromagnetic spectrum, and so NMR is often referred to as a radiofrequency technique. NMR can be used with any nonzero spin nuclei and is most commonly applied to investigate protons (^{1}H). (Atkins & De Paula 2010)

An NMR spectrometer consists of a suitable radiofrequency sources and a magnet capable of producing a very intense and homogenous magnetic field. Modern instruments utilize radiofrequency pulses of different frequencies to cover a frequency range, allowing the acquisition of spectra from multiple different kinds of nuclei. This in in contrast with earlier "continuous-wave" instruments, in which the frequency of the radiation was fixed and instruments usually had to be dedicated to a single type of nucleus. (Mortimer 2000) Magnetic field strengths in excess of 10 T can be attained in modern instruments. Within the instrument, the sample, in an NMR tube, is spun like a top at a fast rate to average out any magnetic inhomogeneities. With samples that contain large molecules the spinning may however lead to irreproducible results. The sample is usually kept at room temperature or alternatively in an enclosure that allows the adjustment of sample temperature. The superconducting magnet responsible for the magnetic field operates and is kept at liquid helium temperature (4 K). (Atkins & De Paula 2010)

The electrons surrounding the nucleus in interaction with the external magnetic field dampen the local magnetic field experienced by the nucleus. The magnitude of the magnetic field perceived by the nucleus is therefore relative to the specific electron density that surrounds the nucleus. This gives rise to the phenomenon of chemical shielding: the experienced magnitude of the magnetic field is different for chemically nonequivalent nuclei due to their different electron densities. As the Larmor frequency, and therefore also the resonance frequency for spin-½ nuclei, is dependent on the effective magnetic field, it too is affected by the chemical shielding. The resonance frequencies of nuclei are expressed using an empirical quantity known as the chemical shift: the resonance frequencies of

protons and ^{13}C are related to those of tetramethylsilane (TMS) to yield chemical shift values. As the resonance frequencies are relative to the magnetic field, using a standard such as TMS permits the comparison of resonance frequencies, and therefore of spectra as well, acquired from different instruments. The chemical shifts are commonly expressed in parts per million (ppm). (Nanny *et al.* 1997) Chemical shielding and chemical shift are inversely related: when the chemical shielding of a nucleus decreases, its chemical shift increases. Nuclei with large chemical shifts are said to be strongly deshielded. Electron-withdrawing elements, such as oxygen in many organic compounds, tend to deshield neighboring nuclei through reduction of the electron density surrounding the neighbors. The chemical environment of a nucleus can in some cases be estimated by comparing its chemical shift to the typical values acquired for nuclei at specific chemical environments. In addition, in an NMR spectrum the resonances from equivalent nuclei are added up and so the relative amounts of different types of chemical environments experienced by nuclei can be derived from the integrals of resonances. (Atkins & De Paula 2010)

In this study, a Bruker Avance III 400 spectrometer was used, with a ^{1}H operation frequency of 400,18 MHz, to a acquire the NMR spectra. All spectra were collected at 300 K. A broadband inverse z-gradient probe (BBI) optimized for proton detection was used. The chemical shifts were referenced internally to TMS using the lock signal of the D_2O. The signal arising from the water molecules present in the solvent was suppressed using a WATERGATE pulse sequence (Piotto *et al.* 1992; Sklenar *et al.* 1993). Spectra were acquired with 32k data points and zero-filled to 64k points. The exponential window functions used had a line broadening factor of 0,05 Hz.

2.2.5. pH measurement

The setup used for pH measurement consisted of a glass combination electrode (Ross) and an Orion 520A pH meter (Thermo Scientific). The system was calibrated daily using pH 4, 7, and 10 standard solutions (Ross).

2.3. Results and discussion

2.3.1. Interaction between Cm(III) and HSA at room temperature

To establish whether Cm(III) interacts with HSA, the spectrum of Cm(III) in the presence of HSA was measured in TRIS-buffered aqueous solution and pH range 3,5 – 11,5 at room temperature using TRLFS. The spectra are shown in Figure 2.2. Initially, two species were identifiable from the spectra: one with a maximum at 593,8 nm and another with a maximum at 602,0 nm. Of these, the former was identified as the Cm(III) aquo ion based on similarity with the known spectra of the aquo ion and the dominance of the species at low pH. The latter was postulated to be the CmHSA species, as the features of the emission band did not correspond to those of Cm(III) hydrolysis species (Wimmer, Klenze *et al.* 1992). The maximum intensity wavelength determined for the CmHSA species relative to the aquo ion (8,2 nm) is in line with other studies that have reported Cm(III) complexes with small biologically relevant organic ligands (Moll *et al.* 2005; Moll & Bernhard 2007), components of microbial cells (Moll *et al.* 2013), and other proteins (Barkleit *et al.* 2016), but significantly lower than what is observed for Cm(III) complexed at the primary Fe(III) binding site of human transferrin (26,5 nm). In the article reporting the CmTF complex, it was postulated that the buried, high coordination environment of the Fe(III) binding site of transferrin was responsible for the extraordinary shift in Cm(III) fluorescence when complexed at the site. (Bauer *et al.* 2014) This suggests that the binding of Cm(III) by HSA does not occur at a buried high coordination site, but at a partial binding site on the surface of the protein.

A measured spectrum is the sum of the spectra of its pure components. The presence of additional species in the Cm-HSA system was suggested by the futility of spectral deconvolution attempts using just the two species mentioned above. In the case of the Cm-HSA system, two additional species need to be taken into account on top of the emission spectra of the Cm(III) aquo ion and the CmHSA species to allow full deconvolution of spectra. One species with an emission maximum of 599,3 nm was identified. It was conjectured that this species might correspond to a solvent species of TRIS and $CmOH^{2+}$ (Cm-OH/TRIS). The speciation of Cm(III) in aqueous solution perhaps suggests that the species might correspond to $CmOH^{2+}$ (Figure 1.8), but the emission band is more pronounced than what is seen in pure H_2O. Therefore, it was postulated that the species is

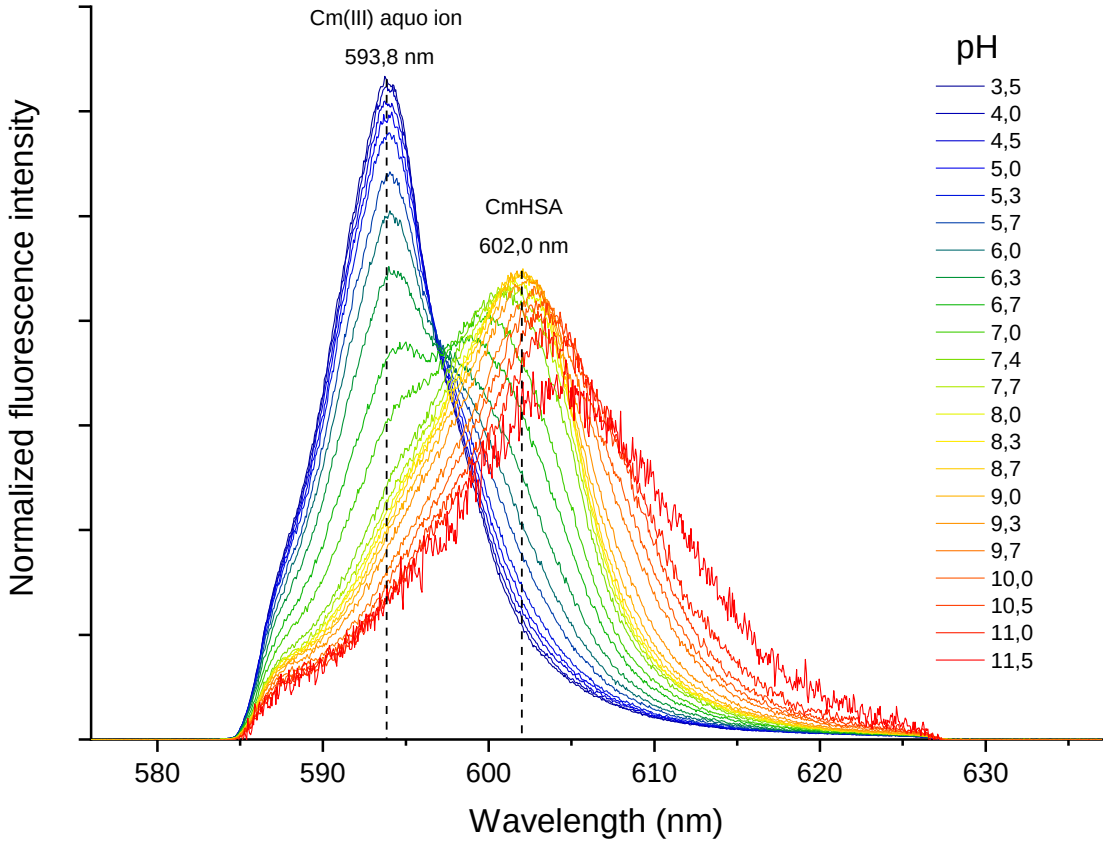

Figure 2.2. The spectra of the Cm-HSA system measured in TRIS buffer at room temperature and at specified pH values in the pH range 3,5 – 11,5. [Cm(III)] = 1×10^{-7} M, [HSA] = 5×10^{-6} M.

not representative of pure $CmOH^{2+}$, and that likely an interaction involving the TRIS buffer molecule exists. It also became clear that an additional species was present at pH values greater than 9,0, as a reduction in fluorescence intensity coupled with a bathochromic shift was observed beyond that pH. The reduction of fluorescence intensity in response to rising pH was deemed not great enough to represent the formation of the second hydrolysis species $Cm(OH)_2^+$, and was thought to arise from the formation of one or more ternary Cm-HSA-OH species. The spectrum at pH 11,5, which comprised of a single slightly asymmetric emission band with a maximum at 603,3 nm, was selected to represent these species. The spectra of the four component species are shown in Figure 2.3.

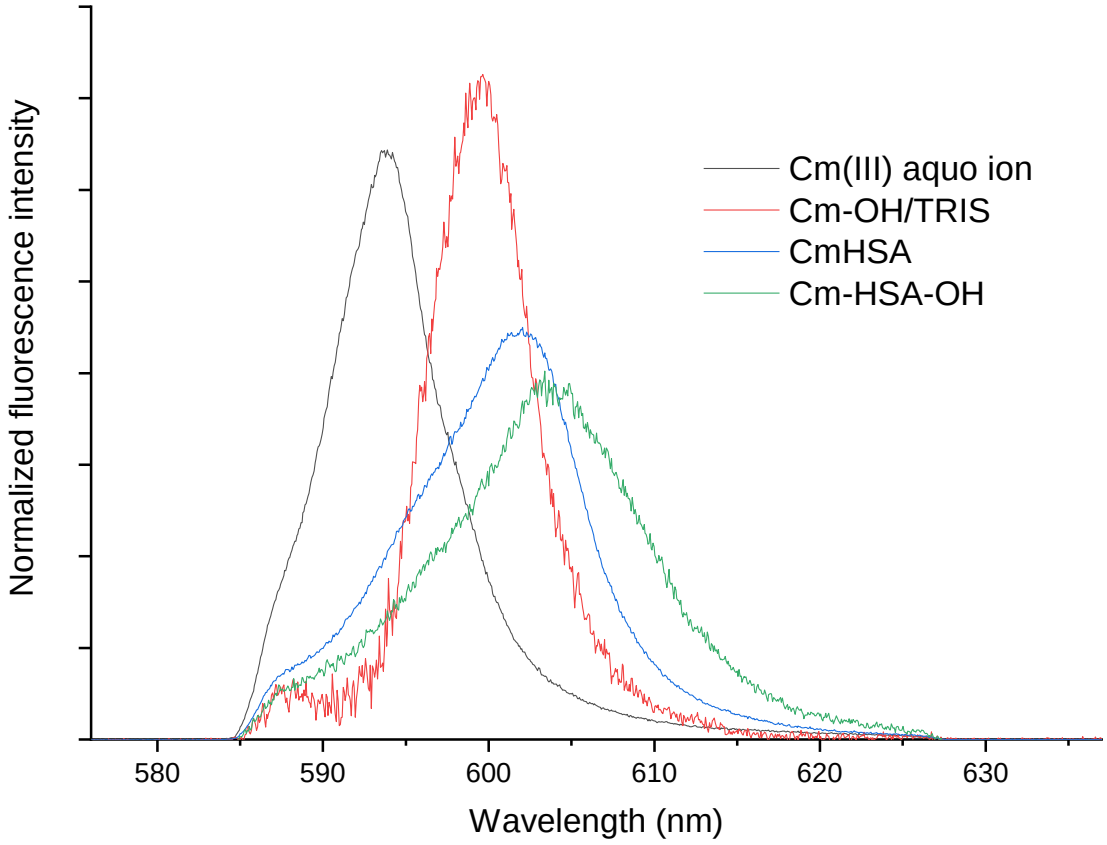

Figure 2.3. The spectra of the species identified in the Cm-HSA system at room temperature in TRIS buffer and pH range 3,5 – 11,5.

The distribution of species as a function of pH in the Cm-HSA system was possible with the pure spectra of the four species laid out in Figure 2.3. The distribution of species as a function of pH for the Cm-HSA system at room temperature is shown in Figure 2.4. The speciation is dominated by the aquo ion in the pH range 3,5 – 6,7, after which CmHSA becomes the dominant species. The fraction of the CmHSA species is at its highest at pH 8,7, where all the curium present is in complex with HSA. At pH > 8,7 the fraction of Cm-HSA-OH is seen to incrementally rise and the CmHSA and Cm-HSA-OH fractions are nigh equal at pH 9,7. At pH > 9,7 Cm-HSA-OH becomes the dominant species. The fraction of the Cm-OH/TRIS species is at its maximum at pH 6,7, where it is represents approximately 19 % of the total curium.

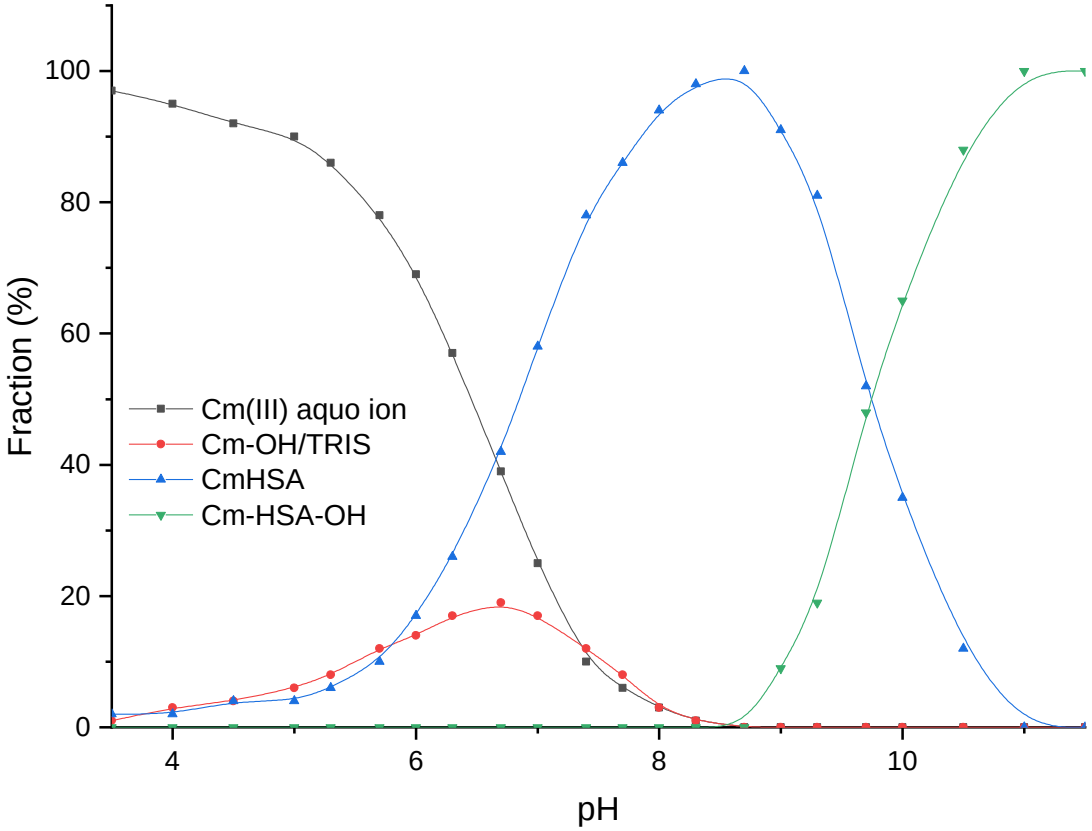

Figure 2.4. Distribution of curium species as a function of pH in the Cm-HSA system in an aqueous solution at room temperature.

2.3.2. Interaction between Cm(III) and HSA at physiological temperature

As the primary interest of this study was to help unravel the behavior of curium in blood, results under experimental conditions resembling physiological conditions are particularly valuable. After the existence of a CmHSA complex appeared to be proven, it was deemed to be of interest to investigate the nature and properties of interaction at physiological temperature. To this end, an otherwise similar pH titration experiment was run at physiological temperature (310 K, 37 °C). The spectra are presented in Figure 2.5. The spectra were deconvoluted using the same pure component species spectra used to deconvolute the room temperature pH titration spectra. The distribution of species as a function of pH for the Cm-HSA system at physiological temperature is shown in Figure 2.6. The speciation at physiological temperature resembles that which was determined at room temperature. However, higher temperature does appear to drive the CmHSA formation to initiate at a lower pH value relative to room temperature, suggesting that the complexation

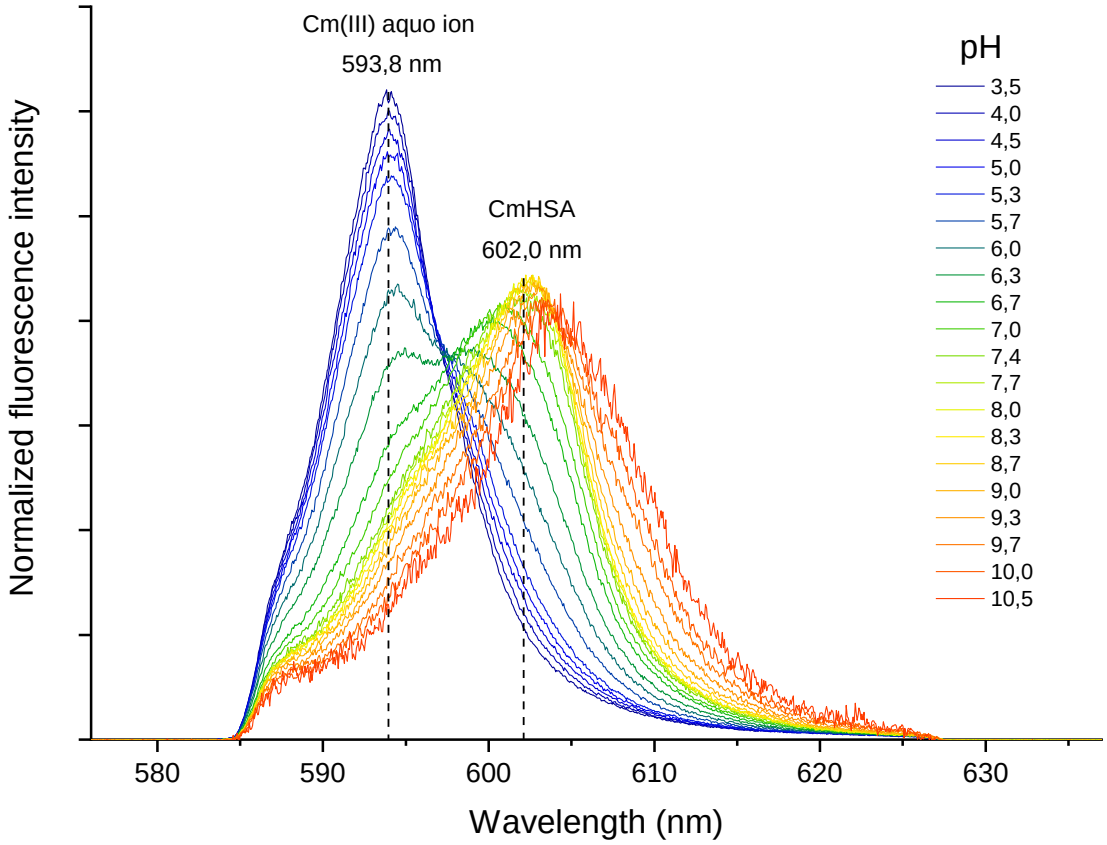

Figure 2.5. Cm(III) fluorescence spectra acquired in the presence of HSA in TRIS buffer at physiological temperature and different pH values in the pH range 3,5 – 10,5. [Cm(III)] = 1×10^{-7} M, [HSA] = 5×10^{-6} M.

reaction is endothermic. This results in a higher fraction of CmHSA at physiological pH (7,4) and physiological temperature (90 %) relative to room temperature (78 %). This is of interest with regard to speciation of Cm(III) in blood *in vivo*, as Cm(III) complexation with HSA at physiological pH appears to be more relevant at physiological temperature than room temperature.

2.3.3. Kinetics of the CmHSA complex

To assess the stability of the CmHSA complex a kinetic study was performed. The experiment was run at pH 8,7, as speciation analysis had revealed the CmHSA species to be present at its highest concentration relative to other species at this pH value at room temperature. HSA was added to a cuvette containing Cm(III) and a fluorescence spectrum

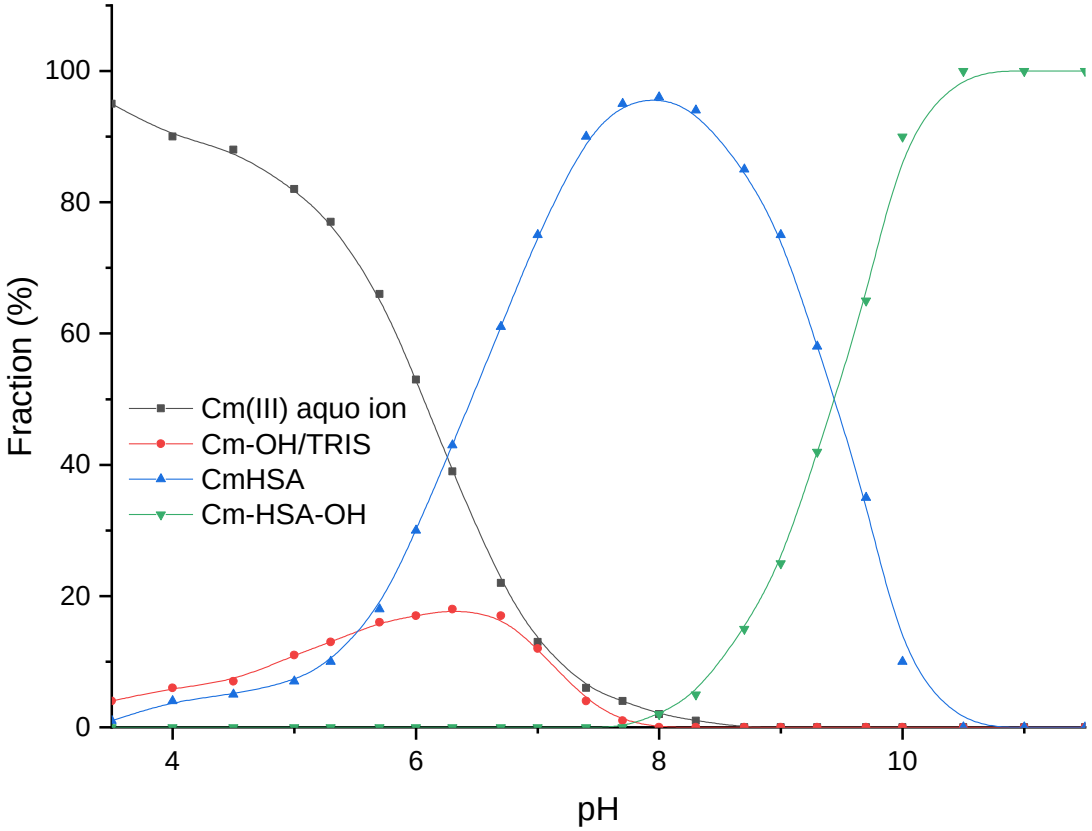

Figure 2.6. Distribution of curium species as a function of pH in the Cm-HSA system at physiological temperature (310 K, 37 °C).

was immediately measured with TRLFS. The same sample cuvette was measured again at specified time points over a total time period of four hours to see if any observable changes in the spectrum occur. The spectra are shown in Figure 2.7. No significant changes in the CmHSA spectrum are observed for the full duration of the experiment, as every acquired spectrum was practically identical to the first acquired spectrum. The measurements show that the complexation reaction is fast enough to facilitate immediate measurement after sample preparation and that the resulting CmHSA complex is stable for time periods long enough to facilitate the experiments performed in this study.

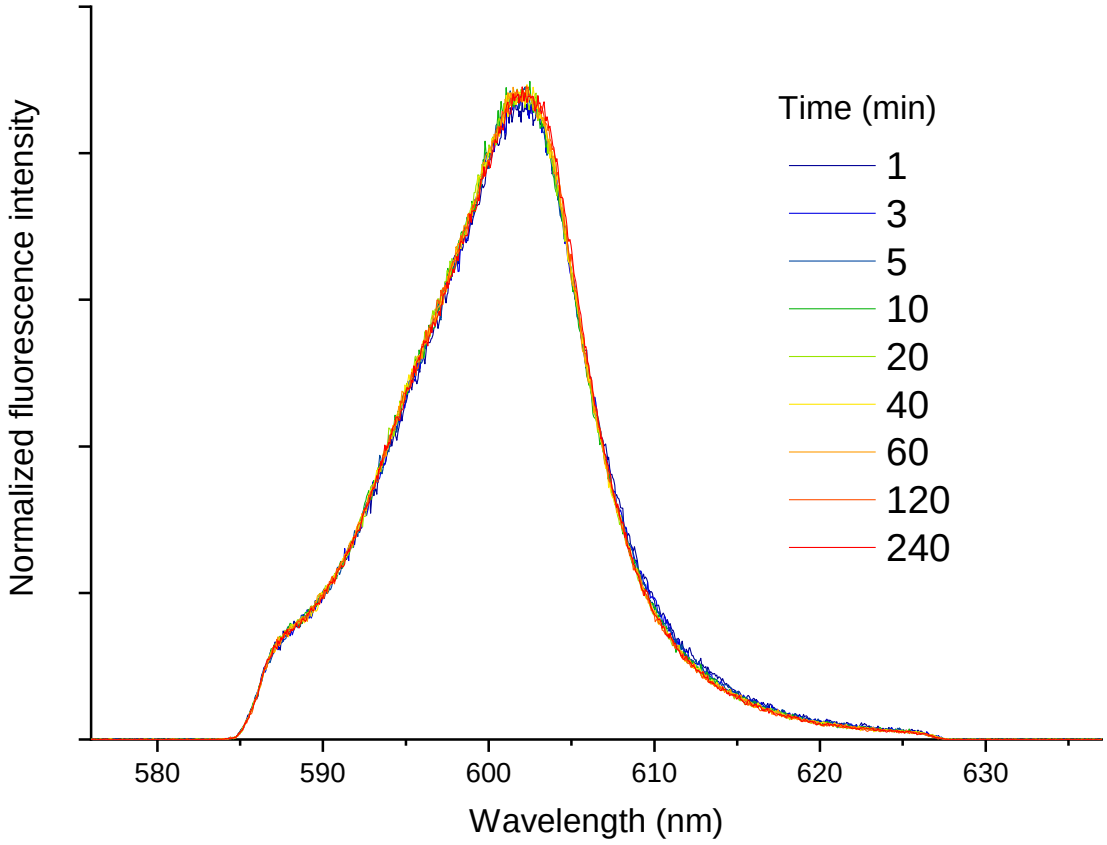

Figure 2.7. Kinetic study of the CmHSA complex in TRIS buffer at pH 8,7 and room temperature over a time frame of one to 240 minutes. The times indicate the time elapsed after the introduction of HSA into the sample. [Cm(III)] = 1×10^{-7} M, [HSA] = 5×10^{-6} M.

2.3.4. The fluorescence lifetime of CmHSA

The fluorescence lifetime of Cm(III) can yield interesting information about the coordination environment of the metal ion, such as the hydration number and the number of coordinating ligands in the first coordination sphere. The lifetime of the CmHSA species was measured at multiple pH values and at Cm:HSA molar ratios of 1:50 and 1:100. When the natural logarithm of fluorescence intensity was plotted as a function of delay time, it was seen that the fluorescence decay dataset was not linear, and hence not representative of a single pure species under any of the conditions used, though the deviation from linearity was small. A dataset measured at pH 8,0 is provided as an example in Figure 2.8. It was postulated that the Cm(III) aquo ion and the Cm(III) hydrolysis species might contribute to the deviation. In this vein, fluorescence lifetimes were derived from plots of fluorescence intensity as a function of delay time using a triexponential decay function. In

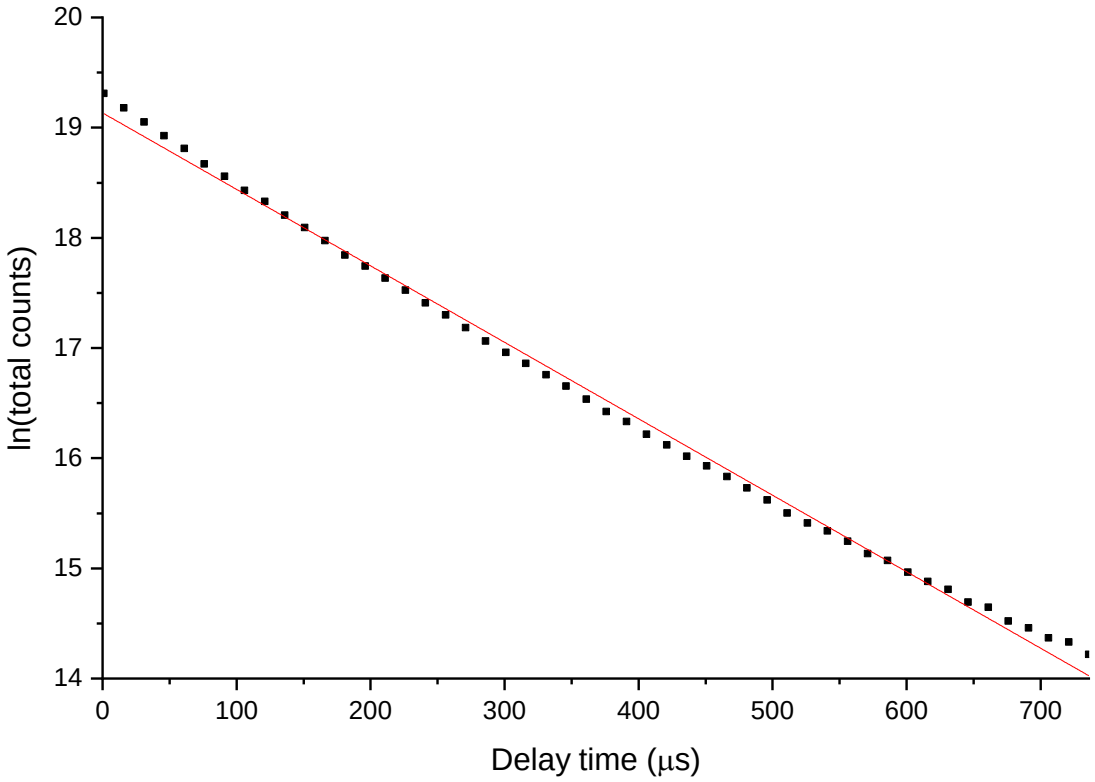

Figure 2.8. Semi-logarithmic plot of total measured counts versus the delay time. A linear fit of the dataset is shown as a red line. Data were collected at pH 8,0. [Cm(III)] = 1×10^{-7} M, [HSA] = 5×10^{-6} M.

accordance with the speciation of Cm(III) (Figure 1.8) and lifetimes of Cm(III) species (Table 1.4) in aqueous solution (Figure 1.8), the two known parameters inserted into the function at pH < 8 were 65 μs (Cm(III) aquo ion) and 72 μs ($CmOH^{2+}$). At pH ≥ 8,0 the known parameters inserted were 72 μs ($CmOH^{2+}$) and 80 μs ($Cm(OH)_2^{+}$). The third component was calculated by the triexponential decay function and was taken to represent the fluorescence lifetime of CmHSA. The conditions of fluorescence lifetime measurements and the calculated lifetimes are summarized in Table 2.1. The average of the calculated lifetimes 152 ± 10 μs was chosen to represent the CmHSA species fluorescence lifetime.

The number of water molecules in the first coordination sphere was calculated by inserting the determined fluorescence lifetime of CmHSA into the Kimura equation (4), and a value of 3,4 ± 0,5 was obtained. This suggests that three to four water molecules, and therefore six to five ligands other than water, are expected in the first coordination sphere of CmHSA.

Table 1.1. Summary of measurements performed to establish the fluorescence lifetime of the CmHSA species. All measurements were performed at room temperature and in TRIS buffer. The concentration of Cm(III) was 1×10^{-7} M. HSA concentration was either 5×10^{-6} or 1×10^{-5} M. The average of lifetimes derived using a triexponential decay function was calculated to be 152 ± 10 µs.

pH	Cm:HSA molar ratio	Fluorescence lifetime (µs)
6,5	1:50	143
7,0	1:50	151
7,4	1:50	145 146 149
8,0	1:50	149
8,5	1:50	148 149
8,5	1:100	162 154
8,7	1:50	144 158
9,0	1:50	164 164

Lifetimes of 120 and 129 µs have been reported for complexes of Cm(III) with proteins porcine α-amylase and human transferrin, and these lifetimes correspond with Cm(III) hydration numbers 4,5 ± 0,5 and 4,2 ± 0,5, respectively (Barkleit *et al.* 2016; Bauer *et al.* 2014). Relative to these complexes, one additional ligand appears to be involved in Cm(III) binding by HSA.

2.3.5. Stoichiometry and the conditional stability constant of CmHSA

To establish the stoichiometry and conditional stability constant of the Cm-HSA interaction, the dependence of the interaction on HSA concentration in the concentration range 0 – $7{,}08 \times 10^{-6}$ M HSA was studied at pH 8,0. The spectra are shown in Figure 2.9. A gradual shift from a solvent species with maximum at 598,3 nm towards the CmHSA species at 602,0 nm was observed.

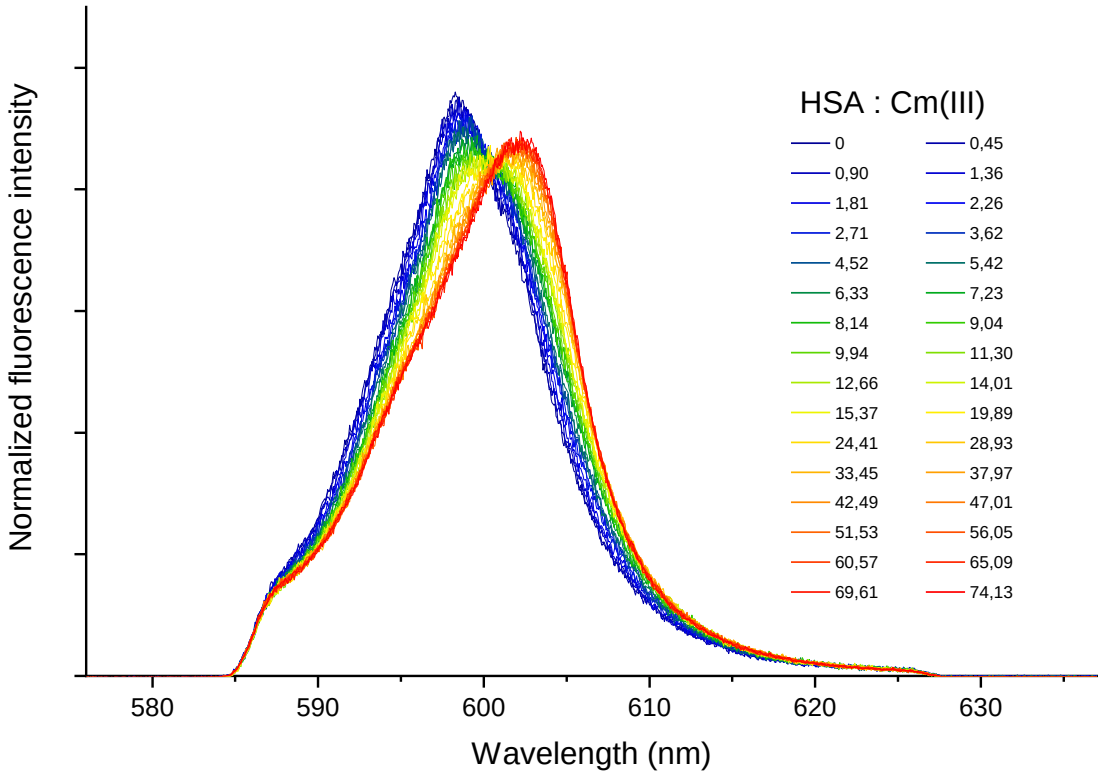

Figure 2.9. Titration of Cm(III) with HSA in TRIS buffer at pH 8,0 and room temperature. The Cm:HSA molar ratios are listed in the figure. [Cm(III)] = 1×10^{-7} M, [HSA] = 0 – $7{,}08 \times 10^{-6}$ M.

The formation of the CmHSA complex can be described using the equation

$$\mathrm{Cm(III)} + \mathrm{HSA} \rightleftharpoons \mathrm{CmHSA} \tag{6}$$

The conditional stability constant *K* of Cm-HSA interaction is calculable using the equation

$$K = \frac{[\mathrm{CmHSA}]_{\mathrm{eq}}}{[\mathrm{Cm}]_{\mathrm{eq}}[\mathrm{HSA}]_{\mathrm{eq}}} \tag{7}$$

Equation (7) may be further transformed into

$$\log\frac{[\mathrm{CmHSA}]_{\mathrm{eq}}}{[\mathrm{Cm}]_{\mathrm{eq}}} = \log[\mathrm{HSA}]_{\mathrm{eq}} + \log K \tag{8}$$

In equation (8) the logarithms of the concentration ratio $[CmHSA]_{eq}/[Cm]_{eq}$ and the concentration $[HSA]_{eq}$ are linearly correlated. The slope of the plot of $\log([CmHSA]_{eq}/[Cm]_{eq})$ versus $\log[HSA]_{eq}$ yields the complexation stoichiometry between Cm(III) and HSA. To calculate the *K* value with equation (7), the concentrations of the species are required. Knowing the total concentration of Cm(III), the fractions of $[CmHSA]_{eq}$, $[Cm\text{-}OH/TRIS]_{eq}$, and $[Cm(OH)_2^+]_{eq}$ are obtained by spectral deconvolution and the concentration $[HSA]_{eq}$ and $[Cm]_{eq}$ (at pH 8,0) can be calculated using

$$[\mathrm{HSA}]_{\mathrm{eq}} = [\mathrm{HSA}]_{\mathrm{tot}} - [\mathrm{CmHSA}]_{\mathrm{eq}} \quad (9)$$

$$[\mathrm{Cm}]_{\mathrm{eq}} = [\mathrm{Cm}]_{\mathrm{tot}} - [\mathrm{CmHSA}]_{\mathrm{eq}} - [\mathrm{Cm\text{-}OH/TRIS}]_{\mathrm{eq}} - [\mathrm{Cm(OH)_2^+}]_{\mathrm{eq}} \quad (10)$$

For the purpose of assessment of stoichiometry and the conditional stability constant, the HSA titration spectra were deconvoluted using previously acquired pure component spectra of CmHSA, Cm-OH/TRIS, and $Cm(OH)_2^+$. Spectral deconvolution and equations (9) and (10) made it possible to determine $[Cm]_{eq}$, $[HSA]_{eq}$, and $[CmHSA]_{eq}$. Conditional log *K* values were calculated by taking a base 10 logarithm of *K* values calculated using equation (7). An average of the log *K* values was then taken to yield a conditional pH 8,0 stability constant log *K* 6,8 ± 0,5. It is assumed here that all present HSA is available for Cm(III) binding. This is not likely, however, as HSA contains a multitude of different protonable sites. HSA likely binds Cm(III) in only one or few protonation states and the equilibrium fraction of each of these states is dependent on the pH. Because the exact nature of the complexing ligands and their pK_a values are not known at this time, a pH-independent stability constant cannot be attained.

The comparison of the calculated log *K* value with previously published values is difficult as no stability constants for HSA interaction with trivalent actinides are available in the literature. Conditional stability constants of HSA with selected lanthanides under physiological-like conditions (*T* = 310 K, *I* = 0,15 M, pH 7,4) that were measured using an equilibrium dialysis method, have been published by Schomäcker *et al*. (1988). The article by Schomäcker *et al*. outlines a trend in which increasing the ionic radius of a lanthanide results in a weaker HSA complex. Eu(III), an ion that is smaller in radius than Cm(III) (David

1986), reportedly formed a HSA complex with a log *K* of 6,41 ± 0,02. Neodymium(III), with an ionic radius slightly larger than Cm(III) (David 1986), on the other hand, formed a HSA complex with a log *K* of 5,39 ± 0,03. Although the measurement conditions and methods are not exactly comparable between the present study and the study published by Schomäcker and colleagues, the reported EuHSA log *K* value and the CmHSA log *K* presented here are in the same order of magnitude. The reported NdHSA log *K*, however, is over an order of magnitude smaller relative to that of CmHSA.

A plot of $\log([CmHSA]_{eq}/[Cm]_{eq})$ versus $\log[HSA]_{eq}$ is shown in Figure 2.10. The slope of the linear fit has a value of 1,38. The existence of a 1:2 Cm:HSA complex, which would give a slope of two, is highly improbable, as the steric hindrance stemming from the inclusion of two molecules of HSA per one Cm(III) in the complex is likely very high. A reaction stoichiometry of 1:1, for which a slope of one is to be expected, is therefore much more feasible. The reason why the slope deviates from 1,00 is most likely the low concentration of the Cm(III) aquo ion relative to other species. As the fraction of Cm(III) aquo ion is low to begin with, ≤ 20 % in all and ≤ 10 % in most spectra, an error of a percentage point or two in the fraction leads to a large relative error. The cumulative effect of these errors is then the deviation of the slope from a value of 1,00.

2.3.6. Thermodynamics of Cm-HSA interaction

In order to acquire the enthalpy and entropy of interaction for the CmHSA complexation reaction, Cm(III) fluorescence spectra in the presence of HSA were acquired at different temperatures while the pH was kept constant. Two datasets were collected, one at pH 7,0 and another at pH 7,4. Spectra were collected in a temperature range 10,0 – 35,0 °C using 2,5 °C temperature steps. The acquired spectra were subsequently deconvoluted using the pure component spectra for the Cm(III) aquo ion, Cm-OH/TRIS, and CmHSA from Figure 2.3. Conditional *K* values were then calculated using equation (7).

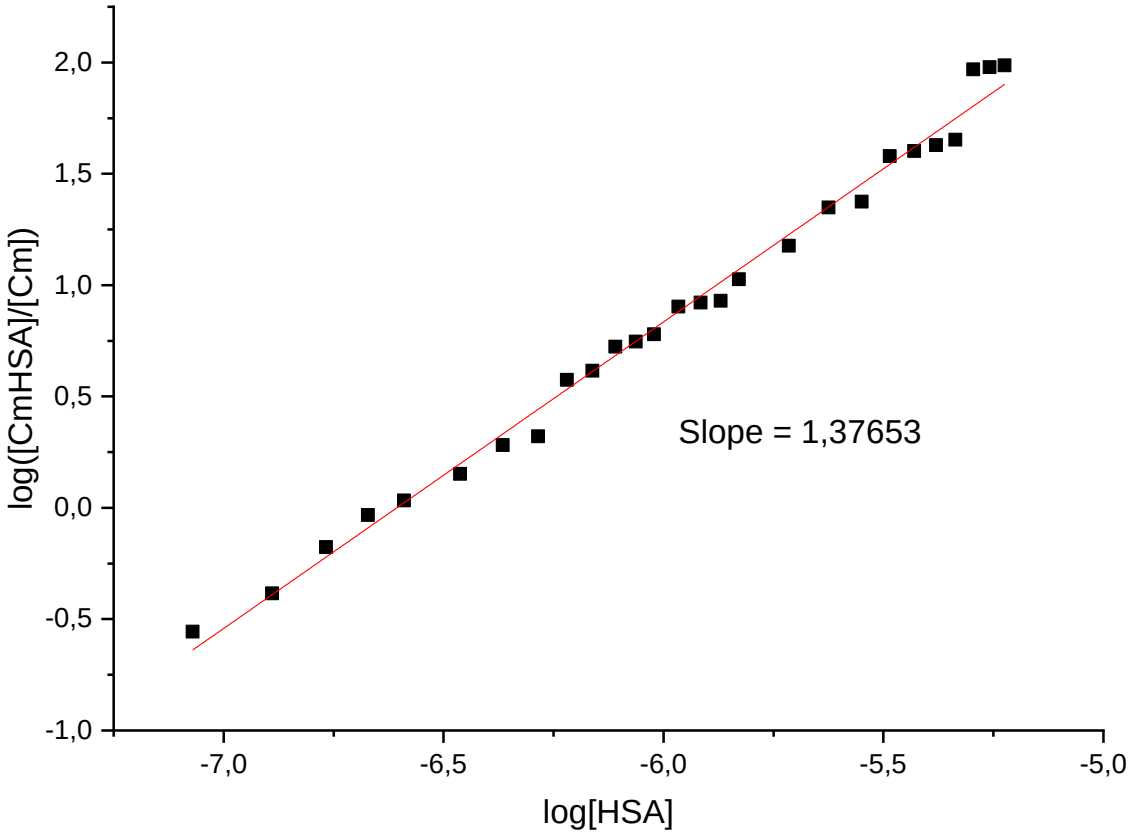

Figure 2.10. A log-log plot of $[CmHSA]_{eq}/[Cm]_{eq}$ versus $[HSA]_{eq}$ with data derived from the deconvolution of spectra acquired from HSA titration of Cm(III). A linear fit of the data is shown in red and has a slope of 1,38.

Values of ln *K* and the reciprocal of the measurement temperature (in K) were plotted in accordance to the linear form of the van't Hoff equation

$$\ln K = -\frac{\Delta H}{RT} + \frac{\Delta S}{R} \qquad (11)$$

where *R* is the gas constant and *T* is the measurement temperature. The van't Hoff plot is shown in Figure 2.11.

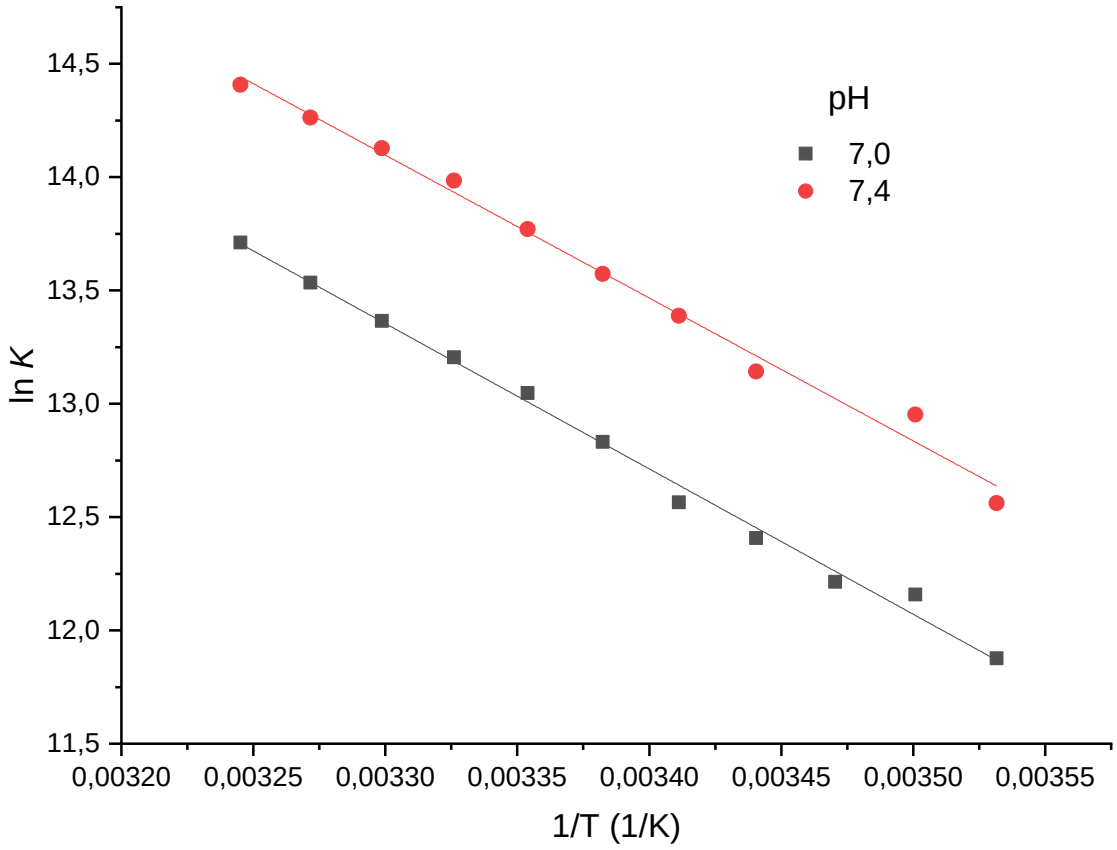

Figure 2.11. A van't Hoff plot for the Cm-HSA interaction at pH values 7,0 (black) and 7,4 (red) in the temperature range 10,0 – 35,0 °C (2,5 °C intervals). Both datasets were fitted using a linear fit, drawn in the figure using the same color as for the respective dataset. All samples were measured in TRIS buffer. [Cm(III)] = 1×10^{-7}, [HSA] = 5×10^{-6}.

The thermodynamic parameters Δ*H* and Δ*S* were calculated from linear fits of the datasets using the equations

$$\Delta H = -R \times \text{slope} \quad (12)$$

$$\Delta S = R \times \text{intercept} \quad (13)$$

where *R* is the gas constant. The thermodynamic parameters acquired from the fits are given in Table 2.2.

Table 2.2. The thermodynamic parameters of the Cm-HSA interaction. Errors shown are derived from the errors for slope and the y-intercept of the linear fits.

pH	Δ*H* (kJ mol^{-1})	Δ*S* (J K^{-1} mol^{-1})
7,0	53 ± 2	287 ± 5
7,4	52 ± 2	290 ± 6

The negative slopes of the van't Hoff plot fits indicate that the interaction is endothermic and entropy-driven under the measurement conditions that were used. Considering that the fluorescence lifetime measurements indicate that HSA provides six or five ligands to bind Cm(III) in CmHSA, it is likely that the chelate effect and liberation of waters of hydration are the phenomena responsible for the endothermic nature of the complexation reaction. Interestingly, Cu(II) binding at DAHK tetrapeptide, representing the N-Terminal Site and the Lys4 residue of HSA, is in like manner reported to be entropy-driven (Trapaidze *et al.* 2012). In the DAHK peptide thermodynamic study, it was likewise speculated that the entropy-driven nature of binding is up to the release of water from both the hydrated metal and the ligand as well as the release of protons from the ligand.

2.3.7. Displacement of Cm(III) from HSA by divalent metals

One role of HSA in the human body is the binding and transport of, mostly divalent, metal ions. For many metals, the binding site or sites on HSA are known. Cu(II) and Ni(II) are canonical binders of the N-Terminal Site (NTS), which is comprised of the three first amino acids of HSA. Zn(II), Cu(II), and Cd(II) bind at the Multi-metal Binding Site (MSB) located in a cleft between HSA domains I and II. In addition to binding at the MBS, HSA binds Cd(II) at an additional, yet-uncharacterized binding site, Site B. (Bal *et al.* 2013) To understand the modalities of the Cm-HSA interaction, it is of interest to know if HSA binds Cm(III) at any of the characterized sites. To assess the binding site of Cm(III) on HSA, the CmHSA complex was titrated with three competitor metals: Cu(II) to assess binding at the NTS and MBS, Zn(II) to assess binding at the MBS only, and Cd(II) to assess binding at the MBS and Site B. Titration spectra were collected at pH 8,5, where the CmHSA complex is the dominant species, and in the absence of TRIS, as Cu(II) and Zn(II) have been shown to interact with it (Colombo *et al.* 1987; Peña *et al.* 1990). Prior to the addition of HSA or competitor metals,

a Cm(III) solvent spectrum was collected, which at pH 8,5 is dominated by $Cm(OH)_2^+$ (Figure 1.8).

Titration with Cu(II)

The addition of Cu(II) has a drastic effect on Cm(III) fluorescence, as addition of excess Cu(II) relative to HSA resulted in a hypsochromic shift towards the maximum intensity wavelength of the Cm(III) solvent spectrum (Figure 2.12). At a Cu:HSA ratio of 5:1 and greater, the maximum intensity wavelength of the Cm(III) signal is established at 598,5 nm, very close to that of the Cm(III) solvent species. This result suggests that Cm(III) is displaced by Cu(II) from HSA, likely because binding ligands are shared between the two metals.

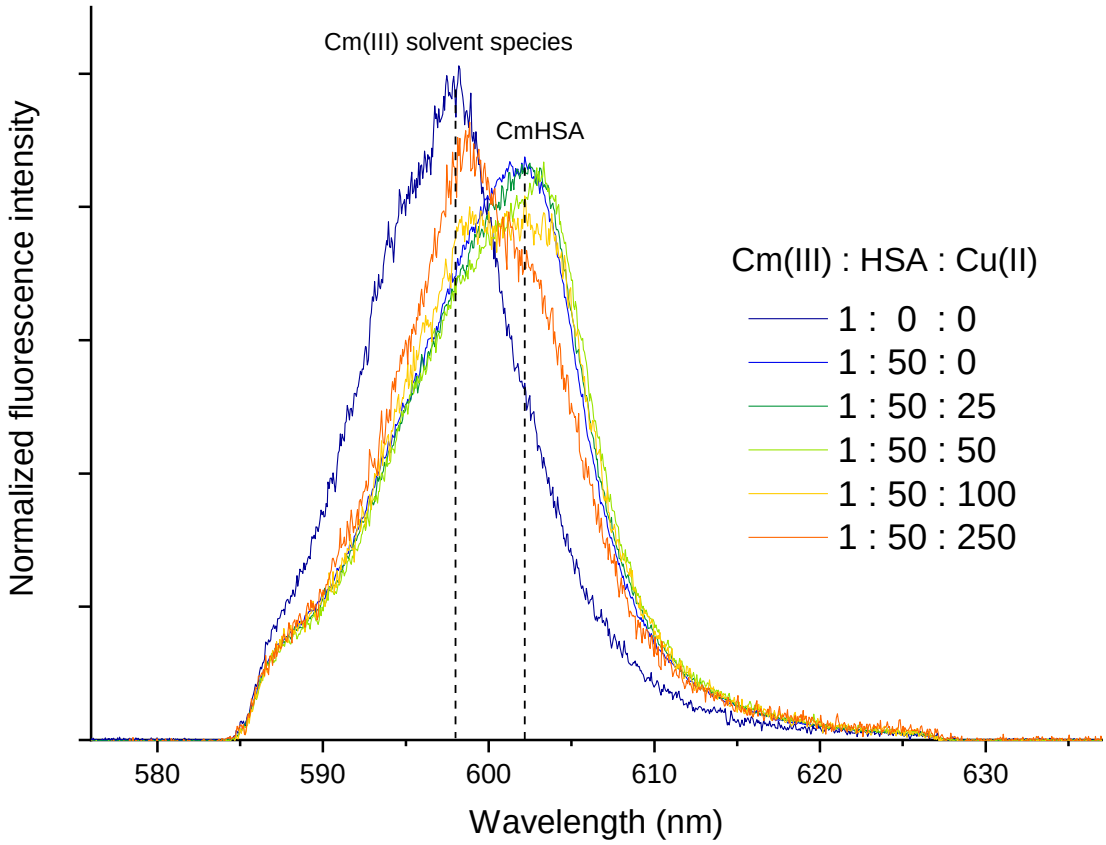

Figure 2.12. The fluorescence spectra of Cm(III) at different concentrations of HSA and Cu(II) in a 150 mM NaCl solution at pH 8,5 and room temperature. The relative concentrations of Cm(III), HSA, and Cu(II) for the shown spectra are depicted in the figure. The maximum intensity wavelengths of the CmHSA and Cm(III) solvent species are highlighted using dashed lines. Only selected spectra are shown for clarity. [Cm(III)] = $1{,}0 \times 10^{-7}$ M, [HSA] = $0 - 5 \times 10^{-6}$ M, [Cu(II)] = $0 - 5 \times 10^{-5}$ M.

Titration with Zn(II)

Addition of Zn(II) in excess relative to the concentration of HSA results in a gradual bathochromic shift towards a maximum of 604,0 nm (Figure 2.13). No change in Cm(III) fluorescence is observed when the concentration of zinc is lower than or equal to the concentration of HSA. As stated earlier, Cu(II) and Zn(II) both bind at the MBS, but Cu(II) binds also at the NTS. Based on the titration data, Cu(II) appears to displace Cm(III). Zn(II), however, does not appear to displace Cm(III). If Cm(III) was to bind at the MBS, a hypsochromic shift similar to what is seen when titrating CmHSA with Cu(II) would be seen when titrating CmHSA with Zn(II). The results, therefore, indicate that HSA binds Cm(III) at or near the NTS. The bathochromic shift induced by Zn(II) might be the result of Zn(II) binding at a site close to the NTS. In some crystal structures of equine serum albumin (ESA) in complex with zinc, a Zn(II) ion can be seen bound by His9, Asp13, and Asp255 (Handing *et al.* 2016). Of the three amino acids, His9 and Asp13 are close to the N-terminus in primary sequence. These two amino acids are also present in the human serum albumin (Meloun *et al.* 1975). It may, therefore, be possible that HSA is also capable of binding Zn(II) at a site that consists at least partly of these residues. The proximity of this site to the NTS could have an impact on the structural features of NTS and hence the fluorescence behavior of Cm(III) complexes at the N-terminus. The reason why the bathochromic shift is seen only when the concentration of Zn(II) exceeds that of HSA is probably that the first molar equivalent of Zn(II) binds at its primary binding site, the MBS. Any excess Zn(II) is then bound at a secondary site or sites.

Titration with Cd(II)

Competition titration with Cd(II) resulted in the broadening of the Cm(III) fluorescence signal and a partial hypsochromic shift (Figure 2.14). Again, no changes were observed until the concentration of Cd(II) exceeded that of HSA, suggesting that the first equivalent of Cd(II) binds at a site that is not proximal to the Cm(III) complexation site. The reason for the changes observed in the fluorescence spectrum of Cm(III) induced by Cd(II) at higher concentrations might be Cd(II) binding at the Site B of HSA, the location of which is unknown. Based on the Cd(II) titration spectra, the direct involvement of Site B in complexation of Cm(III) can, however, be ruled out.

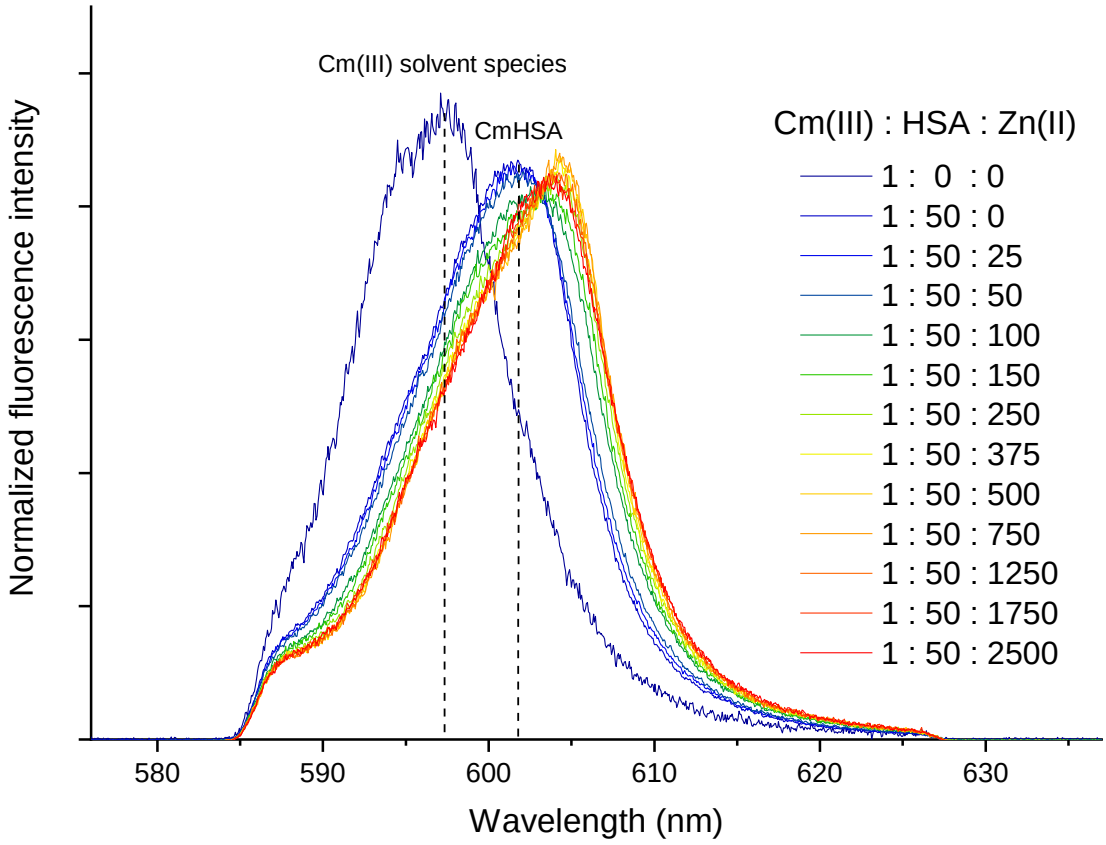

Figure 2.13. The fluorescence spectra of Cm(III) at varying concentrations of HSA and Zn(II) in a 150 mM NaCl solution at pH 8,5 and room temperature. The relative concentrations of Cm(III), HSA, and Zn(II) for the shown spectra are depicted in the figure. The maximum intensity wavelengths of the CmHSA and Cm(III) solvent species are highlighted using dashed lines. [Cm(III)] = $1{,}0 \times 10^{-7}$ M, [HSA] = $0 - 5 \times 10^{-6}$ M, [Zn(II)] = $0 - 1{,}25 \times 10^{-2}$ M.

2.3.8. Interaction of Eu(III) with HSA

Europium in its trivalent state is often used as an analogue for trivalent actinides. To further validate the interaction of HSA with Cm(III) and trivalent f-elements in general, the spectroscopic behavior of Eu(III) in the presence of HSA was investigated. Spectra of the Eu-HSA system in TRIS buffer at room temperature and in the pH range of 3,5 – 11,5 were collected and selected spectra are presented in Figure 2.15. Two emission bands are present in the spectra, the $^5D_0 \rightarrow {}^7F_1$ transition between 580 and 600 nm and the $^5D_0 \rightarrow {}^7F_2$ transition between 610 and 625 nm. At pH 3,5 the shape of the emission bands as well as the relative intensity ratio of F_2 and F_1 bands indicate that Eu(III) is present as its aquo ion. The F_2/F_1 relative intensity is seen to increase with the increase of pH, a phenomenon that

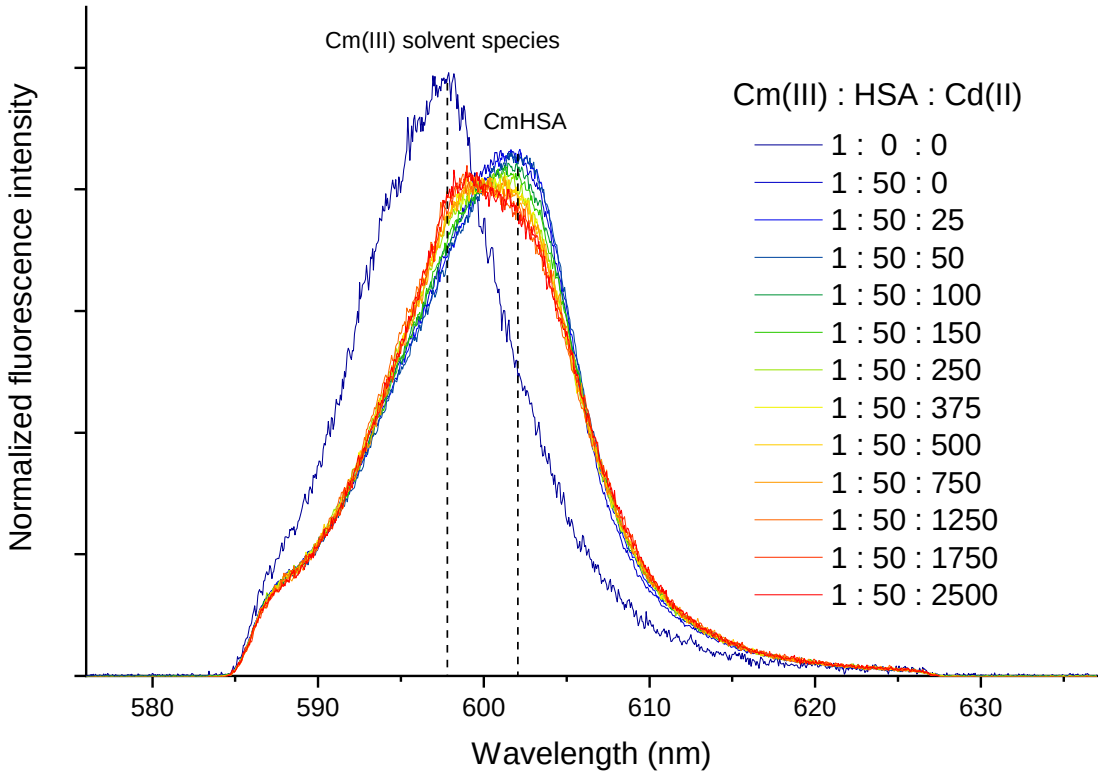

Figure 2.14. The fluorescence spectra of Cm(III) at varying concentrations of HSA and Cd(II) in a 150 mM NaCl solution at pH 8,5 and room temperature. The relative concentrations of Cm(III), HSA, and Cd(II) for the shown spectra are depicted in the figure. The maximum intensity wavelengths of the CmHSA and Cm(III) solvent species are highlighted using dashed lines. [Cm(III)] = $1{,}0 \times 10^{-7}$ M, [HSA] = $0 - 5 \times 10^{-6}$ M, [Cd(II)] = $0 - 1{,}25 \times 10^{-2}$ M.

is commonly interpreted as a sign of complexation and loss of site symmetry (Binnemans 2015). At pH $\geq$ 6,7 the splitting pattern of the F_2 band changes, suggesting a change in the Eu(III) coordination environment, and two fine structure elements can be seen at 612,5 and 614,6 nm. The feature at 612,5 nm is at its maximum intensity at pH 8,0 and the feature at 614,6 nm at pH 8,7. Both features begin to lose intensity as the pH exceeds their respective maximum intensity pH values. The increase in F_2/F_1 ratio and the F_2 band splitting profile observed at pH ≥ 6,7, considering that CmHSA is observed to become the predominant species in the Cm-HSA system at about pH 6,7, indicate complexation of Eu(III) with HSA.

The distribution of Eu(III) species in the presence of HSA as a function of pH was not determined to unambiguity here, as the splitting of emission bands makes it difficult to determine the number of total species and to obtain spectra of the pure components. To

further complicate speciation, Eu(III) reportedly complexes with the buffer molecule TRIS (Pfefferlé & Bünzli 1989). Therefore the spectra are described in qualitative terms only.

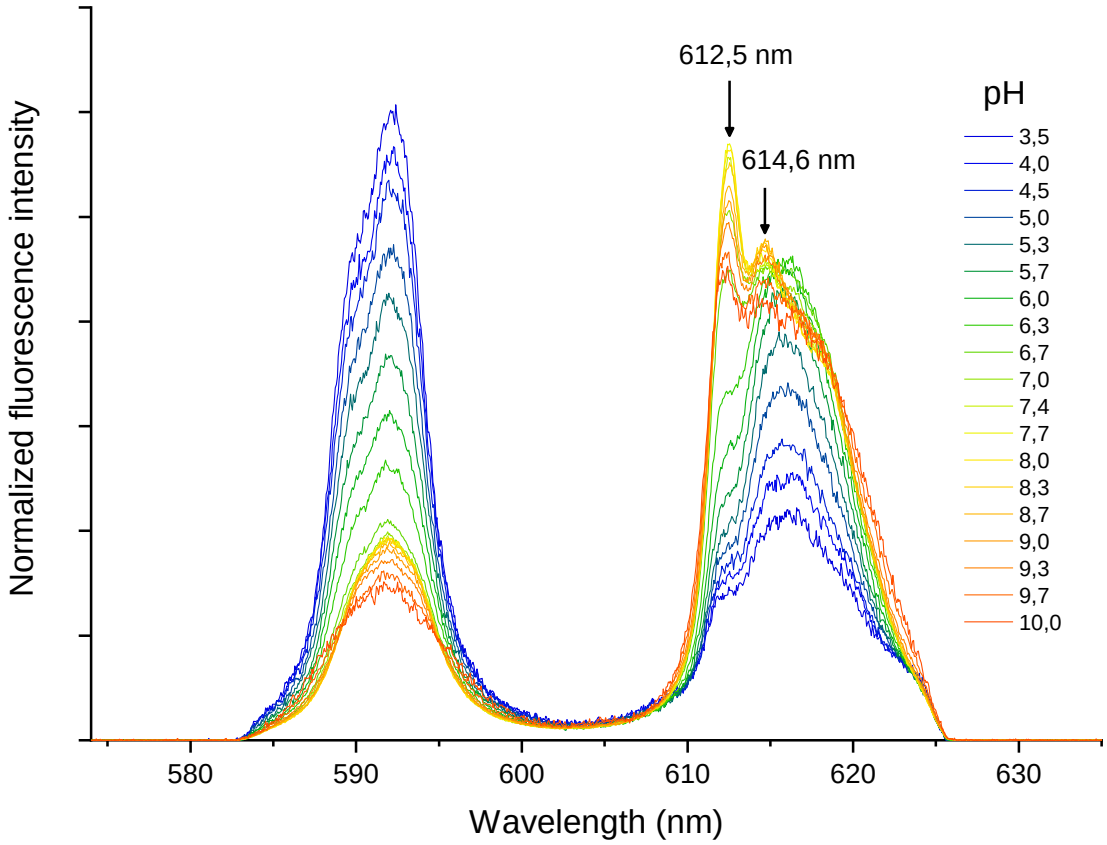

Figure 2.15. The spectra of Eu-HSA system in TRIS buffer at room temperature in the pH range 3,5 – 10,0. Arrows with wavelengths highlight two prominent features of the split F_2 emission band observed at pH ≥ 6,7. [Eu(III)] = 1,0 × 10^{-5} M, [HSA] = 1,8 × 10^{-5} M.

Next, to examine the effect of HSA concentration on Eu(III) fluorescence, Eu(III) was titrated with HSA and spectra were collected in TRIS buffer at pH 8,0 and room temperature. Selected spectra are shown in Figure 2.16. In the absence of HSA, the spectrum represents a Eu(III) solvent species in which the aquo ion and hydrolysis species of Eu(III), and possibly the Eu-TRIS complex, are the component species (Pfefferlé & Bünzli 1989; Plancque *et al.* 2003). A clear change in the fluorescence of Eu(III) is observed immediately with the introduction of HSA. The F_1 emission band at 591,8 nm becomes more symmetric in the presence of HSA relative to the solvent species. Two F_2 emission band fine structure

features appear at 612,5 and 614,6 nm with the addition of HSA. These F_2 transition features match the features seen in the pH titration at pH ≥ 6,7, confirming that their origin is the EuHSA complex.

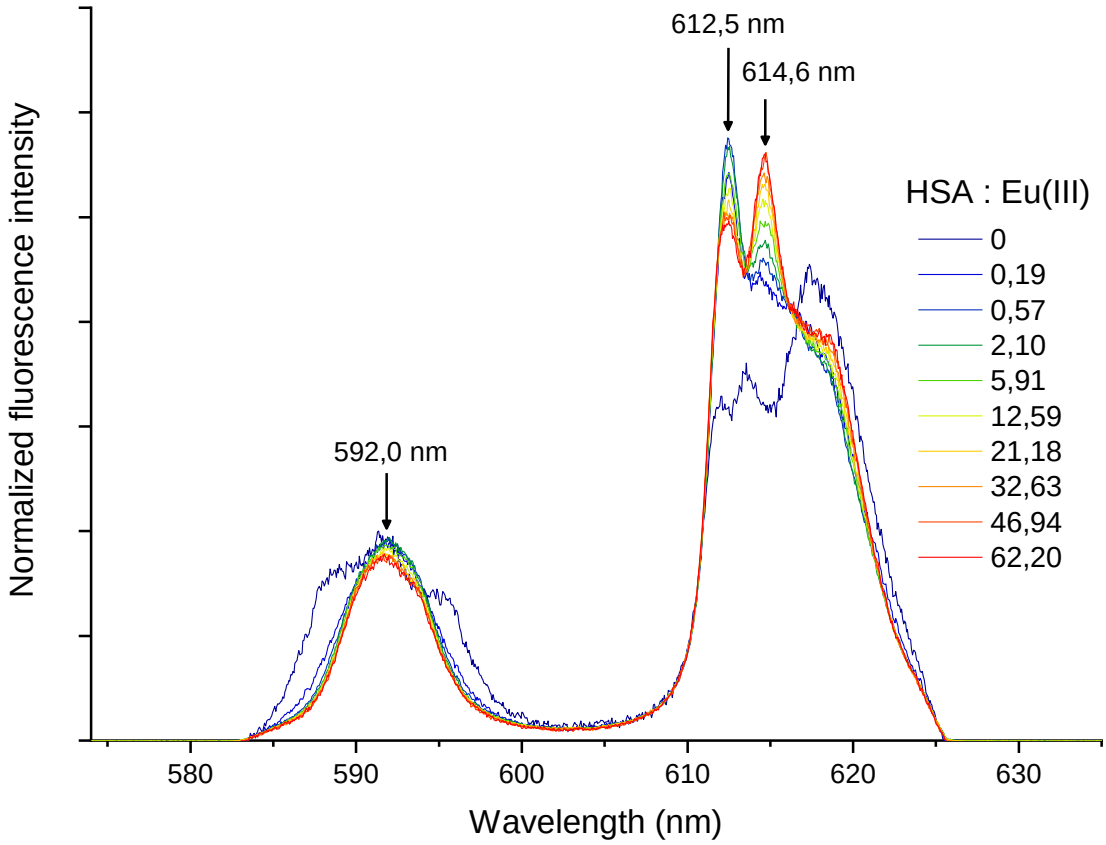

Figure 2.16. Titration of Eu(III) with HSA in TRIS buffer at room temperature and pH 8,0. The Eu:HSA molar ratios for shown spectra are listed in the figure. Arrows with wavelengths indicate the positions of the maxima for the F_1 emission band and the F_2 band fine structure features of EuHSA. [Eu(III)] = 5×10^{-6} M, [HSA] = 0 – $2,7 \times 10^{-4}$ M.

2.3.9. Eu(III) induced transitions in the proton NMR spectrum of HSA

Next, the nature of the Eu-HSA interaction was investigated using NMR. NMR can yield information on the overall fold of the protein as well as specific binding information based on changes in the chemical shift or in the intensity of identifiable resonances. Two chemical shift regions that are of interest in studying protein folding are the amide region at 6 – 10 ppm and the methyl region at −0,5 – 1,5 ppm (McDonald & Phillips 1967; Page *et al.* 2005).

In an unfolded protein most if not all backbone amides and the methyl groups of alanine, valine, leucine, and isoleucine residues are solvent-exposed and therefore have similar chemical shifts. Because of this, the amide and methyl regions of an unfolded protein contain few sharp and distinct peaks. A 1D proton spectrum of HSA was obtained in TRIS buffer at pH 8,0 and 300 K using the WATERGATE pulse sequence (Figure 2.17). The spectrum was used to assess whether HSA was folded or not. The lack of only a few, sharp peaks in the amide and methyl regions in the measured proton NMR spectrum of HSA suggests that the protein is in a folded state.

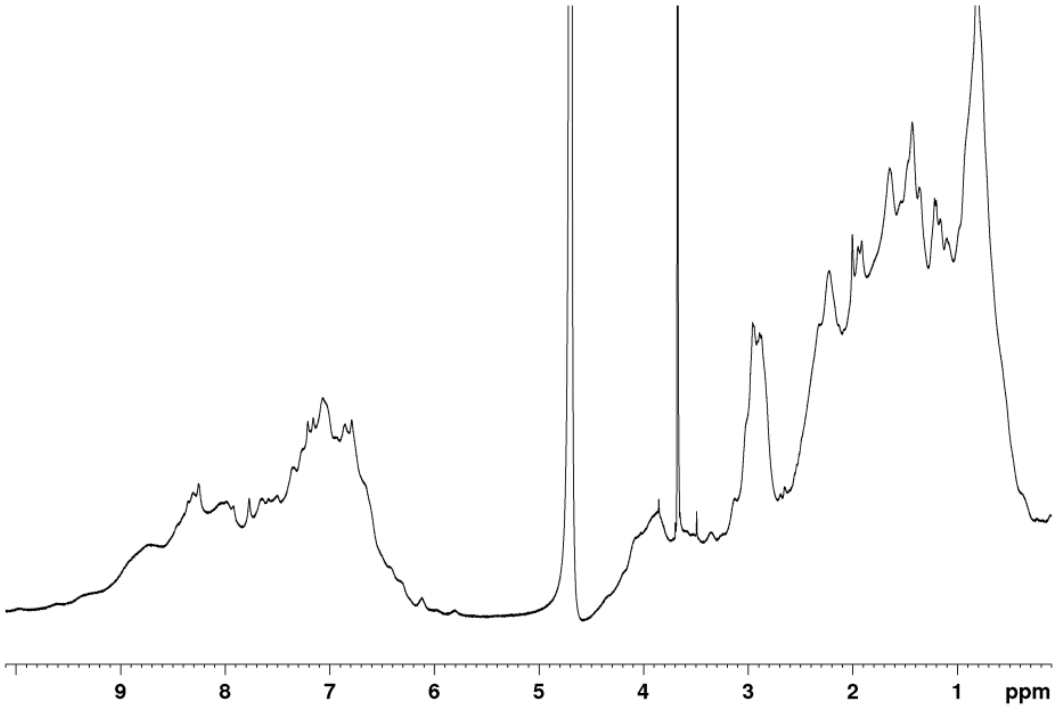

Figure 2.17. Proton NMR spectrum of HSA measured in TRIS buffer at pH 8,0 and 300 K. The signal arising from the protons in the water present in the solvent has been suppressed using the WATERGATE pulse sequence. [HSA] = 1 mM.

The chemical shift range that included the histidine C2 protons was of particular interest, as previous studies have indicated that an NMR resonance at around 7,5 ppm at pH 8,0 can be attributed to the C2 proton of His3 in HSA and that this resonance is sensitive to Cu(II)

complexation at NTS. The sensitivity manifests itself as a considerable decrease of intensity upon Cu(II) binding. (Bos *et al.* 1989). To study the response of the His3 C2 proton resonance to Eu(III), proton spectra of HSA in the presence of zero, one or two molar equivalents of Eu(III) were measured in TRIS buffer at 300 K and pH 8,0. The 7,3 – 7,9 ppm range of the spectra is shown in Figure 2.18. A peak is found at about 7,5 ppm in the absence of Eu(III). The peak is not however observable when one or two molar equivalents of Eu(III) have been added to the sample. The fact that a Eu(III) sensitive peak is observed around 7,5 ppm suggests that HSA binds Eu(III) at the NTS and that the His3 C2 proton resonance is a valid probe for Eu(III), and hence also likely An(III), NTS binding.

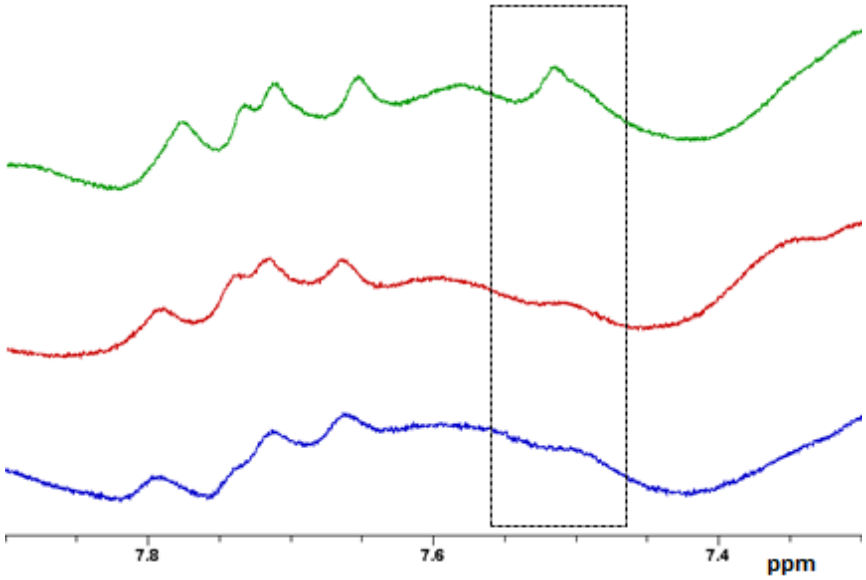

Figure 2.18. Close-up of the 7,3 – 7,9 ppm range of the HSA proton NMR spectrum in the presence and absence of Eu(III). All spectra were measured in TRIS buffer at 300 K and pH 8,0 and the concentration of HSA was 1 mM. The green, red, and blue traces represent spectra acquired in the presence of zero, one or two millimolar Eu(III), respectively. The region that includes the His3 C2 proton resonance has been highlighted with a box.

2.3.10. The nature of the CmHSA complex

Based on the Eu(III) NMR and Cm(III) competitor metal titration results a model can be proposed where the HSA binding locus of trivalent lanthanides and actinides resides in the N-terminus of HSA. This model is supported by published results in which the circular dichroism (CD) and tryptophan fluorescence spectra of HSA were mostly insensitive to the

addition of the trivalent lanthanides Ce(III) and La(III) (Ali *et al.* 2016). The reported results make sense if Ce(III) and La(III) bind at an unstructured site protruding out from the protein (such as the NTS), but not if the binding occurs at a site where binding is coupled to structural rearrangements. Whereas four ligands are provided by HSA for binding of Cu(II) and other divalent transition metals at the NTS (Figure 1.13), the lifetime of CmHSA species measured in this study suggests that five or six non-water ligands are involved in the complexation, so one or two additional ligands are required. The coordination geometry of Cm(III) or Eu(III) bound to HSA will likely deviate from the canonical square planar geometry of the NTS due to the preferred tricapped trigonal prismatic geometry of these f-element ions in their nonahydrated forms. Both Cm(III) and Eu(III) are hard Lewis acids that prefer hard donor atoms such as oxygen, whereas the chemical hardness of Cu(II) is a borderline case (House 2013; Panak & Geist 2013). Therefore, not just the number but also the chemical nature of HSA ligands recruited to complex Cm(III) and Eu(III) will likely differ from those involved in Cu(II) binding at the NTS. Furthermore, both Eu(III) and Cm(III) are trivalent, not divalent like the canonical NTS binding metals, so the involvement of an additional negatively charged ligand seems likely for charge negation purposes. A possible additional ligand could be the sidechain carboxyl group of Asp1, the involvement of which in Cu(II) and Ni(II) binding at the NTS has been suggested (Laussac & Sarker 1984). The sidechain of Lys4, another suggested NTS ligand (Sadler *et al.* 1994), is likely to be protonated and positively charged in the pH range in which CmHSA is a relevant species, and is therefore unlikely to participate in binding (Pace *et al.* 2009). It may also be possible that ligands from HSA residues that are distant from the NTS in primary structure but close to it in tertiary structure are involved in binding.

2.4. Summary and outlook

The interactions between human serum albumin and two trivalent f-elements, the actinide Cm(III) and the lanthanide Eu(III), were investigated with spectroscopic methods in the present study. The binding of Cm(III) by HSA was characterized here for the first time. At room temperature, the CmHSA complex is the dominant species in the pH range 6,7 – 9,7. At physiological temperature and pH, about 90 % of all available Cm(III) is in the CmHSA complex. The measured lifetime of the CmHSA species suggests that five or six coordinating

ligands are present in the first coordination sphere of Cm(III). A conditional stability constant log *K* of 6,8 ± 0,5 was determined for complex formation at pH 8,0. The complexation reaction was determined to be endothermic in nature and entropy-driven. In addition, it was determined that the HSA binding locus of Cm(III) and Eu(III) resides in the N-terminal end of the protein. Cu(II), a metal known to bind HSA at the NTS and the MBS, displaces Cm(III) from HSA. No such effect is observed for Zn(II), a metal that binds HSA at the MBS, suggesting that the NTS is involved in Cm(III) binding. Furthermore, a decrease in NMR resonance assigned to the C2 proton of His3 of HSA is seen upon Eu(III) introduction, exactly what is expected to happen upon metal complexation at the NTS. Based on the competitor metal titration and NMR results a conclusion can be made that trivalent actinides and lanthanides bind HSA at the N-terminus.

The results presented in this study provide a fertile ground for further studies on the interaction between trivalent actinides and human serum albumin. Additional experiments could be performed to further validate the model presented here in which trivalent actinides bind HSA at the N-terminus. An NTS deletion mutant of HSA (i.e. HSA lacking the first three amino acids) could be studied using the TRLFS methods outlined in this study to further validate that the primary binding site of Cm(III) resides at the NTS and also perhaps probe whether a secondary binding site exists. If a secondary binding site was to be found, it could possibly be characterized using the very same methods used here to characterize the NTS. The role of, for example, Asp1 sidechain carboxylate could be examined by mutating Asp1 to an amino acid with a non-charged, non-polar sidechain like glycine or perhaps alanine. Whether protons are released from the Asp1-Ala2 and Ala2-His3 peptide bonds upon Cm(III) binding, as is the case when HSA binds divalent transition metals, could possibly be resolved with potentiometric titrations. In addition to full length HSA, peptide analogues of the NTS could be utilized. The behavior of Cm(III) fluorescence in the presence of NTS mimetic short peptides, such as DAH or DAHK, *N*-methyl amide-conjugated at the C-terminus to prevent complexation at the C-terminal carboxylate, could be established using the methods described in this study and compared with the results obtained when full length HSA was used as the source of ligands. The acquisition of NMR spectra using a higher field instrument using a trivalent lanthanide of ionic radius comparable to Cm(III) or Am(III) as the binding metal could be beneficial and a metal titration of HSA with more

steps than the three (zero, one, and two molar equivalents) used here should be performed. As no structures of HSA, NTS or NTS mimetic peptides with a bound trivalent metal cation are available, the acquisition of one could help solve the binding geometry and the nature of ligands involved in the binding of Cm(III) by the HSA NTS. As peptide analogues of the NTS have been crystallized in the presence of Cu(II) (Camerman *et al.* 1976), the same could be attempted using a trivalent f-element metal cation. Alternatively, the structure could perhaps be resolved using NMR methods, as long as a diamagnetic trivalent f-element representative metal such as La(III) is used, instead of paramagnetic lanthanides or actinides.

The results also paint a tantalizing picture in which HSA, considering its ubiquity in the blood, could facilitate the distribution of trivalent actinides in the human blood and body. To gauge the feasibility of such a scenario, it might be of interest to determine the CmHSA stability constant under more physiological-like conditions. Furthermore, Cm(III) could be introduced into blood samples or a blood simulant, followed by fractionation and analysis by TRLFS, to assess whether CmHSA is a relevant species *in vivo*.

3. References

Aas, W., Steinle, E., Fanghänel Th. & Kim, J.I. Thermodynamics of Cm(III) in Concentrated Electrolyte Solutions. Fluoride Complexation in 0-5 m NaCl at 25°C, *Radiochim. Acta* ***84*** (1999) 85.

Ali, M., Kumar, A., Kumar, M. & Pandey, B.N. The interaction of human serum albumin with selected lanthanide and actinide ions: Binding affinities, protein unfolding and conformational changes, *Biochimie* ***123*** (2016) 117-129.

Altmaier, M., Gaona, X. & Fanghänel, T. Recent Advances in Aqueous Actinide Chemistry and Thermodynamics, *Chem. Rev.* ***113*** 2 (2013) 901-943.

Anraku, M., Chuang, V.T.G., Maruyama, T. & Otagiri, M. Redox properties of serum albumin, *Biochim. Biophys. Acta, Gen. Subj.* ***1830*** 12 (2013) 5465-5472.

Appleton, D.W. & Sarkar, B. The Absence of Specific Copper(II)-binding Site in Dog Albumin: A COMPARATIVE STUDY OF HUMAN AND DOG ALBUMINS, *J. Biol. Chem.* ***246*** 16 (1971) 5040-5046.

Asprey, L.B., Ellinger, F.H., Fried, S. & Zachariasen, W.H. Evidence for quadrivalent curium: x-ray data on curium oxides, *J. Am. Chem. Soc.* ***77*** 6 (1955) 1707-1708.

Asprey, L.B., Ellinger, F.H., Fried, S. & Zachariasen, W.H. Evidence for quadrivalent curium. ii. curium tetrafluoride, *J. Am. Chem. Soc.* ***79*** 21 (1957) 5825.

Atkins, P. & De Paula, J. *Atkins' Physical Chemistry,* 9th ed., W.H. Freeman, Oxford ; New York, 2010.

Atkins, P. & De Paula, J. *Atkins' Physical Chemistry,* 10th ed., Oxford University Press, Oxford, 2014.

Atwood, D.A. *Radionuclides in the Environment,* Wiley, New York, 2010.

Audi, G., Kondev, F.G., Wang, M., Huang, W.J. & Naimi, S. The NUBASE2016 evaluation of nuclear properties, *Chin. Phys. C* ***41*** 3 (2017) 030001.

Aziz, A. & Lyle, S.J. Equilibrium constants for aqueous fluoro complexes of scandium, yttrium, americanium(III) and curium(III) by extraction into di-2-ethylhexyl phosphoric acid, *J. Inorg. Nucl. Chem.* ***31*** 11 (1969) 3471-3480.

Bal, W., Christodoulou, J., Sadler, P.J. & Tucker, A. Multi-metal binding site of serum albumin, *J. Inorg. Biochem.* ***70*** 1 (1998) 33-39.

Bal, W., Sokołowska, M., Kurowska, E. & Faller, P. Binding of transition metal ions to albumin: Sites, affinities and rates, *Biochim. Biophys. Acta, Gen. Subj.****1830*** 12 (2013) 5444-5455.

Bar-Or, D., Gerald, C., Nagaraja, R., Nick, B. & Edward, L. Characterization of the Co2+ and Ni2+ binding amino-acid residues of the N-terminus of human albumin, *Eur. J. Biochem.* ***268*** 1 (2001) 42-48.

Barkleit, A., Wilke, C., Heller, A., Stumpf, T. & Ikeda-Ohno, A. Trivalent f-elements in human saliva: a comprehensive speciation study by time-resolved laser-induced fluorescence spectroscopy and thermodynamic calculations, *Dalton Trans.* ***46*** 5 (2017) 1593-1605.

Barkleit, A., Heller, A., Ikeda-Ohno, A. & Bernhard, G. Interaction of europium and curium with alpha-amylase, *Dalton Trans.* ***45*** 21 (2016) 8724-8733.

Bauer, N., Fröhlich, D.R. & Panak, P. Interaction of Cm(iii) and Am(iii) with human serum transferrin studied by time-resolved laser fluorescence and EXAFS spectroscopy, *Dalton Trans.* ***43*** 18 (2014) 6689-6700.

Bauer, N., Smith, V.C., MacGillivray, R.T.A. & Panak, P.J. Complexation of Cm(iii) with the recombinant N-lobe of human serum transferrin studied by time-resolved laser fluorescence spectroscopy (TRLFS), *Dalton Trans.* ***44*** 4 (2015) 1850-1857.

Beck, H.L. & Bennett, B.G. Historical overview of atmospheric nuclear weapons testing and estimates of fallout in the continental United States, *Health. Phys.* ***82*** 5 (2002) 591-608.

Beitz, J.V., Bowers, D.L., Doxtader, M.M., Maroni, V.A. & Reed, D.T. Detection and Speciation of Transuranium Elements in Synthetic Groundwater via Pulsed-Laser Excitation, *Radiochim. Acta* ***44-45*** (1988) 87.

Beitz, J.V. Laser-induced Fluorescence Studies of Cm3+ Complexes in Solution, *Radiochim. Acta* ***52-53*** (1991) 35.

Beitz, J.V. & Hessler, J.P. Oxidation State Specific Detection of Transuranic Ions in Solution, *Nucl. Technol.* ***51*** 2 (1980) 169-177.

Ben-Bolie, G., Ele Abiama, P. & Owono Ateba, P. Impact of Plant Growth in Waste-Contaminated Areas, in publication *Radionuclide Contamination and Remediation through Plants,* ed(s). Gupta, D.K. & Walther, C., Springer International Publishing, Cham, 2014, 139-160.

Bhattacharya, A.A., Grüne, T. & Curry, S. Crystallographic analysis reveals common modes of binding of medium and long-chain fatty acids to human serum albumin, *J. Mol. Biol.* ***303*** 5 (2000) 721-732.

Binnemans, K. Interpretation of europium(III) spectra, *Coord. Chem. Rev.* ***295*** (2015) 1-45.

Birkett, D.J., Myers, S.P. & Sudlow, G. Effects of Fatty Acids on Two Specific Drug Binding Sites on Human Serum Albumin, *Mol. Pharmacol.* ***13*** 6 (1977) 987-992.

Bonanata, J., Turell, L., Antmann, L., Ferrer-Sueta, G., Botasini, S., Méndez, E., Alvarez, B. & Coitiño, E.L. The thiol of human serum albumin: Acidity, microenvironment and mechanistic insights on its oxidation to sulfenic acid, *Free Radical Biol. Med.* ***108*** (2017) 952-962.

Boocock, G. & Popplewell, D.S. In vitro Distribution of Americium in Human Blood Serum Proteins, *Nature* ***210*** (1966) 1283.

Bos, O.J., Labro, J.F., Fischer, M.J., Wilting, J. & Janssen, L.H. The molecular mechanism of the neutral-to-base transition of human serum albumin. Acid/base titration and proton nuclear magnetic resonance studies on a large peptic and a large tryptic fragment of albumin. *J. Biol. Chem.* ***264*** 2 (1989) 953-959.

Bruno, J., Cera, E., Duro, L., Jordana, S., Pablo, J. & Savage, D. Determination of radionuclide solubility limits to be used in SR 97 Uncertainties associated to calculated solubilities, (1997)

Bruynesteyn, A. Mineral biotechnology, *J. Biotechnol.* ***11*** 1 (1989) 1-10.

Buckau, G., Kim, J.I., Klenze, R., Rhee, D.S. & Wimmer, H. A Comparative Spectroscopic Study of the Fulvate Complexation of Trivalent Transuranium Ions, *Radiochim. Acta* ***57*** (1992) 105.

Camerman, N., Sarkar, B. & Camerman, A. Molecular design to mimic the copper(II) transport site of human albumin. The crystal and molecular structure of copper(II) - glycylglycyl-L-histidine-N-methyl amide monoaquo complex, *Can. J. Chem.* ***54*** 8 (1976) 1309-1316.

Campbell, J.A., Stromatt, R.W., Smith, M.R., Bean, R.M., Jones, T.E. & Strachan, D.M. Organic Analysis at the Hanford Nuclear Site, *Anal. Chem.* ***66*** 24 (1994) 1215A.

Carnall, W.T., Fields, P.R. & Rajnak, K. Electronic Energy Levels of the Trivalent Lanthanide Aquo Ions. II. Gd3+, *J. Chem. Phys.* ***49*** 10 (1968a) 4443-4446.

Carnall, W.T., Fields, P.R. & Rajnak, K. Electronic Energy Levels of the Trivalent Lanthanide Aquo Ions. IV. Eu3+, *J. Chem. Phys.* ***49*** 10 (1968b) 4450-4455.

Carnall, W.T. & Rajnak, K. Electronic energy level and intensity correlations in the spectra of the trivalent actinide aquo ions. II. Cm3+ , *J. Chem. Phys.* ***63*** 8 (1975) 3510-3514.

Cavellec, R., Lucas, C., Simoni, E., Hubert, S. & Edelstein, N. Structural Characterization of Sorption Complexes of Cm(III) at the Phosphate Minerals-Solution Interface Using Laser Spectrofluorimetry, *Radiochim. Acta* ***82*** (1998) 221.

Cernochova, K., Mathur, J.N. & Choppin, G.R. Chemical speciation of Am, Cm and Eu with EDTA at high ionic strength: thermodynamics and laser fluorescence spectroscopy studies, *Radiochim. Acta* ***93*** (2009) 733.

Chatwal, G.R. & Anand, S.K. *Spectroscopy : Atomic and Molecular,* Global Media, Mumbai, 2008.

Chipperfield, A.R. & Taylor, D.M. Binding of Plutonium and Americium to Bone Glycoproteins, *Nature* ***219*** (1968) 609.

Choppin, G., Liljenzin, J., Rydberg, J. & Ekberg, C. *Radiochemistry and Nuclear Chemistry*, 4th ed., Elsevier, Saint Louis, 2013.

Christelle, H., Eury, H., Guillot, R., Christian, B., Sayen, S., Solari, P., Emmanuel, G., Peter, F. & Pierre, D. X-ray and Solution Structures of Cu(II)GHK and Cu(II)DAHK Complexes: Influence on Their Redox Properties, *Chem. Eur. J.* ***17*** 36 (2011) 10151-10160.

Chung, KH., Klenze, R., Park, KK., Paviet-Hartmann, P. & Kim, J.I. A Study of the Surface Sorption Process of Cm(III) on Silica by Time-Resolved Laser Fluorescence Spectroscopy (I), *Radiochim. Acta* ***82*** (1998) 215.

Collins, R.N., Saito, T., Aoyagi, N., Payne, T.E., Kimura, T. & Waite, T.D. Applications of Time-Resolved Laser Fluorescence Spectroscopy to the Environmental Biogeochemistry of Actinides, *J. Environ. Qual.* ***40*** 3 (2011) 731-741.

Colombo, M.F., Austrilino, L., Nascimento, O.R., Castellano, E.E. & Tabak, M. On the interaction of copper with tris(hydroxymethyl)aminomethane, *Can. J. Chem.* ***65*** 4 (1987) 821-826.

Correia, I., Jakusch, T., Cobbinna, E., Mehtab, S., Tomaz, I., Nagy, N.V., Rockenbauer, A., Costa Pessoa, J. & Kiss, T. Evaluation of the binding of oxovanadium(iv) to human serum albumin, *Dalton Trans.* ***41*** 21 (2012) 6477-6487.

Cotton, S. *Lanthanide and Actinide Chemistry,* John Wiley & Sons, Chichester, 2006.

Courdouan, A., Christl, I., Meylan, S., Wersin, P. & Kretzschmar, R. Characterization of dissolved organic matter in anoxic rock extracts and in situ pore water of the Opalinus Clay, *Appl. Geochem.* ***22*** 12 (2007a) 2926-2939.

Courdouan, A., Christl, I., Meylan, S., Wersin, P. & Kretzschmar, R. Isolation and characterization of dissolved organic matter from the Callovo–Oxfordian formation, *Appl. Geochem.* ***22*** 7 (2007b) 1537-1548.

Curry, S., Mandelkow, H., Brick, P. & Franks, N. Crystal structure of human serum albumin complexed with fatty acid reveals an asymmetric distribution of binding sites, *Nat. Struct. Biol.* ***5*** (1998) 827.

Czerwinski, KR., Kim, J.I., Rhee, D.S. & Buckau, G. Complexatíon of Trivalent Actinide Ions (Am3+, Cm3+) with Humic Acid: The Effect of Ionic Strength, *Radiochim. Acta* ***72*** (1996) 179.

D'Angelo, P., Martelli, F., Spezia, R., Filipponi, A. & Denecke, M.A. Hydration Properties and Ionic Radii of Actinide(III) Ions in Aqueous Solution, *Inorg. Chem.* ***52*** 18 (2013) 10318-10324.

David, F. Thermodynamic properties of lanthanide and actinide ions in aqueous solution, *J. Less-Common Met.* ***121*** (1986) 27-42.

David, F.H. & Vokhmin, V. Thermodynamic properties of some tri- and tetravalent actinide aquo ions, *New. J. Chem.* ***27*** 11 (2003) 1627-1632.

de Bettencourt-Dias, A. Introduction to Lanthanide Ion Luminescence, in publication *Luminescence of Lanthanide Ions in Coordination Compounds and Nanomaterials,* ed(s). de Bettencourt-Dias, A., Wiley, Chichester, 2014.

de Carvalho, R.G. & Choppin, G.R. Lanthanide and actinide sulfate complexes—I: Determination of stability constants, *J. Inorg. Nucl. Chem.* ***29*** 3 (1967) 725-735.

Dixon, J.W. & Sarkar, B. Isolation, Amino Acid Sequence and Copper(II)-binding Properties of Peptide (1-24) of Dog Serum Albumin, *J. Biol. Chem.* ***249*** 18 (1974) 5872-5877.

Dodson, C.M. & Zia, R. Magnetic dipole and electric quadrupole transitions in the trivalent lanthanide series: Calculated emission rates and oscillator strengths, *Phys. Rev. B* ***86*** 12 (2012) 125102.

Domínguez-Gadea, L., Cerezo, L. Decontamination of radioisotopes. *Rep. Pract. Oncol. Radiother*. ***16*** 4 (2011) 147-52.

Domino, E.F., Krause, R.R., Thiessen, M.M. & Batsakis, J.G. Blood protein fraction comparisons of normal and schizophrenic patients, *Arch. Gen. Psychiatry,* ***32*** 6 (1975) 717-721.

Duff, M.R. & Kumar, C.V. Site-Selective Photocleavage of Proteins by Uranyl Ions, *Angew. Chem.* ***118*** 1 (2006) 143-145.

Dugaiczyk, A., Law, S.W. & Dennison, O.E. Nucleotide sequence and the encoded amino acids of human serum aibumin mRNA, *Proc. Natl. Acad. Sci. USA* ***79*** 6 (1982) 2124.

Durbin, P.W. Actinides in Animals and Man, in publication *The Chemistry of the Actinide and Transactinide Elements,* ed(s). Morss, L.R., Edelstein, N.M. & Fuger, J., Springer Netherlands, Dordrecht, 2006.

Dutkiewicz, M.S., Apostolidis, C., Walter, O. & Arnold, P.L. Reduction chemistry of neptunium cyclopentadienide complexes: from structure to understanding, *Chem. Sci.* ***8*** 4 (2017) 2553-2561.

Edelstein, N.M. Comparison of the electronic structure of the lanthanides and actinides, *J. Alloys Compd.* ***223*** 2 (1995) 197-203.

Edelstein, N.M., Fuger, J., Katz, J.J. & Morss, L.R. Summary and Comparison of Properties of the Actinide and Transactinide Elements, in publication *The Chemistry of the Actinide and Transactinide Elements,* ed(s). Morss, L.R., Edelstein, N.M. & Fuger, J., Springer Netherlands, Dordrecht, 2011.

Edelstein, N.M., Klenze, R., Fanghänel, T. & Hubert, S. Optical properties of Cm(III) in crystals and solutions and their application to Cm(III) speciation, *Coord. Chem. Rev.* ***250*** 7–8 (2006) 948-973.

Eikenberg, J., Beer, H. & Bajo, S. Anthropogenic radionuclide emissions into the environment, *Spec. Publ. – Geol. Soc. London* ***236*** 1 (2004) 143-151.

Eisenbud, M. & Gesell, T.F. *Environmental Radioactivity from Natural, Industrial & Military Sources: From Natural, Industrial and Military Sources*, 4th ed., Academic Press, San Diego, 1997.

Engel, T. & Reid, P. *Physical Chemistry,* 3rd ed., Pearson, Harlow, Essex, 2014.

Fanali, G., Cao, Y., Ascenzi, P. & Fasano, M. Mn(II) binding to human serum albumin: A 1H-NMR relaxometric study, *J. Inorg. Biochem.* ***117*** (2012) 198-203.

Fanali, G., di Masi, A., Trezza, V., Marino, M., Fasano, M. & Ascenzi, P. Human serum albumin: From bench to bedside, *Mol. Aspects Med.* ***33*** 3 (2012) 209-290.

Fanali, G., Fesce, R., Agrati, C., Ascenzi, P. & Fasano, M. Allosteric modulation of myristate and Mn(III)heme binding to human serum albumin, *FEBS J* ***272*** 18 (2005) 4672-4683.

Fanghänel, T., Weger, HT, Könnecke Th., Neck, V., Paviet-Hartmann, P., Steinle, E. & Kim, J.I. Thermodynamics of Cm(III) in Concentrated Electrolyte Solutions. Carbonate Complexation at Constant Ionic Strength (1 m NaCl), *Radiochim. Acta* ***82*** (1998) 47.

Fanghänel, T., Kim, J.I., Paviet, P., Klenze, R. & Hauser, W. Thermodynamics of Radioactive Trace Elements in Concentrated Electrolyte Solutions: Hydrolysis of Cm3+ in NaCl-Solutions, *Radiochim. Acta* ***66-67*** (1994) 81.

Fanghänel, T., Könnecke, T., Weger, H., Paviet-Hartmann, P., Neck, V. & Kim, J.I. Thermodynamics of Cm(III) in Concentrated Salt Solutions: Carbonate Complexation in NaCl Solution at 25°C, *J. Solution Chem.* ***28*** 4 (1999) 447-462.

Fanghänel, T., Kim, J.I., Klenze, R. & Kato, Y. Formation of Cm(III) chloride complexes in CaCl2 solutions, *J. Alloys Compd.* ***225*** 1 (1995) 308-311.

Flora, S.J.S. & Pachauri, V. Chelation in Metal Intoxication, *Int. J. Environ. Res. Public Health* ***7*** 7 (2010) 2745-2788.

Francis, A.J. Biotransformation of uranium and other actinides in radioactive wastes, *J. Alloys Compd.* ***271-273*** (1998) 78-84.

Francis, A.J., Gillow, J.B., Dodge, C.J., Dunn, M., Mantione, K., Strietelmeier, B.A., Pansoy-Hjelvik, ME. & Papenguth, H.W. Role of Bacteria as Biocolloids in the Transport of Actinides from a Deep Underground Radioactive Waste Repository, *Radiochim. Acta* ***82*** (1998) 347.

Fröhlich, D.R., Skerencak-Frech, A. & Panak, P.J. A spectroscopic study on the formation of Cm(iii) acetate complexes at elevated temperatures, *Dalton Trans.* ***43*** 10 (2014) 3958-3965.

Gabriella, F., Alessio, B., Paolo, A. & Mauro, F. Modulation of heme and myristate binding to human serum albumin by anti-HIV drugs, *FEBS J* ***274*** 17 (2007) 4491-4502.

García-Olivares, A. & Iranzo, C.E. Resuspension and transport of plutonium in the Palomares area, *J. Environ. Radioact.* ***37*** 1 (1997) 101-114.

Garland, J.A. & Wakeford, R. Atmospheric emissions from the Windscale accident of October 1957, *Atmos. Environ.* ***41*** 18 (2007) 3904-3920.

Ghuman, J., Zunszain, P.A., Petitpas, I., Bhattacharya, A.A., Otagiri, M. & Curry, S. Structural Basis of the Drug-binding Specificity of Human Serum Albumin, *J. Mol. Biol.* ***353*** 1 (2005) 38-52.

Gill, S.C. & von Hippel, P.H. Calculation of protein extinction coefficients from amino acid sequence data, *Anal. Biochem.* ***182*** 2 (1989) 319-326.

Giroux, E.L. & Henkin, R.I. Competition for zinc among serum albumin and amino acids, *Biochim. Biophys. Acta, Gen. Subj.****273*** 1 (1972) 64-72.

Gray, S.A., Pearce, M.J., Stradling, G.N., Wilson, I., Hodgson, A. & Isaacs, K.R. Optimising the removal of inhaled plutonium and americium from the rat by administration of ZnDTPA in drinking water, *Hum. Exp. Toxicol.* ***14*** 11 (1995) 902-908.

Grenthe, I. On the Stability of the Acetate and Glycolate Complexes of Trivalent Curium, *Acta Chem. Scand.* ***17*** (1963) 1814-1815.

Griffiths, T.L., Martin, L.R., Zalupski, P.R., Rawcliffe, J., Sarsfield, M.J., Evans, N.D.M. & Sharrad, C.A. Understanding the Solution Behavior of Minor Actinides in the Presence of EDTA4–, Carbonate, and Hydroxide Ligands, *Inorg. Chem.* ***52*** 7 (2013) 3728-3737.

Haigh, C.W. The Theory of Atomic Spectroscopy: jj Coupling, Intermediate Coupling, and Configuration Interaction, *J. Chem. Educ.* ***72*** 3 (1995) 206.

Handing, K.B., Shabalin, I.G., Kassaar, O., Khazaipoul, S., Blindauer, C.A., Stewart, A.J., Chruszcz, M. & Minor, W. Circulatory zinc transport is controlled by distinct interdomain sites on mammalian albumins, *Chem. Sci.* ***7*** 11 (2016) 6635-6648.

Harford, C. & Sarkar, B. Amino Terminal Cu(II)- and Ni(II)-Binding (ATCUN) Motif of Proteins and Peptides: Metal Binding, DNA Cleavage, and Other Properties, *Acc. Chem. Res.* ***30*** 3 (1997) 123-130.

Harris, N.S. & Winter, W.E. *Multiple Myeloma and Related Serum Protein Disorders: An Electrophoretic Guide,* Demos Medical, New York, NY, 2012.

Hayashi, T., Era, S., Kawai, K., Imai, H., Nakamura, K., Onda, E. & Yoh, M. Observation for redox state of human serum and aqueous humor albumin from patients with senile cataract, *Pathophysiology* ***6*** 4 (2000) 237-243.

He, X.M. & Carter, D.C. Atomic structure and chemistry of human serum albumin, *Nature* ***358*** (1992) 209.

Heller, A., Barkleit, A. & Bernhard, G. Chemical Speciation of Trivalent Actinides and Lanthanides in Biological Fluids: The Dominant in Vitro Binding Form of Curium(III) and Europium(III) in Human Urine, *Chem Res Toxicol* ***24*** 2 (2011) 193-203.

Heller, A., Barkleit, A., Foerstendorf, H., Tsushima, S., Heim, K. & Bernhard, G. Curium(iii) citrate speciation in biological systems: a europium(iii) assisted spectroscopic and quantum chemical study, *Dalton Trans.* ***41*** 45 (2012) 13969-13983.

Högberg, L. Root Causes and Impacts of Severe Accidents at Large Nuclear Power Plants, *Ambio* ***42*** 3 (2013) 267-284.

House, J.E. *Inorganic Chemistry,* 2. ed., Academic Press, Waltham, MA, 2013.

Huang, H., Chaudhary, S. & Van Horn, J.D. Uranyl−Peptide Interactions in Carbonate Solution with DAHK and Derivatives, *Inorg. Chem.* ***44*** 4 (2005) 813-815.

Hudson, M.J., Harwood, L.M., Laventine, D.M. & Lewis, F.W. Use of Soft Heterocyclic N-Donor Ligands To Separate Actinides and Lanthanides, *Inorg. Chem.* ***52*** 7 (2013) 3414-3428.

Huittinen, N., Rabung, T., Lützenkirchen, J., Mitchell, S.C., Bickmore, B.R., Lehto, J. & Geckeis, H. Sorption of Cm(III) and Gd(III) onto gibbsite, α-Al(OH)3: A batch and TRLFS study, *J. Colloid Interface Sci.* ***332*** 1 (2009) 158-164.

Huittinen, N., Thomas, R., Andrieux, P., Jukka, L. & Geckeis, H. A comparative batch sorption and time-resolved laser fluorescence spectroscopy study on the sorption of Eu(III) and Cm(III) on synthetic and natural kaolinite, *Radiochim. Acta* ***98*** (2010) 613.

Hunt, G.J. & Smith, B.D. The radiological impact of actinides discharged to the Irish Sea, *J. Environ. Radioact.* ***44*** 2 (1999) 389-403.

Hänsch T.W. Repetitively Pulsed Tunable Dye Laser for High Resolution Spectroscopy, *Appl. Opt.* ***11*** 4 (1972) 895-898.

Ikäheimonen, T.K., Ilus, E., Klemola, S., Dahlgaard, H., Ryan, T. & Eriksson, M. Plutonium and americium in the sediments off the Thule air base, Greenland, *J. Radioanal. Nucl.* ***252*** 2 (2002) 339-344.

Ivanov, A.I., Christodoulou, J., Parkinson, J.A., Barnham, K.J., Tucker, A., Woodrow, J. & Sadler, P.J. Cisplatin Binding Sites on Human Albumin, *J. Biol. Chem.* ***273*** 24 (1998) 14721-14730.

Jones, S. Windscale and Kyshtym: a double anniversary, *J. Environ. Radioact.* ***99*** 1 (2008) 1-6.

Kaltsoyannis, N. & Scott, P. *The f Elements,* Oxford university press, Oxford, 1999.

Karmel, S.I., Batrice, J.R. & Eisen, S.M. Catalytic Organic Transformations Mediated by Actinide Complexes, *Inorganics* ***3*** 4 (2015) 392-428.

Karpas, Z. *Analytical Chemistry of Uranium: Environmental, Forensic, Nuclear, and Toxicological Applications,* CRC Press, Boca Raton, 2015.

Kassaar, O., Schwarz-Linek, U., Blindauer, C.A. & Stewart, A.J. Plasma free fatty acid levels influence Zn2+-dependent histidine-rich glycoprotein–heparin interactions via an allosteric switch on serum albumin, *J. Thromb. Haemost.* ***13*** 1 (2015) 101-110.

Keenan, T.K. First observation of aqueous tetravalent curium, *J. Am. Chem. Soc.* ***83*** 17 (1961) 3719-3720.

Khopkar, P.K. & Mathur, J.N. Thiocyanate complexing of some trivalent actinides and lanthanides, *J. Inorg. Nucl. Chem.* ***36*** 12 (1974) 3819-3825.

Khopkar, P.K. & Mathur, J.N. Complexing of californium(III) and other trivalent actinides by inorganic ligands, *J. Inorg. Nucl. Chem.* ***42*** 1 (1980) 109-113.

Kim, J.I., Wimmer, H. & Klenze, R. A Study of Curium(III) Humate Complexation by Time Resolved Laser Fluorescence Spectroscopy (TRLFS), *Radiochim. Acta* ***54*** (1991) 35.

Kimura, T. & Choppin, G.R. Luminescence study on determination of the hydration number of Cm(III), *J. Alloys Compd.* ***213*** (1994) 313-317.

Kimura, T., Choppin, G.R., Yoshiharu, K. & Zenko, Y. Determination of the Hydration Number of Cm(III) in Various Aqueous Solutions, *Radiochim. Acta* ***72*** (1996) 61.

Kimura, T., Kato, Y., Takeishi, H. & Choppin, G.R. Comparative study on the hydration states of Cm(III) and Eu(III) in solution and in cation exchange resin, *J. Alloys Compd.* ***271*** (1998) 719-722.

Könnecke, T., Fanghänel, T. & Kim, J.I. Thermodynamics of Trivalent Actinides in Concentrated Electrolyte Solutions: Modelling the Chloride Complexation of Cm(III), *Radiochim. Acta* ***76*** (1997) 131.

Kragh-Hansen, U. Molecular and practical aspects of the enzymatic properties of human serum albumin and of albumin–ligand complexes, *Biochim. Biophys. Acta, Gen. Subj.****1830*** 12 (2013) 5535-5544.

Kragh-Hansen, U. Human Serum Albumin: A Multifunctional Protein, in publication *Albumin in Medicine: Pathological and Clinical Applications,* ed(s). Otagiri, M. & Chuang, V.T.G., Springer Singapore, Singapore, 2016.

Kragh-Hansen, U., Watanabe, H., Nakajou, K., Iwao, Y. & Otagiri, M. Chain Length-dependent Binding of Fatty Acid Anions to Human Serum Albumin Studied by Site-directed Mutagenesis, *J. Mol. Biol.* ***363*** 3 (2006) 702-712.

Krey, P.W. Atmospheric Burnup of a Plutonium-238 Generator, *Science* ***158*** 3802 (1967) 769-771.

Krey, P.W., Leifer, R., Benson, W.K., Dietz, L.A., Hendrikson, H.C. & Coluzza, J.L. Atmospheric Burnup of the Cosmos-954 Reactor, *Science* ***205*** 4406 (1979) 583-585.

Kumar, V., Goel, R., Chawla, R., Silambarasan, M., Sharma, R.K. Chemical, biological, radiological, and nuclear decontamination: Recent trends and future perspective. *J. Pharm. Bioallied Sci*. ***2*** 3 (2010) 220-38.

Laussac, J.P. & Sarker, B. Characterization of the copper(II) and nickel(II) transport site of human serum albumin. Studies of copper(II) and nickel(II) binding to peptide 1-24 of human serum albumin by carbon-13 and proton NMR spectroscopy, *Biochemistry (NY)* ***23*** 12 (1984) 2832-2838.

Lehto, J. & Hou, X. *Chemistry and Analysis of Radionuclides: Laboratory Techniques and Methodology,* Wiley-VCH, US, 2010.

Lewenstein M., Balcou P., Ivanov M.Y., L'Huillier A. & Corkum P.B. Theory of high-harmonic generation by low-frequency laser fields, *Phys. Rev. A* ***49*** 3 (1994) 2117-2132.

Li, Y., Yan, X., Chen, Xia, Y. & Jiang, Y. Human Serum Albumin−Mercurial Species Interactions, *J. Proteome. Res.* ***6*** 6 (2007) 2277-2286.

Lindqvist-Reis, P., Apostolidis, C., Rebizant, J., Morgenstern, A., Klenze, R., Walter, O., Fanghänel, T. & Haire, R. The Structures and Optical Spectra of Hydrated Transplutonium Ions in the Solid State and in Solution, *Angew. Chem. Int. Ed.* ***46*** 6 (2007) 919-922.

Lindqvist-Reis, P., Klenze, R., Schubert, G. & Fanghänel, T. Hydration of Cm3+ in Aqueous Solution from 20 to 200 °C. A Time-Resolved Laser Fluorescence Spectroscopy Study, *J. Phys. Chem. B* ***109*** 7 (2005) 3077-3083.

Lindqvist-Reis, P., Walther, C., Klenze, R. & Edelstein, N.M. Optical Spectra and Crystal-Field Levels of Cm(H2O)9]3+ Ions with C3h Symmetry in Isotypic Rare-Earth Triflate and Ethyl Sulfate Salts, *J. Phys. Chem. C* ***113*** 1 (2009) 449-458.

Lindqvist-Reis, P., Walther, C., Klenze, R., Eichhöfer, A. & Fanghänel, T. Large Ground-State and Excited-State Crystal Field Splitting of 8-fold-Coordinate Cm3+ in Y(H2O)8]Cl3·15-crown-5, *J. Phys. Chem. B* ***110*** 11 (2006) 5279-5285.

Lloyd, J.R., Chesnes, J., Glasauer, S., Bunker, D.J., Livens, F.R. & Lovley, D.R. Reduction of Actinides and Fission Products by Fe(III)-Reducing Bacteria, *Geomicrobiol. J.* ***19*** 1 (2002) 103-120.

Lloyd, R.D., Atherton, D.R., Mays, C.W., McFarland, S.S. & Williams, J.L. The Early Excretion, Retention and Distribution of Injected Curium Citrate in Beagles, *Health. Phys.* ***27*** 1 (1974).

Lo Sasso, T., Cohen, N. & Wrenn, M.E. Distribution and Retention of ^{243,244}Cm in the Adult Baboon, *Radiat. Res.* ***85*** 1 (1981) 173-183.

Lu, J., Stewart, A.J., Sleep, D., Sadler, P.J., Pinheiro, T.J.T. & Blindauer, C.A. A Molecular Mechanism for Modulating Plasma Zn Speciation by Fatty Acids, *J. Am. Chem. Soc.* ***134*** 3 (2012) 1454-1457.

Lumetta, G.J., Thompson, M.C., Penneman, R.A. & Eller, P.G. Curium, in publication *The Chemistry of the Actinide and Transactinide Elements,* ed(s). Morss, L.R., Edelstein, N.M. & Fuger, J., Springer Netherlands, Dordrecht, 2011.

MacDonald, M.R., Fieser, M.E., Bates, J.E., Ziller, J.W., Furche, F. & Evans, W.J. Identification of the +2 Oxidation State for Uranium in a Crystalline Molecular Complex, K(2.2.2-Cryptand)](C5H4SiMe3)3U], *J. Am. Chem. Soc.* ***135*** 36 (2013) 13310-13313.

Marjolaine, R., Philippe, R., Singh, N.R., Evelyne, T. & Emmanuel, B. The antioxidant properties of serum albumin, *FEBS Lett.* ***582*** 13 (2008) 1783-1787.

Markus, G. & Karush, F. The Disulfide Bonds of Human Serum Albumin and Bovine γ-Globulin1, *J. Am. Chem. Soc.* ***79*** 1 (1957) 134-139.

Maruyama, K., Nishigoro, H. & Iwatsuru, M. Characterization of the Benzodiazepine Binding Site (Diazepam Site) on Human Serum Albumin, *Chem. Pharm. Bull.* ***33*** 11 (1985) 5002-5012.

Masaru, S., Seiichi, E., Shunji, N., Kazuo, K., Kimihiro, K., Kiyoshi, M., Hiroshi, I., Eiji, S., Shigeo, H. & Shigeki, S. HPLC-studies on nonmercapt-mercapt conversion of human serum albumin, *Int. J. Pept. Protein. Res.* ***25*** 4 (1985) 398-402.

Masuoka, J. & Saltman, P. Zinc(II) and copper(II) binding to serum albumin. A comparative study of dog, bovine, and human albumin. *J. Biol. Chem.* ***269*** 41 (1994) 25557-25561.

Mathur, J.N., Cernochova, K. & Choppin, G.R. Thermodynamics and laser luminescence spectroscopy of binary and ternary complexation of Am3+, Cm3+ and Eu3+ with citric acid, and citric acid+EDTA at high ionic strength, *Inorg. Chim. Acta* ***360*** 6 (2007) 1785-1791.

Mathur, J.N., Thakur, P., Dodge, C.J., Francis, A.J. & Choppin, G.R. Coordination Modes in the Formation of the Ternary Am(III), Cm(III), and Eu(III) Complexes with EDTA and NTA: TRLFS, 13C NMR, EXAFS, and Thermodynamics of the Complexation, *Inorg. Chem.* ***45*** 20 (2006) 8026-8035.

Mauro, F., Stephen, C., Enzo, T., Monica, G., Gabriella, F., Pasquale, N., Stefania, N. & Paolo, A. The extraordinary ligand binding properties of human serum albumin, *IUBMB Life* ***57*** 12 (2008) 787-796.

Mboulou, M.O., Hurtgen, C., Hofkens, K. & Vandecasteele, C. Vertical distributions in the Kapachi soil of the plutonium isotopes (238Pu, 239,240Pu, 241Pu), of 241Am, and of 243,244Cm, eight years after the Chernobyl accident, *J. Environ. Radioact.* ***39*** 3 (1998) 231-237.

McClellan, R.O., Boyd, H.A., Gallegos, A.F. & Thomas, R.G. Retention and Distribution of ^{244}Cm Following Inhalation of $^{244}CmCl_3$ and $^{244}CmO_{1.73}$ by Beagle Dogs, *Health. Phys.* ***22*** 6 (1972) .

McDonald, C.C. & Phillips, W.D. Manifestations of the tertiary structures of proteins in high-frequency nuclear magnetic resonance, *J. Am. Chem. Soc.* ***89*** 24 (1967) 6332.

McDowell, W.J. & Coleman, C.F. The sulfate complexes of some trivalent transplutonium actinides and europium, *J. Inorg. Nucl. Chem.* ***34*** 9 (1972) 2837-2850.

Means, J.L. & Alexander, C.A. The environmental biogeochemistry of chelating agents and recommendations for the disposal of chelated radioactive wastes, *Nucl. Chem. Waste Manage.* ***2*** 3 (1981) 183-196.

Meinrath, G. & Kim, J.I. The Carbonate Complexation of the Am(III) Ion, *Radiochim. Acta* ***52-53*** (1991) 29.

Meloun, B., Morávek, L. & Kostka, V. Complete amino acid sequence of human serum albumin, *FEBS Lett.* ***58*** 1 (1975) 134-137.

Merlot, A.M., Kalinowski, D.S. & Richardson, D.R. Unraveling the mysteries of serum albumin—more than just a serum protein, *Front. Physiol.* ***5*** (2014) 299.

Michon, J., Frelon, S., Garnier, C. & Coppin, F. Determinations of Uranium(VI) Binding Properties with some Metalloproteins (Transferrin, Albumin, Metallothionein and Ferritin) by Fluorescence Quenching, *J. Fluoresc.* ***20*** 2 (2010) 581-590.

Milić, N., Djurdjević, P. & Niketić, S. Effect of acetate and EDTA ligands on Hydrolysis of the Iron(III) Ion in sodium chloride medium, *Z. Anorg. Allg. Chem.* ***571*** 1 (1989) 174-180.

Mohapatra, P.K. & Khopkar, P.K. Hydrolysis of actinides and lanthanides: hydrolysis of some trivalent actinide and lanthanide ions studied by extraction with thenoyltrifluoroacetone, *Polyhedron* ***8*** 16 (1989) 2071-2076.

Moll, H., Brendler, V. & Gert, B. Aqueous curium(III) phosphate species characterized by time-resolved laser-induced fluorescence spectroscopy, *Radiochim. Acta* ***99*** (2011) 775.

Moll, H., Stumpf, T., Merroun, M., Rossberg, A., Selenska-Pobell, S. & Bernhard, G. Time-Resolved Laser Fluorescence Spectroscopy Study on the Interaction of Curium(III) with Desulfovibrio äspöensis DSM 10631T, *Environ. Sci. Technol.* ***38*** 5 (2004) 1455-1459.

Moll, H. & Bernhard, G. Complex formation of curium(III) with amino acids of different functionalities: L-threonine and O -phospho-L-threonine, *J. Coord. Chem.* ***60*** 16 (2007) 1795-1807.

Moll, H., Geipel, G. & Bernhard, G. Complexation of curium(III) by adenosine 5'-triphosphate (ATP): A time-resolved laser-induced fluorescence spectroscopy (TRLFS) study, *Inorg. Chim. Acta* ***358*** 7 (2005) 2275-2282.

Moll, H., Glorius, M. & Bernhard, G. Curium(III) Complexation with Desferrioxamine B (DFO) Investigated Using Fluorescence Spectroscopy, *Bull. Chem. Soc. Jpn.* ***81*** 7 (2008) 857-862.

Moll, H., Johnsson, A., Schäfer, M., Pedersen, K., Budzikiewicz, H. & Bernhard, G. Curium(III) complexation with pyoverdins secreted by a groundwater strain of Pseudomonas fluorescens, *Biometals* ***21*** 2 (2008) 219-228.

Moll, H., Lütke, L., Barkleit, A. & Bernhard, G. Curium(III) Speciation Studies with Cells of a Groundwater Strain of Pseudomonas fluorescens, *Geomicrobiol. J.* ***30*** 4 (2013) 337-346.

Montavon, G., Apostolidis, C., Bruchertseifer, F., Repinc, U. & Morgenstern, A. Spectroscopic study of the interaction of U(VI) with transferrin and albumin for speciation of U(VI) under blood serum conditions, *J. Inorg. Biochem.* ***103*** 12 (2009) 1609-1616.

Montero, R.P. & Sánchez, M.A. Plutonium contamination from accidental release or simply fallout: study of soils at Palomares (Spain), *J. Environ. Radioact.* ***55*** 2 (2001) 157-165.

Moore, K.T. & van der Laan, G. Nature of the 5f states in actinide metals, *Rev. Mod. Phys.* ***81*** 1 (2009) 235-298.

Moreno, L.M. *Europium: Compounds, Production and Applications,* Nova Science Publishers, Inc., Hauppauge, 2011.

Mortimer, R.G. *Physical Chemistry,* Elsevier Science & Technology, San Diego, 2000.

Mothes, E. & Faller, P. Evidence that the Principal CoII-Binding Site in Human Serum Albumin Is Not at the N-Terminus: Implication on the Albumin Cobalt Binding Test for Detecting Myocardial Ischemia, *Biochemistry (NY)* ***46*** 8 (2007) 2267-2274.

Moulin Valérie, Jan, T. & Gerald, O. Actinide Speciation in the Presence of Humic Substances in Natural Water Conditions, *Radiochim. Acta* ***58-59*** (1992) 179.

Mycielska, M.E., Patel, A., Rizaner, N., Mazurek, M.P., Keun, H., Patel, A., Ganapathy, V. & Djamgoz, M.B.A. Citrate transport and metabolism in mammalian cells, *Bioessays* ***31*** 1 (2009) 10-20.

Nanny, M.A., Minear, R.A. & Leenheer, J.A. *Nuclear Magnetic Resonance Spectroscopy in Environmental Chemistry,* Oxford University Press, Incorporated, Cary, 1997.

Nesmerak, K. Lanthanide/Actinide Toxicity, in publication *Encyclopedia of Metalloproteins,* ed(s). Kretsinger, R.H., Uversky, V.N. & Permyakov, E.A., Springer New York, New York, NY, 2013.

Nikipelov, B.V., Romanov, G.N., Buldakov, L.A., Babaev, N.S., Kholina, Y.B. & Mikerin, E.I. Report on a radiological accident in the southern Urals on 29 September 1957, (1989).

Nouhi, A., Hajjoul, H., Redon, R., Gagné, J.P. & Mounier, S. Time-resolved laser fluorescence spectroscopy of organic ligands by europium: Fluorescence quenching and lifetime properties, *Spectrochim. Acta, Part A* ***193*** (2018) 219-225.

Orchard, A.F. *Magnetochemistry,* Oxford University Press, Oxford : New York, 2003.

Ottavia, S., Domenico, S., Simone, C., Andrea, B., Vincenzo, V., De, C.M., Raffaella, P., Simona, F., Antonios, M., Di, G.D., Di, S.P. & Neri, N. A structurally driven analysis of thiol reactivity in mammalian albumins, *Biopolymers* ***95*** 4 (2011) 278-285.

Ozaki, T., Kimura, T., Ohnuki, T., Yoshida, Z. & Francis, A.J. Association mechanisms of europium(III) and curium(III) with Chlorella vulgaris, *Environ. Toxicol. Chem.* ***22*** 11 (2003) 2800-2805.

Pace, C.N., Grimsley, G.R. & Scholtz, J.M. Protein Ionizable Groups: pK Values and Their Contribution to Protein Stability and Solubility, *J. Biol. Chem.* ***284*** 20 (2009) 13285-13289.

Page, R., Peti, W., Wilson, I.A., Stevens, R.C. & Wüthrich, K. NMR screening and crystal quality of bacterially expressed prokaryotic and eukaryotic proteins in a structural genomics pipeline, *Proc. Natl. Acad. Sci. USA* ***102*** 6 (2005) 1901-1905.

Panak, P., Klenze, R. & Kim, J.I. A Study of Ternary Complexes of Cm(III) with Humic Acid and Hydroxide or Carbonate in Neutral pH Range by Time-Resolved Laser Fluorescence Spectroscopy, *Radiochim. Acta* ***74*** (1996) 141.

Panak, P.J. & Geist, A. Complexation and Extraction of Trivalent Actinides and Lanthanides by Triazinylpyridine N-Donor Ligands, *Chem. Rev.* ***113*** 2 (2013) 1199-1236.

Pauling, L. *General Chemistry,* Dover Publications, Inc, New York, 1988.

Paviet, P., Fanghänel Th., Klenze, R. & Kim, J.I. Thermodynamics of Curium(III) in Concentrated Electrolyte Solutions : Formation of Sulfate Complexes in NaCl/Na2SO4 Solutions, *Radiochim. Acta* ***74*** (1996) 99.

Pearson, R.G. Hard and Soft Acids and Bases, *J. Am. Chem. Soc.* ***85*** 22 (1963) 3533-3539.

Peña, M.J., Arevalillo, A., Rucandio, I. & Jiménez, J.S. Complex species of Zn(II) and Cu(II) in tris buffer solutions—I. Zn(II), *Electrochim. Acta* ***35*** 3 (1990) 673-677.

Penneman, R.A. & Keenan, T.K. The Radiochemistry of Americium and Curium, 1960.

Petitpas, I., Bhattacharya, A.A., Twine, S., East, M. & Curry, S. Crystal Structure Analysis of Warfarin Binding to Human Serum Albumin: Anatomy of drug site I, *J. Biol. Chem.* ***276*** 25 (2001) 22804-22809.

Pfefferlé, J. & Bünzli, J.G. Interaction between the buffer Tris and the eu(III) ion: Luminescence and potentiometric investigation, *Helv. Chim. Acta* ***72*** 7 (1989) 1487-1494.

Piciu, D. *Nuclear Endocrinology,* Springer, Berlin; Heidelberg, 2012.

Piotto, M., Saudek, V. & Sklenář, V. Gradient-tailored excitation for single-quantum NMR spectroscopy of aqueous solutions, *J. Biomol. NMR* ***2*** 6 (1992) 661-665.

Plancque, G., Moulin, V., Toulhoat, P. & Moulin, C. Europium speciation by time-resolved laser-induced fluorescence, *Anal. Chim. Acta* ***478*** 1 (2003) 11-22.

Predki, P.F., Harford, C., Brar, P. & Sarkar, B. Further characterization of the *N*-terminal copper(II)- and nickel(II)-binding motif of proteins. Studies of metal binding to chicken serum albumin and the native sequence peptide, *Biochem. J.* ***287*** 1 (1992) 211-215.

Rabung, T., Altmaier, M., Neck, V. & Fanghänel, T. A TRLFS study of Cm(III) hydroxide complexes in alkaline CaCl2 solutions, *Radiochim. Acta* ***96*** (2009) 551.

Ramasubbu, S., Sandeep, V. & Sandeep, K. ATCUN-like metal-binding motifs in proteins: Identification and characterization by crystal structure and sequence analysis, *Proteins* ***58*** 1 (2005) 211-221.

Reddi, A.S. Body Fluid Compartments, in publication *Fluid, Electrolyte and Acid-Base Disorders: Clinical Evaluation and Management,* ed(s). Reddi, A.S., Springer New York, New York, NY, 2014, 1-12.

Rizkalla, E.N. & Choppin, G.R. *Hydration and Hydrolysis of Lanthanides,* Elsevier, Amsterdam, 1991.

Rózga, M., Sokołowska, M., Protas, A.M. & Bal, W. Human serum albumin coordinates Cu(II) at its N-terminal binding site with 1 pM affinity, *JBIC, J. Biol. Inorg. Chem.* ***12*** 6 (2007) 913-918.

Ruff, C.M., Mullich, U., Geist, A. & Panak, P.J. Complexation of Cm(iii) and Eu(iii) with a hydrophilic 2,6-bis(1,2,4-triazin-3-yl)-pyridine studied by time-resolved laser fluorescence spectroscopy, *Dalton Trans.* ***41*** 48 (2012) 14594-14602.

Runde, W. The Chemical Interactions of Actinides in the Environment, *Los Alamos Science* ***26*** (2000) 392-411.

Runde, W. & Neu, M.P. Actinides in the geosphere, in publication *The Chemistry of the Actinide and Transactinide Elements,* ed(s). Morss, L.R., Edelstein, N.M. & Fuger, J., Springer Netherlands, Dordrecht, 2006.

Sadler, P.J., Tucker, A. & Viles, J.H. Involvement of a lysine residue in the N-terminal Ni2+ and Cu2+ binding site of serum albumins, *Eur. J. Biochem.* ***220*** 1 (1994) 193-200.

Sadler, P.J. & Viles, J.H. 1H and 113Cd NMR Investigations of Cd2+ and Zn2+ Binding Sites on Serum Albumin: Competition with Ca2+, Ni2+, Cu2+, and Zn2+, *Inorg. Chem.* ***35*** 15 (1996) 4490-4496.

Sakagami, N., Yamada, Y., Konno, T. & Okamoto, K. Crystal structures and stereochemical properties of lanthanide(III) complexes with ethylenediamine-N,N,N',N'-tetraacetate, *Inorg. Chim. Acta* ***288*** 1 (1999) 7-16.

Schnurr, A., Marsac, R., Rabung, T., Lützenkirchen, J. & Geckeis, H. Sorption of Cm(III) and Eu(III) onto clay minerals under saline conditions: Batch adsorption, laser-fluorescence spectroscopy and modeling, *Geochim. Cosmochim. Acta* ***151*** (2015) 192-202.

Schomäcker, K., Mocker, D., Münze, R. & Beyer, G. Stabilities of lanthanide-protein complexes, *Intl. J. Rad. Appl. Instrum. A* ***39*** 3 (1988) 261-264.

Schönenberger, M. Streulichtmessungen an Plasmaproteinen, *Z. Naturforsch. B* ***10*** (1955) 474.

Schreckhise, R.G. & Cline, J.F. Comparative Uptake and Distribution of Plutonium, Americium, Curium and Neptunium in Four Plant Species, *Health. Phys.* ***38*** 5 (1980) .

Scott, K.G., Axelrod, D.J. & Hamilton, J.G. The metabolism of curium in the rat, *The J. Biol. Chem.* ***177*** 1 (1949) 325.

Shaw, C.F. The Protein Chemistry of Antiarthritic Gold(I) Thiolates and Related Complexes, *Comments Inorg. Chem.* ***8*** 6 (1989) 233-267.

Shen, X., Liang, H., Guo, J., Song, C., He, X. & Yuan, Y. Studies on the interaction between Ag+ and human serum albumin, *J. Inorg. Biochem.* ***95*** 2 (2003) 124-130.

Shin, H.S., Lee, B.H., Choi, J.G. & Moon, H. Complexation of Soil Humic Acid with Trivalent Curium and Europium Ions: A Comparative Study, *Radiochim. Acta* ***69*** (1995) 185.

Silvia, S., Stumpf T., Walther, C., Dirk, B. & Fanghänel T. Sorption of Cm(III) onto different Feldspar surfaces: a TRLFS study, *Radiochim. Acta* ***94*** (2009) 243.

Skanthakumar, S., Antonio, M.R., Wilson, R.E. & Soderholm, L. The Curium Aqua Ion, *Inorg. Chem.* ***46*** 9 (2007) 3485-3491.

Skerencak, A., Panak, P.J. & Fanghänel, T. Complexation and thermodynamics of Cm(iii) at high temperatures: the formation of Cm(SO4)n]3-2n (n = 1, 2, 3) complexes at T = 25 to 200 degree]C, *Dalton Trans.* ***42*** 2 (2013) 542-549.

Sklenar, V., Piotto, M., Leppik, R. & Saudek, V. Gradient-Tailored Water Suppression for 1H-15N HSQC Experiments Optimized to Retain Full Sensitivity, *J. Magn. Reson., Ser. A* ***102*** 2 (1993) 241-245.

Sokołowska, M., Krezel, A., Dyba, M., Szewczuk, Z. & Bal, W. Short peptides are not reliable models of thermodynamic and kinetic properties of the N-terminal metal binding site in serum albumin, *Eur. J. Biochem.* ***269*** 4 (2002) 1323-1331.

Sokołowska, M., Pawlas, K. & Bal, W. Effect of Common Buffers and Heterocyclic Ligands on the Binding of Cu(II) at the Multimetal Binding Site in Human Serum Albumin, *Bioinorg. Chem. Appl.* ***2010*** (2010) 1-7.

Sokołowska, M., Wszelaka-Rylik, M., Poznański, J. & Bal, W. Spectroscopic and thermodynamic determination of three distinct binding sites for Co(II) ions in human serum albumin, *J. Inorg. Biochem.* ***103*** 7 (2009) 1005-1013.

Solomon, H.M., Schrogie, J.J. & Williams, D. The displacement of phenylbutazone-14C and warfarin-14C from human albumin by various drugs and fatty acids, *Biochem. Pharmacol.* ***17*** 1 (1968) 143-151.

Spoor, N.L. The use of EDTA and DTPA for accelerating the removal of deposited transuranic elements from humans, 1977.

Stacey, W.M. *Nuclear Reactor Physics,* Wiley-VCH Verlag GmbH & Co. KGaA, Weinheim, 2007.

Stamler, J.S., Jaraki, O., Osborne, J., Simon, D.I., Keaney, J., Vita, J., Singel, D., Valeri, C.R. & Loscalzo, J. Nitric oxide circulates in mammalian plasma primarily as an S-nitroso adduct of serum albumin. *Proc. Natl. Acad. Sci. USA* ***89*** 16 (1992) 7674-7677.

Steele, M.L. & Wertz, D.L. Solute complexes in aqueous gadolinium(III) chloride solutions, *J. Am. Chem. Soc.* ***98*** 15 (1976) 4424-4428.

Steinhauser, G., Brandl, A. & Johnson, T.E. Comparison of the Chernobyl and Fukushima nuclear accidents: A review of the environmental impacts, *Sci. Total. Environ.* ***470–471*** (2014) 800-817.

Stewart, A.J., Blindauer, C.A., Berezenko, S., Sleep, D. & Sadler, P.J. Interdomain zinc site on human albumin, *Proc. Natl. Acad. Sci. USA* ***100*** 7 (2003) 3701-3706.

Stewart, A.J., Blindauer, C.A., Stephen, B., Darrell, S., David, T. & Sadler, P.J. Role of Tyr84 in controlling the reactivity of Cys34 of human albumin, *FEBS J* ***272*** 2 (2005) 353-362.

Stone, R.S. *Industrial Medicine on the Plutonium Project,* 1st ed., McGraw-Hill, New York, 1951.

Stover, B.J., Bruenger, F.W. & Stevens, W. The Reaction of PuIV with the Iron Transport System in Human Blood Serum, *Radiat. Res.* ***33*** 2 (1968) 381-394.

Stumpf, T., Marques Fernandes, M., Walther, C., Dardenne, K. & Fanghänel, T. Structural characterization of Am incorporated into calcite: A TRLFS and EXAFS study, *J. Colloid Interface Sci.* ***302*** 1 (2006) 240-245.

Stumpf, T., Rabung, T., Klenze, R., Geckeis, H. & Kim, J.I. Spectroscopic Study of Cm(III) Sorption onto γ-Alumina, *J. Colloid Interface Sci.* ***238*** 1 (2001) 219-224.

Stumpf, T. & Fanghänel, T. A Time-Resolved Laser Fluorescence Spectroscopy (TRLFS) Study of the Interaction of Trivalent Actinides (Cm(III)) with Calcite, *J. Colloid Interface Sci.* ***249*** 1 (2002) 119-122.

Sturzbecher-Hoehne, M., Goujon, C., Deblonde, G.J.-., Mason, A.B. & Abergel, R.J. Sensitizing Curium Luminescence through an Antenna Protein To Investigate Biological Actinide Transport Mechanisms, *J. Am. Chem. Soc.* ***135*** 7 (2013) 2676-2683.

Sudlow, G., Birkett, D.J. & Wade, D.N. The Characterization of Two Specific Drug Binding Sites on Human Serum Albumin, *Mol. Pharmacol.* ***11*** 6 (1975) 824-832.

Sudlow, G., Birkett, D.J. & Wade, D.N. Further Characterization of Specific Drug Binding Sites on Human Serum Albumin, *Mol. Pharmacol.* ***12*** 6 (1976) 1052-1061.

Sugio, S., Kashima, A., Mochizuki, S., Noda, M. & Kobayashi, K. Crystal structure of human serum albumin at 2.5 Å resolution, *Protein Eng., Des. Sel.* ***12*** 6 (1999) 439-446.

Sullivan, J.C., Gordon, S., Mulac, W.A., Schmidt, K.H., Cohen, D. & Sjoblom, R. Pulse radiolysis studies of americum(III) and curium(III) ions in perchlorate media. The preparation of Am II, Am IV, Cm II and Cm IV, *Inorg. Nucl. Chem. Lett.* ***12*** 8 (1976) 599-601.

Sun, H., Li, H. & Sadler, P.J. Transferrin as a Metal Ion Mediator, *Chem. Rev.* ***99*** 9 (1999) 2817-2842.

Takahashi, Y., Kimura, T. & Minai, Y. Direct observation of Cm(III)-fulvate species on fulvic acid-montmorillonite hybrid by laser-induced fluorescence spectroscopy, *Geochim. Cosmochim. Acta* ***66*** 1 (2002) 1-12.

Takuo, O., Gillow, J.B., Takaumi, K., Ohnuki, T., Zenko, Y. & Francis, A.J. Sorption behavior of europium(III) and curium(III) on the cell surfaces of microorganisms, *Radiochim. Acta* ***92*** (2009) 741.

Taylor, D.M. The bioinorganic chemistry of actinides in blood, *J. Alloys Compd.* ***271-273*** (1998) 6-10.

Thakur, P., Conca, J.L., De Burgt, L.J.,V.A.N. & Choppin, G.R. Complexation and the laser luminescence studies of Eu(III), Am(III), and Cm(III) with EDTA, CDTA, and PDTA and their ternary complexation with dicarboxylates, *J. Coord. Chem.* ***62*** 23 (2009) 3719-3737.

Thakur, P., Pathak, P.N., Gedris, T. & Choppin, G.R. Complexation of Eu(III), Am(III) and Cm(III) with Dicarboxylates: Thermodynamics and Structural Aspects of the Binary and Ternary Complexes, *J. Solution Chem.* ***38*** 3 (2009) 265.

Thakur, P., Mathur, J.N., Dodge, C.J., Francis, A.J. & Choppin, G.R. Thermodynamics and the structural aspects of the ternary complexes of Am(iii), Cm(iii) and Eu(iii) with Ox and EDTA + Ox, *Dalton Trans.* 40 (2006) 4829-4837.

Thomas, R., Horst, G., Wang, X.K., Rothe Jörg, Denecke, M.A., Klenze, R. & Fanghänel Thomas. Cm(III) sorption onto γ-Al2O3: New insight into sorption mechanisms by time-resolved laser fluorescence spectroscopy and extended X-ray absorption fine structure, *Radiochim. Acta* ***94*** (2009) 609.

Tian, G., Edelstein, N.M. & Rao, L. Spectroscopic Properties and Hydration of the Cm(III) Aqua Ion from 10 to 85 °C, *J. Phys. Chem. A* ***115*** 10 (2011) 1933-1938.

Tian, G., Zhang, Z., Martin, L.R. & Rao, L. Complexation of Curium(III) with DTPA at 10–70 °C: Comparison with Eu(III)–DTPA in Thermodynamics, Luminescence, and Coordination Modes, *Inorg. Chem.* ***54*** 4 (2015) 1232-1239.

Toste, A.P. The gamma-radiolysis of HEDTA in a simulated, mixed waste, *J. Radioanal. Nucl.* ***249*** 2 (2001) 283-288.

Toste, A.P., Osborn, B.C., Polach, K.J. & Lechner-Fish, T. Organic analyses of an actual and simulated mixed waste: Hanford's organic complexant waste revisited, *J. Radioanal. Nucl.* ***194*** 1 (1995) 25-34.

Trapaidze, A., Hureau, C., Bal, W., Winterhalter, M. & Faller, P. Thermodynamic study of Cu2+ binding to the DAHK and GHK peptides by isothermal titration calorimetry (ITC) with the weaker competitor glycine, *JBIC, J. Biol. Inorg. Chem.* ***17*** 1 (2012) 37-47.

Trumm, M., Wagner, C., Schimmelpfennig, B., Geist, A. & Panak, P.J. A closer look on the coordination of soft nitrogen-donor ligands to Cm(iii): SO3-Ph-BTBP, *Dalton Trans.* ***45*** 31 (2016) 12308-12311.

Turner, G.A. & Taylor, D.M. The Transport of Plutonium, Americium and Curium in the Blood of Rats, *Phys. Med. Biol.* ***13*** 4 (1968) 535.

UNSCEAR. UNSCEAR 2000 Report, Vol. I, Sources and effects of ionizing radiation, 2000.

UNSCEAR. UNSCEAR 2008 Report, Vol. II, Sources and effects of ionizing radiation, 2008.

USAF. Project Crested Ice: USAF B-52 Accident At Thule, Greenland, 21 January 1968, *USAF Nuclear Safety* ***65*** 1 (1970).

USDOE. Operation Morning Light, U.S. Department of Energy Report NV-198, 1978.

Valko, M., Morris, H., Mazúr, M., Telser, J., McInnes, E.J.L. & Mabbs, F.E. High-Affinity Binding Site for Copper(II) in Human and Dog Serum Albumins (an EPR Study), *J. Phys. Chem. B* ***103*** 26 (1999) 5591-5597.

Vallee, B.L. & Ulmer, D.D. Biochemical Effects of Mercury, Cadmium, and Lead, *Annu. Rev. Biochem.* ***41*** 1 (1972) 91-128.

Vercouter, T., Vitorge, P., Amekraz, B., Giffaut, E., Hubert, S. & Moulin, C. Stabilities of the Aqueous Complexes Cm(CO3)33- and Am(CO3)33- in the Temperature Range 10−70 °C, *Inorg. Chem.* ***44*** 16 (2005) 5833-5843.

Wally, J., Halbrooks, P.J., Vonrhein, C., Rould, M.A., Everse, S.J., Mason, A.B. & Buchanan, S.K. The Crystal Structure of Iron-free Human Serum Transferrin Provides Insight into Inter-lobe Communication and Receptor Binding, *J. Biol. Chem.* ***281*** 34 (2006) 24934-24944.

Wang, X.K., Thomas, R., Horst, G., Panak, P.J., Klenze, R. & Fanghänel Thomas. Effect of humic acid on the sorption of Cm(III) onto γ-Al2O3 studied by the time-resolved laser fluorescence spectroscopy, *Radiochim. Acta* ***92*** (2009) 691.

Weller, M., Overton, T., Rourke, J. & Armstrong, F. *Inorganic Chemistry,* 6th ed., Oxford University Press, Oxford, 2014.

Wiberg, E., Wiberg, N. & Holleman, A.F. *Inorganic Chemistry,* Academic Press ; De Gruyter, San Diego; Berlin; New York, 2001.

Wilting, J., van der Giesen, W F, Janssen, L.H., Weideman, M.M., Otagiri, M. & Perrin, J.H. The effect of albumin conformation on the binding of warfarin to human serum albumin. The dependence of the binding of warfarin to human serum albumin on the hydrogen, calcium, and chloride ion concentrations as studied by circular dichroism, fluorescence, and equilibrium dialysis. *J. Biol. Chem.* ***255*** 7 (1980a) 3032-3037.

Wilting, J., 'T Hart, B.J. & De Gier, J.J. The role of albumin conformation in the binding of diazepam to human serum albumin, *Biochim. Biophys. Acta, Prot. Struct.* ***626*** 2 (1980b) 291-298.

Wimmer, H., Kim, J.I. & Klenze, R. A Direct Speciation of Cm(III) in Natural Aquatic Systems by Time-Resolved Laser-Induced Fluorescence Spectroscopy (TRLFS), *Radiochim. Acta* ***58-59*** (1992) 165.

Wimmer, H., Klenze, R. & Kim, J.I. A Study of Hydrolysis Reaction of Curium(III) by Time Resolved Laser Fluorescence Spectroscopy, *Radiochim. Acta* ***56*** (1992) 79.

Windorff, C.J., Chen, G.P., Cross, J.N., Evans, W.J., Furche, F., Gaunt, A.J., Janicke, M.T., Kozimor, S.A. & Scott, B.L. Identification of the Formal +2 Oxidation State of Plutonium: Synthesis and Characterization of {PuIIC5H3(SiMe3)2]3}−, *J. Am. Chem. Soc.* ***139*** 11 (2017) 3970-3973.

Yamasaki, K., Chuang, V.T.G., Maruyama, T. & Otagiri, M. Albumin–drug interaction and its clinical implication, *Biochim. Biophys. Acta, Gen. Subj.* ***1830*** 12 (2013) 5435-5443.

Yamasaki, K., Hyodo, S., Taguchi, K., Nishi, K., Yamaotsu, N., Hirono, S., Chuang, V.T.G., Seo, H., Maruyama, T. & Otagiri, M. Long chain fatty acids alter the interactive binding of ligands to the two principal drug binding sites of human serum albumin, *PLOS ONE* ***12*** 6 (2017) e0180404.

Yamasaki, K., Maruyama, T., Kragh-Hansen, U. & Otagiri, M. Characterization of site I on human serum albumin: concept about the structure of a drug binding site, *Biochim. Biophys. Acta, Prot. Struct. Mol. Enzymol.* ***1295*** 2 (1996) 147-157.

Yang & Bursten, B.E. Speciation of the Curium(III) Ion in Aqueous Solution: A Combined Study by Quantum Chemistry and Molecular Dynamics Simulation, *Inorg. Chem.* ***45*** 14 (2006) 5291-5301.

Zhang, Y., Akilesh, S. & Wilcox, D.E. Isothermal Titration Calorimetry Measurements of Ni(II) and Cu(II) Binding to His, GlyGlyHis, HisGlyHis, and Bovine Serum Albumin: A Critical Evaluation, *Inorg. Chem.* ***39*** 14 (2000) 3057-3064.

Zheng, J., Tagami, K., Watanabe, Y., Uchida, S., Aono, T., Ishii, N., Yoshida, S., Kubota, Y., Fuma, S. & Ihara, S. Isotopic evidence of plutonium release into the environment from the Fukushima DNPP accident, *Sci. Rep.* ***2*** (2012) 304.